Simulation of natural convective flow in an experimental reactor cavity cooling system facility

PF Niemand

22134530

Dissertation submitted in partial fulfilment of the requirements for the degree Master of Engineering in Nuclear Engineering at the Potchefstroom Campus of the North-West University

Supervisor: Prof CG du Toit

May 2017

Abstract

The very high temperature reactor (VHTR) has many safety features. One of these features is the reactor cavity cooling system (RCCS). This system is intended to remove decay heat from the reactor cavity during upset conditions. The Korea Atomic Energy Research Institute (KAERI) constructed a facility that represents a ¼ scale model of the RCCS of a VHTR. The preliminary testing on the facility has been completed and a simulation model has been set up for the facility, using the system code GAMMA+. GAMMA+ was intended to be used to simulate the phenomena in gas-cooled reactors, particularly the PMR200 (under development by KAERI).

This study aims to simulate the facility using the 1D CFD program Flownex SE and compare the results with the results obtained with GAMMA+. The Flownex simulation was set up as close as possible to the GAMMA+ model by using the same initial- and boundary conditions. The fluid and surface temperatures, as well as the mass flow rates in the riser tubes, were compared to determine the agreement of the results. The results show very good agreement. There are differences in the philosophies of the programs, as well as some differences in the calculation of the fluid properties. The small differences in the results are attributed to these factors.

The mixed convection regime was found to be present and therefore the relevant correlations were used to calculate the heat transfer. The convection heat transfer coefficient had to be calculated based on a Nusselt number which is a combination of the forced and free convection Nusselt numbers.

The mixed convection regime can either increase or decrease the amount of heat that is transferred. In this particular study, the heat transfer was impeded, since the forced convection and free convection was orientated in the same direction while in the flow was in the turbulent regime. This was due to a laminarizational effect that the mixed convection regime can have on the boundary layer.

Key words: reactor cavity cooling system, thermal radiation, mixed convection, natural convection, experimental facility.

Opsomming

Die vierde generasie hoë temperatuur gasverkoelde reaktore het verskillende veiligheidsmeganismes. Een van die meganismes, is die reaktor ruimte verkoeling sisteem (RCCS). Die sisteem is ontwerp om hitte uit die ruimte rondom die reaktor drukvat te verwyder om sodoende die temperatuur in hierdie ruimte onder die aanvaarbare limiet te handhaaf. Alvorens die sisteem in die ontwerp ge-integreer kan word, moet daar bewys word dat die termo-hidroliese verskynsels in die sisteem akkuraat voorspel kan word. Die stelsel kode GAMMA+ is ontwikkel deur die Korea Atoomenergie Navorsingsinstituut (KAERI) om die verskynsels in die PMR200 kernkrag reaktor te simuleer. Die kode is ook ingespan om die verskynsels in die RCCS te voorspel. Die NACEF toetsfasiliteit is gebou om die kode GAMMA+ te valideer. Hierdie fasiliteit is `n skaal model van die lugverkoelde RCCS van `n PMR200 reaktor.

Die GAMMA+ resultate is in die studie vergelyk met resultate verkry deur die gebruik van die stelsel kode, Flownex. Die begin- en randwaardes van die Flownex model is dieselfde gekies as die ooreenstemmende GAMMA+ model sodat die vergelyking sinvol is. Die resultate blyk om baie goeie ooreenstemming te hê. Die temperature en massavloeitempo in die sisteem is vergelyk en het gedien as maatstaaf van die ooreenstemming.

Daar is gevind dat die vloei in die gemengde konveksie gebied val, wat beteken het dat daar as`t ware ge-interpoleer moes word tussen die Nusselt-getalle van natuurlike- en forseerde konveksie. Die konveksie hitteoordrag koeffisient is vervolgens bereken gebaseer op die gemengde konveksie Nusselt-getal.

Gemengde konveksie kan twee moontlike effekte hê op die hitte-oordrag. In die turbulente gebied, word die hitte-oordrag verbeter deurdat die geforseerde en natuurlike konveksie in teenoorgestelde rigtings vloei. Tweedens, die hitte-oordrag word gekniehalter wanneer die dryfkragte en geforseerde konveksie in dieselfde rigting inwerk. In hierdie studie is gevind dat die laasgenoemde geval geld, wat `n “laminariserende” effek het op die vloei.

Sleutel woorde: reaktor ruimte verkoeling stelsel, termiese straling, gemengde konveksie, natuurlike konveksie, eksperimentele fasiliteit.

Acknowledgements

I would like to thank Professor Jat du Toit for his help and guidance throughout the writing of this dissertation. The GAMMA+ models were all set up and simulated by Professor Jat du Toit. The EES results and the Flownex results in the verification chapter were supplied by Prof. Du Toit.

I would like to thank Dr Nam-il Tak from KAERI for his suggestions in the use of GAMMA+ when the results didn`t show satisfactory agreement.

I would like to thank mr. Vincent Britz at M-Tech Industrial for the instruction in the use of the scripting components in Flownex.

Thank you to my family and friends for their moral support and their prayers.

Soli Deo Gloria.

Declaration

I, Peter Niemand hereby declare that the work in this dissertation is my own original work. It has not been submitted to any other academic institution. Proper credit is given to the authors of the cited work.

P.F. Niemand

Contents

List of Figures

List of Tables

Nomenclature

List of abbreviations

ANL	Argonne National Laboratory
CFD	Computational Fluid Dynamics
DTHT	Deteriorated Turbulence Heat Transfer
EES	Engineering Equation solver
ECCS	Emergency Core Cooling System
GAMMA+	General Analyser for Multi-component and Multi-dimensional Transient Application
GT-MHR	Gas Turbine Modular Helium Reactor
IAEA	International Atomic Energy Agency
KAERI	Korea Atomic Energy Research Institute
LOFC	Loss of Forced Coolant
LWR	Light Water Reactor
NACEF	Natural Cooling Experimental Facility
NNR	National Nuclear Regulator
NSTF	Natural Circulation Shutdown Heat Removal Test Facility
RCCS	Reactor Cavity Cooling System
VHTR	Very High Temperature Reactor
SAR	Safety Analysis Report
SCS	Shutdown Cooling System

List of symbols

Symbol	Description	Units
A	Flow area	m^2
$\mathrm{C_p}$	Specific heat capacity	$\frac{J}{kg-K}$
D	Diameter	m
E_{bi}	Emissive power	$\frac{W}{m^2}$
f	Friction factor	-
f_r	Fraction	-

F_{ij}	View factor from i to j	-
g	Gravitational acceleration	$\frac{m}{s^2}$
Gr	Grashof number	-
h_0	Enthalpy	$\frac{J}{kg}$
h	Convection heat transfer coefficient	$\frac{W}{m^2 - K}$
J	Radiosity	$\frac{W}{m^2}$
k	Thermal conductivity	$\frac{W}{m - K}$
K	Secondary loss coefficient	-
L	Length	m
$\dot{m}$	Mass flow rate	$\frac{kg}{s}$
Nu	Nusselt number	-
P	Pressure	Pa
Pr	Prandtl Number	-
Q	Heat	W
R	Gas constant	$\frac{J}{kg - K}$
Ra	Rayleigh number	-
Re	Reynolds number	-
T	Temperature	K
t	time	s
V	Velocity	$\frac{m}{s}$
~~V~~	Volume	m^3
W	Work	W
x	Distance	m
z	Elevation	m

Greek letters

Symbol	Description	Units
β	Expansion coefficient	-
ε	Surface emissivity	-
η	Fluid property index	-
μ	Dynamic viscosity	$\frac{Ns}{m}$
ν	Kinematic viscosity	$\frac{m^2}{s}$
ρ	Density	$\frac{kg}{m^3}$
σ	Stefan-Boltzmann constant	$\frac{W}{m^2 - K^4}$

Subscripts

e	Property at outlet
i	Property at inlet
0	Stagnation properties

Chapter 1 - Introduction

1.1 Introduction

The fourth generation nuclear power plant designs have many safety features. One of these features is the reactor cavity cooling system (RCCS). This system is designed to passively remove decay heat from the reactor cavity. The system will remove heat under all operating conditions, but is intended especially to remove the decay heat in a natural and passive manner during a loss of forced coolant (LOFC) accident. The aim is to keep the temperature low enough to maintain the structural integrity of the concrete enclosure.

1.2 Background

1.2.1 Loss of forced coolant (LOFC) accidents

The heat generated by the fuel is removed by passing a coolant through the core. The coolant, depending on the type of reactor, may be helium, carbon dioxide, and water, liquid metal or molten salts (Lamarsh & Baratta, 2014).

In the event that the coolant flow is interrupted the heat will be trapped in the reactor core. This may have serious consequences, including causing a meltdown of the fuel. The melted fuel would still undergo fission reactions, which produce heat, which would be unable to escape. The heat build-up could lead to the melting of the pressure vessel and subsequently, radioactive material may leak out of the pressure vessel.

Fourth generation nuclear reactors are designed with a negative temperature reactivity coefficient. The negative coefficient aims to prevent a meltdown from occurring. Whenever the temperature increases, the reactivity decreases, causing in turn that the temperature decreases. This effectively causes the nuclear chain reaction to shut itself down when the coolant is lost. There is however still the problem of the decay heat which would still be produced long after the reactor has been shut down. The RCCS is implemented specifically to remove the decay heat.

When it would seem that a shutdown is necessary, the fuel can be cooled by systems such as the emergency core cooling system (ECCS) in Light Water Reactors (LWRs) or the Shutdown Cooling System (SCS) in the GT-MHR design. This system is intended to remove heat under normal conditions. It would be effective in removing a large portion of the fission heat. The SCS is not intended for prolonged use under upset conditions, hence the need for

the RCCS. The RCCS would remain in operation indefinitely since it requires neither an input from an operator, a power source, or manual refilling of the coolant.

1.2.2 The purpose of the reactor cavity cooling system

Decay heat is emitted from the reactor pressure vessel, mainly by the mechanism of thermal radiation (Lisowski & Farmer, 2014). This heat energy causes the temperature within the reactor cavity to rise. The RCCS is installed to remove the decay heat from the reactor cavity, to keep the temperatures at acceptable levels. The temperatures of the containment structure, the pressure vessel and the vessel support structures are hereby kept below the design limits (IAEA, 2008).

The RCCS needs to be fully passive, to remain independent of any system or operator.

The amount of heat removed by the RCCS is low compared to the heat generated at normal operating conditions. In the PMR200 design, the RCCS removes 0.3-0.6% of the total heat when the reactor is at full power (Bae, et al., 2012). It is therefore effective at removing heat under upset conditions while not liable for significant parasitic losses during normal operation.

1.2.3 Working principle

The basis of the RCCS can be explained by the ideal gas law. The density of air decreases as the temperature increases (Munson, et al., 2010). When there is a temperature increase in the hot leg of the RCCS, a temperature difference is created between the hot and cold legs, resulting in a buoyancy force. Since the air in the cold leg has a higher density, it forces the warmer air in the hot leg upwards and out of the system. The mass transfer of the air means that heat transfer also occurs, such that heat is removed from the system. This principle is used in a RCCS.

1.2.4 Types of RCCS configurations

Water cooled RCCS:

The water cooled RCCS uses water sourced from a reservoir as the cooling fluid. The Pebble Bed Modular Reactor (PBMR) design utilizes a water cooled RCCS (Tzanos & Farmer, 2006). The system removes more heat than an air cooled RCCS, but its disadvantages include needing a reservoir and some of the coolant being lost due to evaporation (Tzanos & Farmer, 2006).

Air cooled RCCS:

The GT-MHR design makes use of the air cooled RCCS. Air that is drawn from the atmosphere serves as the cooling fluid (General Atomics, 1996). Since the coolant is drawn from atmosphere, the source is considered to be infinite. A disadvantage is that it doesn`t remove as much heat as a water cooled RCCS, due to the poor heat transfer characteristics of air compared to water.

1.3 *High temperature gas cooled reactors*

High temperature gas-cooled reactors have two different fuel configurations, namely the prismatic block (such as the PMR200 and GT-MHR) and the pebble bed (such as the PBMR and HTR10). In a prismatic block reactor the fuel particles, called TRISO (tri-isotropic) particles (Figure 1.2-1) are compacted into cylindrical rods, which are assembled into hexagonal prismatic blocks. In the pebble bed configuration, the TRISO particles are compacted into spherical fuel elements about the size of tennis balls, which are then randomly packed in the core. The fuel particles consist of a uranium oxide kernel, which is surrounded by two different layers of carbon and silicon carbide. (Allan, et al., 2010).

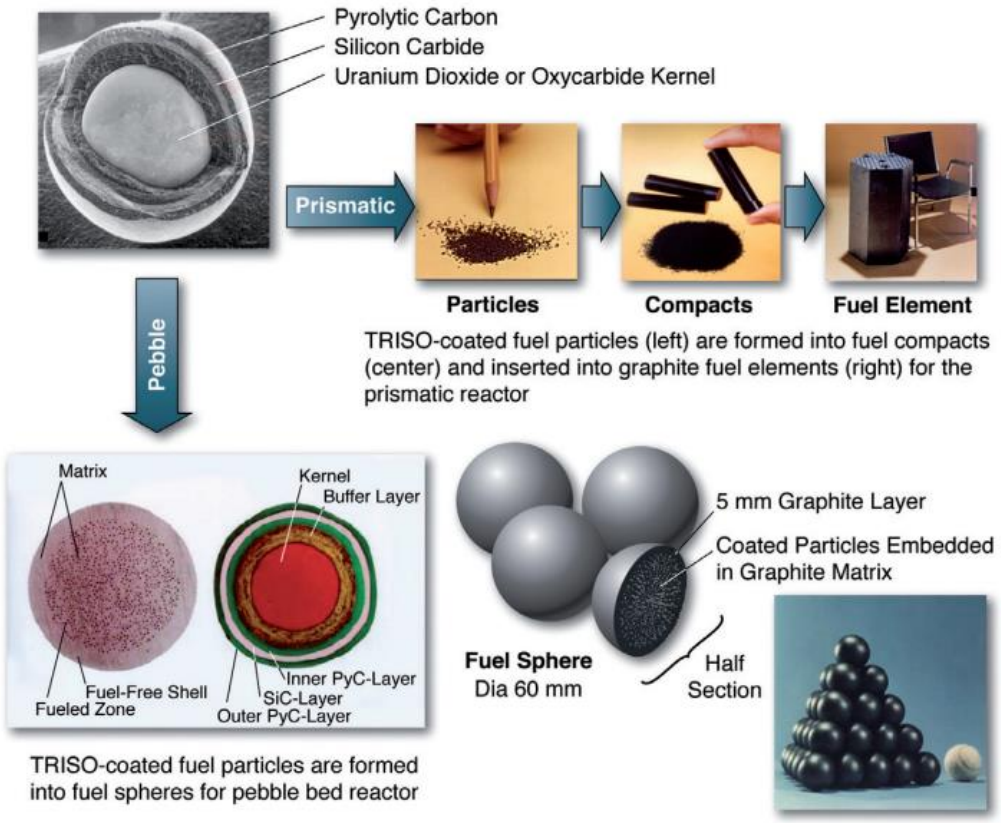

Figure 1.2-1. Fuel used in gas cooled reactors (Allan, et al., 2010).

Gas cooled reactors can use either a direct Brayton cycle or indirect Rankine cycle. The direct Brayton cycle has a higher efficiency than the indirect Rankine cylce. In addition the

plant can be more compact, since the intermediate steam cycle is eliminated. (Chapin, et al., 2004).

The helium coolant used in the direct Brayton cycle doesn`t become radioactive in this process, since helium is inert in this regard. The coolant does however transport other elements which may have become radioactive (Lamarsh & Baratta, 2014), which means that sufficient shielding should be implemented on the gas lines, turbines etc.

Figure 1.2-2 shows the reactor pressure vessel and the power conversion vessel in the GT-MHR design, while Figure 1.2-3 shows the process flow of the design. The hot helium leaves the reactor vessel through the inner tube of the annular cross vessel (Figure 1.2-2,Figure 1.2-3), where it drives the turbine which in turn provides power to the generator and the compressors. After leaving the turbine, the helium flows through the recuperator, which recuperates some of the energy for the cycle. The helium then enters the precooler and the intercooled compressor, where after it passes through the recuperator and flows back into the reactor pressure vessel by means of the cross vessel. (General Atomics, 1996).

Also worth noting is the shutdown cooling system (Figure 1.2-2). The system is water cooled and removes heat from the reactor core via the shutdown heat exchanger. The shutdown cooling system is intended to be kept in standby mode under normal operating conditions, when it will remove a maximum of 1.3 MW(t) from the shutdown heat exchanger. (General Atomics, 1996).

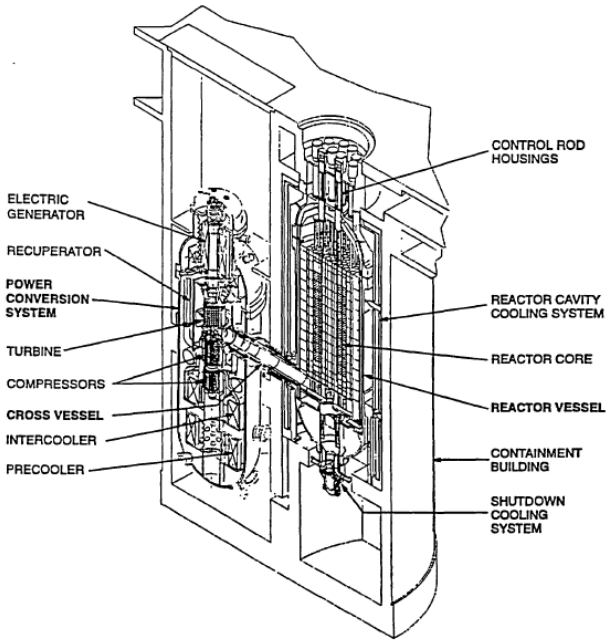

Figure 1.2-2. The pressure vessel and power conversion vessel of the GT-MHR. (General Atomics, 1996).

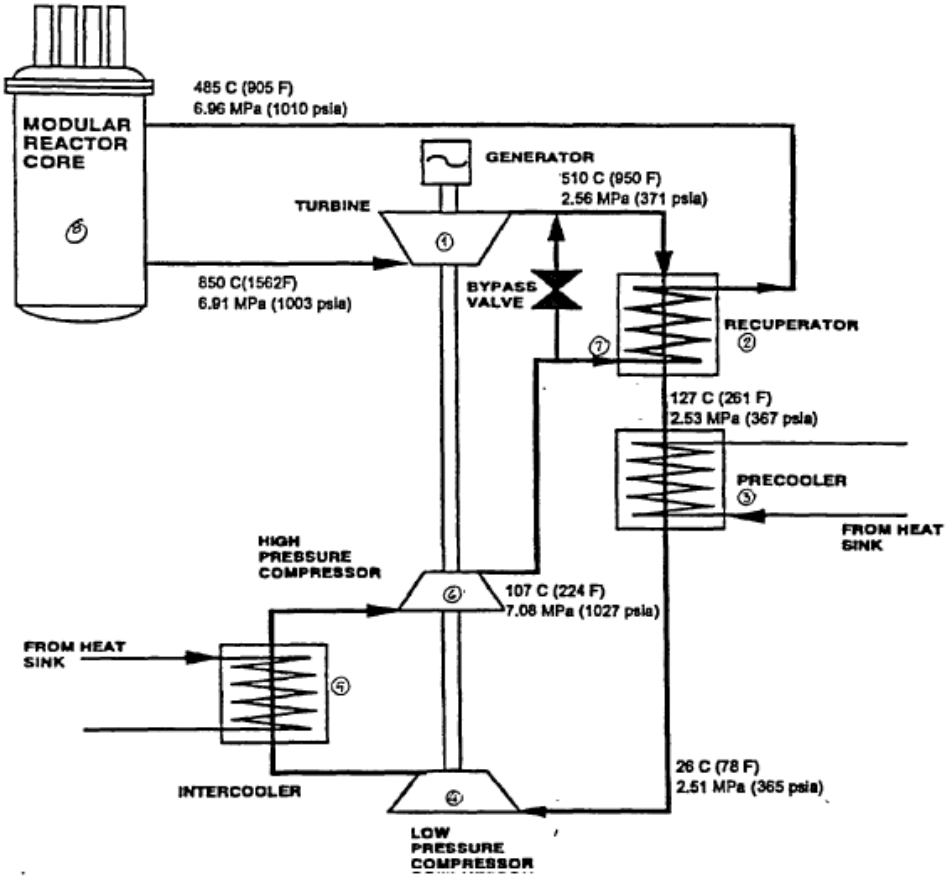

Figure 1.2-3. The process flow diagram for the GT-MHR. (General Atomics, 1996).

1.4 *Gas cooled reactor RCCS*

The RCCS design of a Very High Temperature Reactor (VHTR) is shown in Figure 1.2-4.

Cold air is drawn into and down through the cold ducts from the atmosphere (Figure 1.2-4(c)) where it enters the lower plenum. The air never enters the cavity; it is separated from the cavity by the riser walls. As the air is heated up, it rises through the hot duct system (Figure 1.2-4(b)), exiting the system through the hot duct outlet.

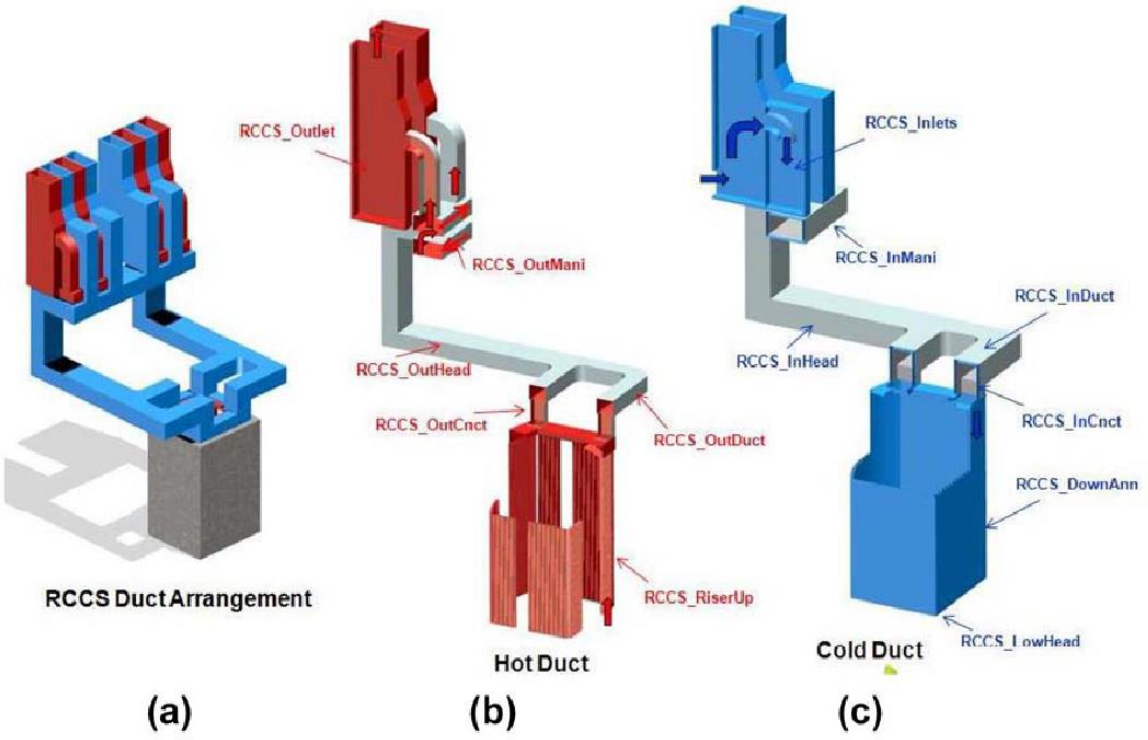

Figure 1.2-4. RCCS system of a VHTR. The assembled RCCS is shown in (a). (b) and (c) show the hot and cold ducts respectively (Du Toit et al. 2014).

1.5 *Experimental Facilities*

Experimental RCCS facilities were built by Argonne National Laboratory (Argonne National Laboratory, 2015) and the Korean Atomic Energy Research Institute as part of the licencing procedure. In building a nuclear power plant, among other things, certain technical documentation, including the Safety Analysis Report (SAR), needs to be submitted to the relevant licencing authority. The technical documentation needs to include all relevant calculations accompanied by the solutions. The solutions need to be verified and validated.

The results can be verified by comparing the simulation results obtained using different simulation software. The results are validated by comparing the simulation results with measured results, obtained by experimentation in an experimental facility or analytical results where available.

The approximation is often made that the cavity geometry could be considered axially symmetric. (Frisani, et al., 2010), (Kim, et al., 2008), (Lisowski & Farmer, 2014). Therefore

only a small radial slice is emulated in a facility. The results for the radial slice would then be extrapolated for the entire cavity.

1.6 *Introduction to the NACEF facility*

The Natural Cooling Experimental Facility (NACEF) was constructed by the Korea Atomic Energy Research Institute (KAERI) to investigate the air cooled RCCS of the PMR200 design. The facility is shown in Figure 1.2-5 and is described in detail in Chapter 3.

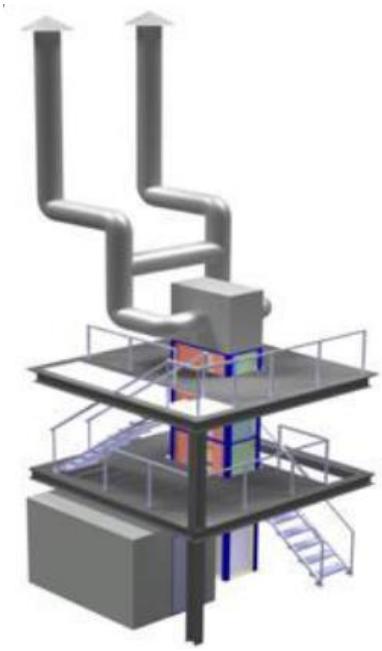

Figure 1.2-5. Natural cooling test facility (Minhwan, 2015).

1.7 Problem statement

The natural cooling test facility (NACEF) has been simulated using a variety of commercial simulation codes; as well as GAMMA+, which is a multi-dimensional simulation code developed by KAERI. However, it has not been simulated using Flownex. It is important in the context of licencing by the National Nuclear Regulator (NNR) that simulation codes that are applied to nuclear systems be verified and validated. For this reason the Flownex software must be tested and evaluated.

1.8 Aim

The aim was to simulate the air flow and heat transfer in an experimental RCCS facility using Flownex SE and compare the results obtained with Flownex with the results obtained by using GAMMA+.

1.9 Scope

The study focussed on simulating the NACEF facility. Flownex was used to calculate the required variables to be compared with the GAMMA+ results. The same geometry and boundary conditions were used for the comparison to be valid. The same simplifying assumptions were used in Flownex as in GAMMA+. Where Flownex was unable to calculate the value of a certain physical quantity, the corresponding GAMMA+ value was used.

1.10 Deliverables

A simulation model that represents the GAMMA+ NACEF model as accurately as possible had to be set up. The necessary output variables had to be generated by the simulation model for comparison with the corresponding GAMMA+ results. The variables included mass flow rates and temperature distribution in the facility.

1.11 Verification

Verification of results could be done by comparing the results obtained using Flownex with the results obtained by using GAMMA+. Both codes use the conservation of mass, momentum and energy to solve the thermal-fluid mechanics of a system. Similar mathematical correlations are implemented in the codes, but there are significant differences in the algorithms used to obtain the solutions. Solving a system with the same geometry and boundary conditions should yield similar results for both programs.

1.12 Layout of work

Chapter two is a literature survey, describing previous work on the subject.

Chapter three describes in greater detail, the system to be simulated. A description of the physical model and the GAMMA+ model will be given.

Chapter four covers the theoretical background and mathematical formulation necessary to solve the problem.

Chapter five describes the various verification exercises which had to be done to verify the model`s constituent parts.

Chapter six describes the Flownex simulation models and boundary conditions of the study.

Chapter seven contains the results and discussion of said results.

In chapter eight the conclusions of the study are given and recommendations are made for further study.

1.13 Conclusion

The need for a RCCS in a nuclear reactor has been outlined. The licencing procedure entails validating simulation codes such as GAMMA+ and Flownex that are used in the design and analysis of nuclear plants. It is therefore important to build experimental facilities such as the NACEF to demonstrate the ability of a simulation code to simulate the thermo-hydraulic phenomena which occurs in a RCCS. The NACEF has not previously been simulated using Flownex. This study aimed to demonstrate how Flownex can be used to simulate the NACEF. The simulation was set up to match the geometry and boundary conditions of the GAMMA+ simulation. Since both programs are based on the same conservation equations for calculating the thermal-fluid mechanics, it was expected that the results would show good agreement.

Chapter 2 - Literature survey

The literature that is important to the study is discussed in this chapter. There are several experimental facilities which were constructed specifically to study natural circulation. The facilities have been simulated numerically to try to predict the thermo-fluid phenomena that would occur. Previous work on the subject of mixed convection is also discussed.

2.1 Simulations involving experimental facilities

The RCCS configurations have been simulated by a number of authors.

The Korea Atomic Energy Research Institute (KAERI) constructed a ¼ scale reactor cavity cooling system. The Natural Cooling Experimental Facility (NACEF) is based on the reactor cavity cooling system of the PMR200. The facility has two heating plates to emulate a reactor pressure vessel. The heaters are enclosed in a cuboid box, which represents the reactor cavity. Six riser tubes are installed vertically in the cuboid. Temperature sensors are installed on the riser tube surfaces and on the heaters. Kim et al. (2015) conducted tests on the facility to gauge the response to the heating phenomena. The temperatures were measured on various surfaces and the convection heat transfer coefficient was calculated based on the experimental results. The predicted convection heat transfer coefficient, calculated by using GAMMA+ was compared to the value of the coefficient obtained from the experimental results. The GAMMA+ coefficient showed good agreement except at the lowest elevation. The authors report that it was possibly due to heat losses to the unheated section of the facility.

Khoza et al. (2015) used GAMMA+ to simulate the experimental facility and the results were compared with the preliminary experimental results. The measured heater temperature was found to be 10 °C higher than predicted by the GAMMA+ model. The riser tube front surface temperatures were in good agreement. The measured and calculated mass flow rates were found to be almost the same. The reflector wall (wall opposite to the heater) showed the largest difference in the predicted vs. measured temperature. It is noted that it was possibly because steady state conditions were not yet reached when the measurements were taken.

Park et al. (2006) simulated natural circulation in the HERMES-HALF facility (Hydraulic Evaluation of Reactor cooling Mechanism by External Self-induced flow – HALF scale). The facility is a ½ scale model of the RCCS used in the APR1400 design. The facility was designed to investigate the effectiveness of a method of cooling the reactor pressure vessel. The method involves circulating water in the annular space between the reactor pressure vessel wall and its insulating material The facility consisted of a test section, which is a

vessel surrounded by insulation material, with water filling the annular space between the vessel and insulating material. A water and air supply system was connected to the test section. The facility did not use a heater, but rather an air flow system to emulate the equivalent circulation which would be induced by a heater. The air flow system injected air into the annular space at various locations. The inlet and outlet areas of the water circulation system were varied and the measured results were compared with the numerically predicted results. The commercial CFD code RELAP5/MOD3 was used to simulate the facility. The code showed general agreement with the measured results. The water mass flow rate showed a dependency on the water inlet and outlet areas, as well as the air flow rate.

Lomperski et al. (2011) used the CFD code STAR CCM+ to simulate the natural circulation of air in the NSTF facility (Natural Circulation Shutdown heat removal Testing Facility). The facility is a scale model of the GT-MHR design. In vertical height, the facility is ½ scale, while the lateral scale is 1:1. The facility consists of an air duct system which passes through a heated cavity. The duct system divides the air into twelve riser tubes in the cavity section before re-joining the streams in an outlet plenum. From the outlet plenum the air is guided upwards via chimneys to the outlet. The STAR CCM+ model predicted a uniform temperature distribution at the highest elevation in all twelve riser tubes. The velocity profiles in the tubes were different, owing to the asymmetrical inlet conditions at the inlet to the riser tubes.

Kim et al. (2008) simulated a HTGR RCCS under accident conditions using GAMMA+ and FLUENT. The RCCS riser tubes are installed circumferentially around the reactor pressure vessel in the HTGR design. Since the geometry is symmetric, it was assumed that the phenomena would be symmetric. Building on this assumption, only a small radial slice was simulated. The implication was that only a single riser tube was simulated of the possible 292. In the representation of the riser tubes, two different approaches were investigated. The first approach was to model the radial slice as a 3D entity. The second approach assumes axisymmetric geometry, so that a 2D model is valid in representing the radial slice. Both of the approaches showed radiation heat transfer as the dominant form of heat transfer. There are notable differences in the results attributed to the 2D model`s inability to model the full geometry of the riser tube. The advantage in using the 2D model was that it required less computational resources to simulate than the 3D model.

Du Toit et al. (2014) simulated the RCCS of the PMR200, a prismatic core VHTR. The commercial CFD programs Flownex SE and GAMMA+ were used to set up numerical models of the design. The RCCS has a geometry similar to a U-tube; the inlet and the outlet

are at the same elevation. The riser and downcomer are installed in the cavity, with a layer of insulation between the hot leg (riser) and cold leg (downcomer). The GAMMA+ model used multi-dimensional interconnected control volumes, while the Flownex model was built up using 1D interconnected control volumes. A fixed temperature boundary condition was placed on the surface representing the reactor pressure vessel and the subsequent heat transfer was studied. The results from both programs for this case showed good agreement. A transient simulation in Flownex showed that the system was prone to flow reversals, which led to an increase in the surface temperature of the concrete enclosure. It was concluded that the two codes solve the fundamental equations in a similar manner, as is implied by the good agreement between the results. It was noted that the results still needed to be validated by experimental data.

Frisani et al. (2010) used STAR CCM to simulate an experimental facility built by Texas A&M University. The facility consisted of a cuboid, representing the reactor cavity, as well as 5 riser tubes, installed in the cavity. A copper vessel, also installed in the cavity, which is electrically heated, emulates the reactor pressure vessel. Two different configurations were simulated, namely water cooling and air cooling. In each case the different coolant would be supplied to the riser tubes and the associated heat transfer phenomena would be simulated. It was found that the water-cooled configuration removed more heat than the air-cooled configuration.

Lee et al. (2009) studied mixed convection in an experimental facility using gas as the working fluid. The experiment was carried out with nitrogen and carbon dioxide. The facility consisted of a closed loop which included a heater section, a chimney, a heat exchanger and a downcomer. Temperature transducers were installed in the heater section to compare the measured results with the numerically predicted results. GAMMA and RELAP5-3D were used to numerically analyse the facility. RELAP5-3D calculates the convection heat transfer coefficient of the gas in the forced laminar, forced turbulent and free convection regime and then uses the maximum value of the three. The implication was that the coefficient in the experimental facility was overestimated. GAMMA used the Aicher criterion, as well as the Burmeister parameter to determine the regime of the flow. In this study, the GAMMA code was adjusted to correct for the deteriorated turbulent heat transfer (DTHT). The turbulence deteriorates in this case, since the forced and free convection are in the same direction. The aiding flow has a laminarization effect on the regime, which means heat transfer is impaired. It was found that the GAMMA model accounting for DTHT predicted the convection heat transfer coefficients more accurately than RELAP5-3D. The latter overestimated the heat transfer coefficients, which led to an underestimation of the riser wall temperature.

2.2 Flow reversals in the RCCS

The RCCS is sensitive flow reversals which can be brought about by windy conditions. ANL noted a flow reversal in the NSTF during experimentation (Lisowski & Farmer, 2014).
The NSTF is shown in Figure 2.2-1. The baseline path is shown in orange. In this configuration, the air exits the exit plenum ("E" in Figure 2.2-1), travels up the chimneys and exits the system. The blue path was used to investigate the effect of a reduced height outlet. In this configuration, the valves in the orange lines are closed.

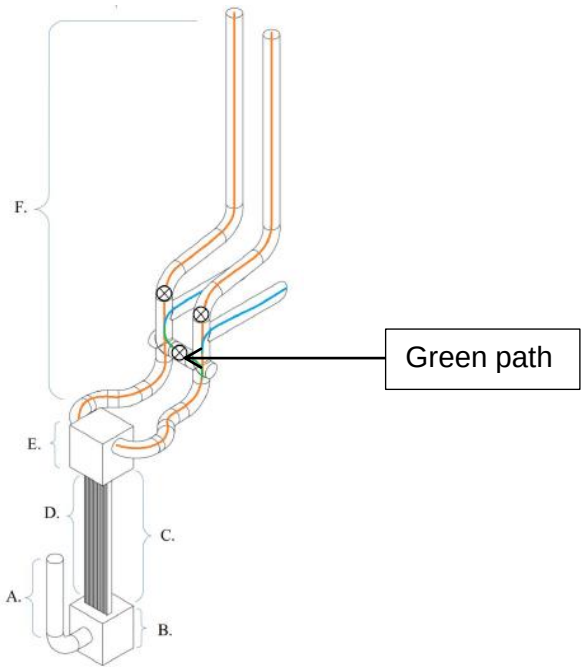

Figure 2.2-1. Simplified model of ½ scale NSTF. A. inlet downcomer, B. inlet plenum, C. heated cavity, D. riser tubes, E. outlet plenum, F. chimney. Flow paths for varying chimney roles: Baseline (orange), reduced discharge (blue), single chimney (green). Crossed circles represent manual valves. (Lisowski & Farmer, 2014).

The flow reversal was caused by strong winds, resulting in one of the chimneys becoming a secondary inlet. This means that air is fed to the outlet plenum from the riser tubes and one of the chimneys. A complete reversal was observed when the reduced discharge (blue lines in Figure 2.2-1) path was investigated. The reduced hydrostatic height made this configuration especially sensitive to a reversal in the flow direction. The reversal resulted in an increased temperature in the riser inlet (bottom of "D" in Figure 2.2-1).

The reversal was corrected by choking the flow by means of a valve. This causes the flow to build up enough pressure to overcome the external pressure caused by meteorological conditions (Lisowski & Farmer, 2014).

The NACEF, built by KAERI also appears to be prone to flow reversals. In the preliminary testing of the facility, an upward mass flow only persisted in one of the two chimneys (Kim, et al., 2014).

2.3 Mixed convection

There are three different possible modes for convection, namely forced- , free- and mixed convection. Figure 2.3-1 illustrates the regime map proposed by Metais & Eckert (1964) for vertical flow in a tube. The Reynolds number is plotted against the product of the Grashof number, Prandtl number and diameter to length ratio (of the pipe in which the fluid flow occurs). The graph shows that the mixed convection regime, falls between the free- and forced convection regimes. Mixed convection occurs for both laminar and turbulent flows. The graph also implies that if the Reynolds number is much larger than the Grashof number, the regime is forced convection. Conversely if the Grashof number is much larger than the Reynolds number, the regime is free convection.

Aicher and Martin (1996) developed a new correlation for calculating the heat transfer associated with mixed convection. The correlation interpolates between the forced and free convection Nusselt numbers. The manner in which the interpolation is applied is dependent on whether the forced and free convection is in the same direction (aiding flow) or in opposite directions (opposing flow). The study also investigated the influence of the geometry on the heat transfer by varying the parameter D/L, which represents the diameter to length ratio of a vertical pipe.

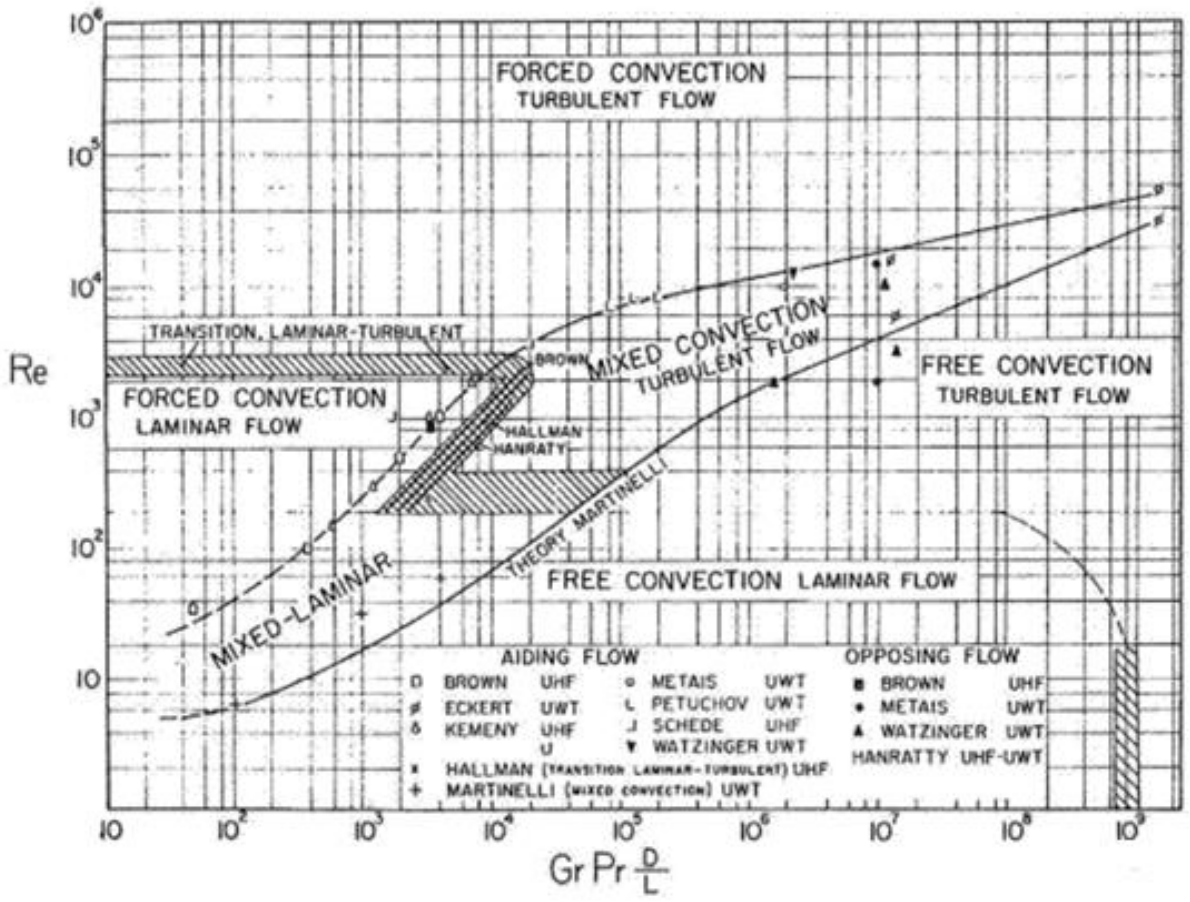

Figure 2.3-1. Regime map to determine whether the flow is forced-, free- or mixed convection (Metais & Eckert, 1964).

Celata et al. (1998) conducted experiments on convection in water flowing upwards in a pipe. The regime ranged from forced- to free convection. Experimental data was compared to the results calculated theoretically. Firstly, the theoretical results were calculated using the k-ε model, which accurately predicted the Nusselt number vs. the buoyancy number. It was noted that this model is complex to solve and therefore the need for a simpler practical method was made apparent. Secondly, the formulation proposed by Martinelli & Boelter (cited by Celata et al., 1998) was tested against experimental results. The formulation produces a mathematical error where the forced and free convection Nusselt numbers are equal. Thirdly, a new method was proposed in which a Gaussian curve equation function is used to adjust the calculated Nusselt number slightly.

Mei et al. (2015) simulated natural convection on galvanized plates. The plates were placed vertically in a furnace and lifted up into a cooling zone where jet nozzles sprayed cooling air onto the plate. The Reynolds number was calculated for the jet nozzles and Grashof

number was calculated for the natural circulation brought about by the heater. The Reynolds and Grashof numbers were varied and the subsequent heat transfer was studied. The higher the Grashof numbers, resulted in higher surface temperatures on the plate. The forced convection (jet nozzles) was orientated in the opposite direction to the free convection (buoyancy forces). It was found that that the higher the Reynolds number from the jet nozzles, the higher the surface temperature of the plate. The conclusion was thus that the heater power could possibly be decreased if the jet nozzle air pressure was increased.

Travis & El-Genk (2013) developed a correlation for the use in predicting heat transfer in a prismatic block helium cooled VHTR. The correlation predicts the convection heat transfer of the helium in the mixed convection regime. The authors considered correlations such as Dittus-Boelter, Sieder-Tate, Taylor and McEligot. The problem faced in the study by Travis and El-Genk, was that the entrance and exit of the coolant channel was difficult to simulate. The mixing of the fluid at these locations of the coolant channel made the flow difficult to predict. The results differed by as much as 20% between the results predicted by the different correlations. The correlations of Taylor and McEligot were preferred as these correlations correct for the change in fluid viscosity at the wall relative to the bulk region. The correlations are valid for a fixed heat flux boundary condition, which is not the case within the coolant channel within the core. The axial power distribution in the coolant channel is a cosine function, which results in a non-uniform axial heat flux. The results were compared between the cosine function and constant heat flux boundary condition. The axial temperature distributions of the two different profiles show similar trends, but are generally higher in the case where a cosine function axial power distribution was applied. Furthermore, the authors compared the results of a STAR CCM+ 3D model with a 1D model using the newly developed correlation, both for the constant heat flux and cosine function heat flux boundary condition. The results were in good agreement which led to the conclusion that the newly developed correlation was valid and that the 1D simplification adequately simulated the heat transfer.

McEligot et al. (2006) did experimental studies on mixed convection of gas in the deteriorated turbulence heat transfer (DTHT) regime. The fluid flow under investigation was vertical flow in a circular tube. The DTHT regime can occur as a result of the acceleration effect or the buoyancy effect. The former is caused by flow laminarization because of the fluid expanding as result of a temperature increase. Hall and Jackson (1964) explain that due to the buoyancy effect the temperature increases on the heated surface resulting in decreased shear stresses in the fluid closest to the wall. The decreased shear stresses lead to a decrease in turbulence near the wall. McEligot at al. (2006) subsequently developed

correlations for the DTHT regime based on the Gnielinski correlation, which was modified to account for the geometry of the specific experimental facility. Correlations from literature were also used calculate the heat transfer. It was found that the correlations from literature over predicted the Nusselt number in the DTHT regime, while the newly developed correlations were more accurate.

Kawaji et al. (2015) studied forced and natural circulation in an experimental facility in which the coolant could be chosen as air, nitrogen or helium. The facility layout was a U-tube configuration in which one of the legs was heated. The modified Dittus-Boelter correlation was used to calculate the Nusselt number in the heated section, which was compared with the Nusselt number obtained by experiments. The correlation accurately predicted the Nusselt number in the heated section. A laminarization effect was noted in the study, which the authors ascribed to the flow acceleration parameter and the buoyancy parameter. The former is a result of the expanding gas accelerating due to the rise in temperature. The buoyancy parameter is a function of the relative temperature difference between the wall and bulk fluid temperatures. Where the acceleration and buoyancy parameters passed a certain threshold the correlations increasingly deviated from the experimental results.

2.4 Concluding remarks

When experimental facilities are simulated, simplifying assumptions need to be made. Thereby computational time and resources can be optimized. A common simplification made by many authors in literature is to assume that the phenomena occur axi-symmetric. The implication is that only a small radial slice of the geometry can be simulated and the results would, in theory, extrapolate to the rest of the geometry. The assumption was made when designing the NACEF.

Flow reversals have been known to occur in RCCS facilities, where the meteorological conditions overpower the pressure at the outlet of the facility. From the mixed convection theory, the meteorological conditions can have multiple effects. If the flow in the chimneys is turbulent and meteorological conditions cause opposing flow, heat transfer is improved. In contrast, if the conditions at the outlet are such that aiding flow occurs, heat transfer is hampered. The inverse is true if the flow in the facility is laminar. Aiding flow causes a laminarizational effect in the boundary layer of the flow, in that the fluid close to the wall is accelerated, which impedes the turbulence production and transport that is necessary for effective heat transfer to occur.

Mixed convection heat transfer can be calculated by interpolating between free- and forced convection Nusselt numbers. The heat transfer is also dependent on the geometry as is evident by the inclusion of D/L in the regime map in Figure 2.3-1.

Chapter 3 - Description of the NACEF

In this chapter the natural cooling experimental facility will be described. Distinction must be made between the physical model and the mathematical model. The physical model is described first, followed by the mathematical model. The mathematical model consists of the facility as represented by the simulation code GAMMA+.

3.1 The experimental facility

The implementation of an air cooled RCCS in the PMR200 is shown in Figure 3.1-1. The heat transfer phenomena are also shown in the figure (refer to the legend of Figure 3.1-1). The heat originates from the fuel elements in the core, where the heat is transferred radially outwards by conduction. Thermal radiation and free convection transfers heat from the core to the reactor pressure vessel. The heat travels through the reactor wall by means of conduction. The reactor pressure vessel transfers heat to the RCCS risers through radiation and convection. The heat travels through the riser wall by means of conduction so that the air inside the riser is heated up by convection heat transfer. There is also radiative heat transfer between the riser walls. The heat transfer results in a density gradient developing, causing natural circulation in the pressure vessel, cavity and riser.

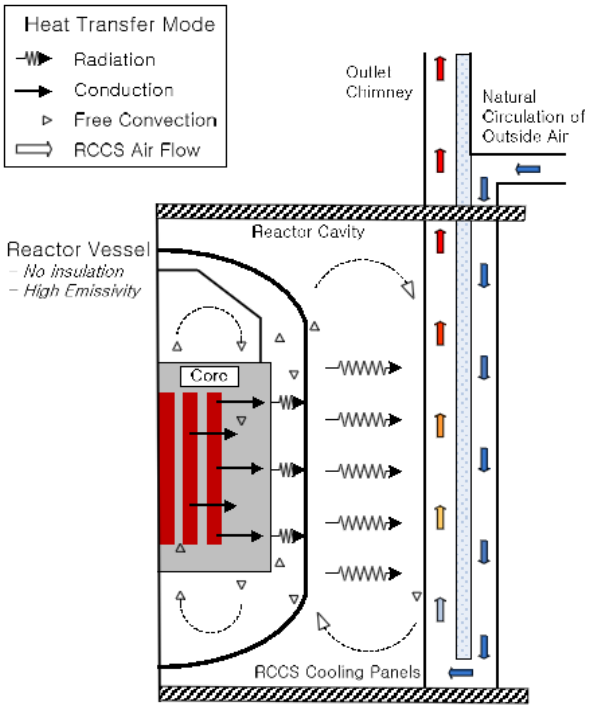

Figure 3.1-1. Heat transfer phenomena in the reactor cavity. From Kim et al. (2014).

The NACEF was developed from the PMR200 nuclear reactor design. Since a full scale model would be costly, it was built to be ¼ scale vertically, but scale 1:1 laterally. The configuration of the RCCS in the cavity is that the risers are placed circumferentially in the cavity, creating a symmetrical cylindrical geometry. The assumption is made that the phenomena occurs axi-symmetric, which means that only a small radial slice (in Figure 3.1-1) needs to be simulated. The results could then be extrapolated for the rest of the geometry, if the assumption is true.

The axi-symmetric phenomena assumption also simplifies the mathematical model of the facility. Since the only a small radial slice is considered, the model contains only 6 riser tubes instead of the actual number, 220. The small slice would therefore require less computational resources when modelled numerically.

The reactor core is emulated by heater elements in the heated section (Figure 3.1-2). Air enters the heated section via the inlet plenum, where after it passes through the exit plenum and finally rises through the chimneys (Figure 3.1-1, Figure 3.1-3).

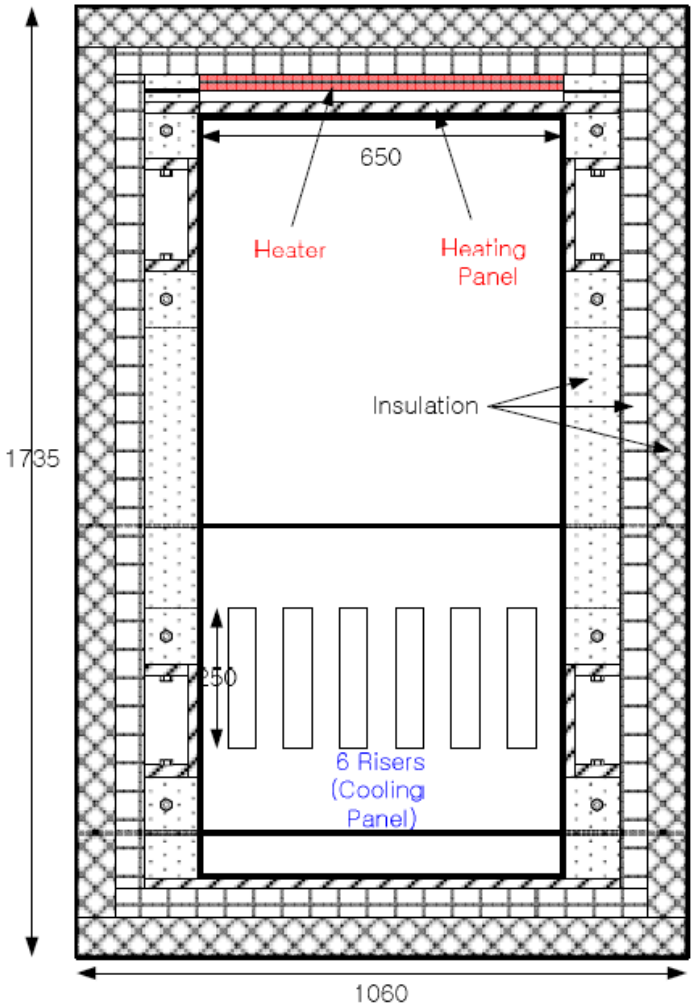

Figure 3.1-2. Top view of the heated cavity. (Kim et al. 2014).

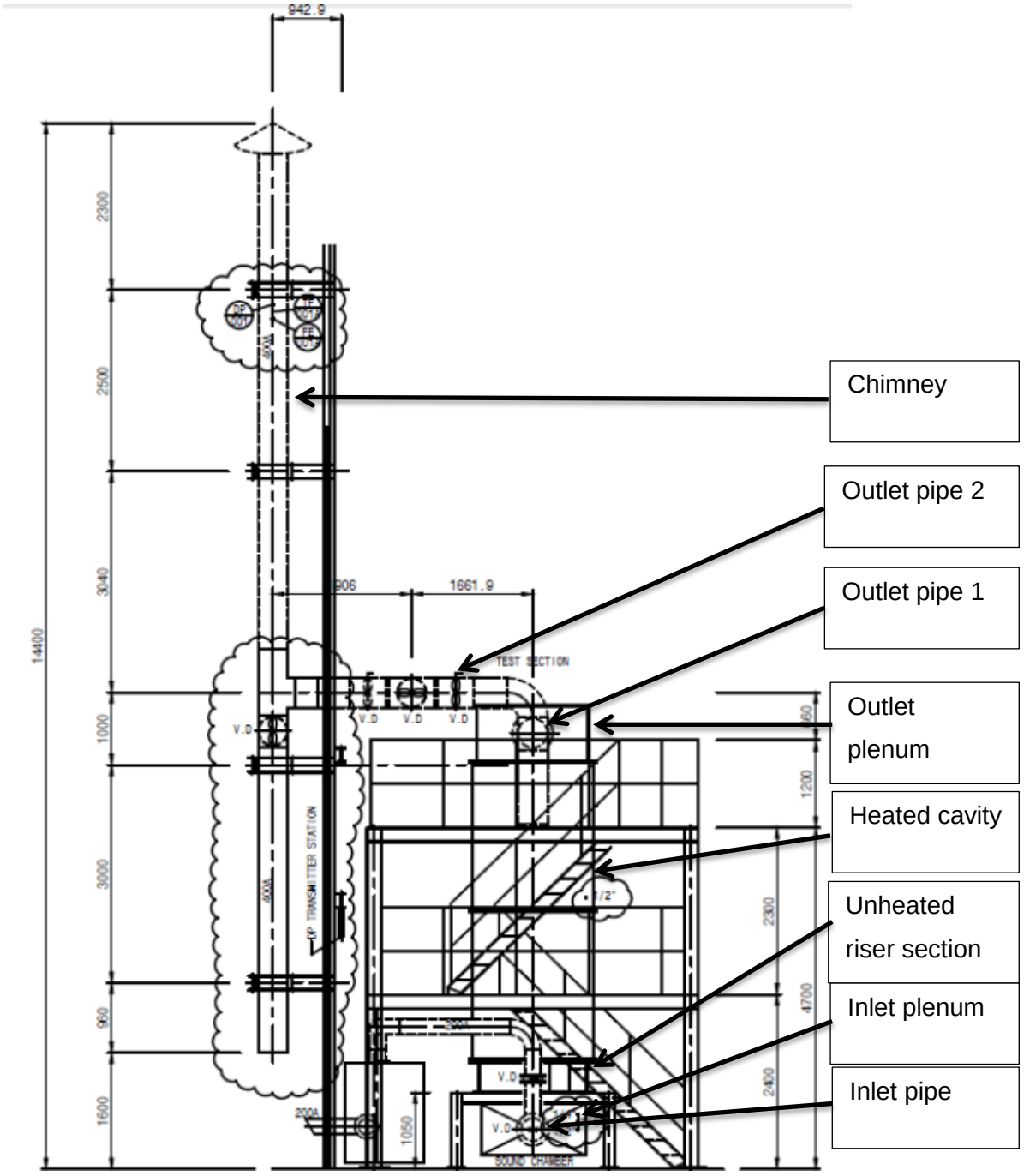

Figure 3.1-3. The NACEF, as viewed from the side. From Kim et al. (2014).

Figure 3.1-2 shows a top section view of the heated test section. The air travels through the rectangular riser tubes as it is heated up. The 52 kW ceramic heater element can deliver a maximum heat flux of 20 kW/m^2 resulting in a temperature close to 420 °C. The emissivity of the heated wall is 0.75 and the unheated walls have an emissivity of 0.1. The heated section is insulated to minimize heat loss to the environment. (Kim, et al., 2014).

3.2 GAMMA+ model of the experimental facility

The GAMMA+ model is made up of fluid blocks connected by junction blocks. Solids are represented by 2-D blocks. The fluid blocks are control volumes that account for the fluid volume in the system. The fluid density, temperature and pressure are associated with the fluid blocks and the fluid blocks thus account for mass and energy conservation of the fluid. The junction blocks provide for the mass, momentum and energy transfer between the fluid blocks and thus account for momentum conservation. The solid blocks are control volumes that account for the solid volume in the system. The solid temperature is associated with the solid blocks thus account for energy conservation of the solid. Conduction accounts for the heat transfer between solid blocks and radiation for the heat transfer between solid surfaces. Convection accounts for the heat transfer between the solid surfaces and the adjacent fluid.

Figure 3.2-1 shows the GAMMA+ model of the NACEF. The convention is that solid parts' names are preceded with "W", fluid blocks' names are preceded by "F" and boundary conditions are preceded by "BC". The air enters the system at the inlet pipes ("F1_Loop_Inpipe"), flows through the inlet plenum ("F1_Loop_InCham"), then up the riser tube ("F1_LoopRiser"), into the outlet plenum ("F1_Loop_OutCham"). For the purpose of simplifying the simulation, "F1_Loop_OutLpipe1" is choked, allowing air to flow only into "F1_Loop_OutRpipe1". There after the air flows through the second outlet pipe ("F1_Loop_OutRpipe2") and then through the chimney ("F1_Loop_RChimney"). The conduction heat transfer in the heater wall and riser tube walls are represented by "W2_Heater" and "W3_RiserTube".

The boundary conditions of the GAMMA+ model were used in the Flownex model and will be described in detail in Chapter 5.

The riser tubes, although defined as rectangular, are modelled as cylindrical with the outside and inside surface areas the same as for the rectangular tubes. However, this leads to a wall thickness of 6.36 mm instead of 5 mm.

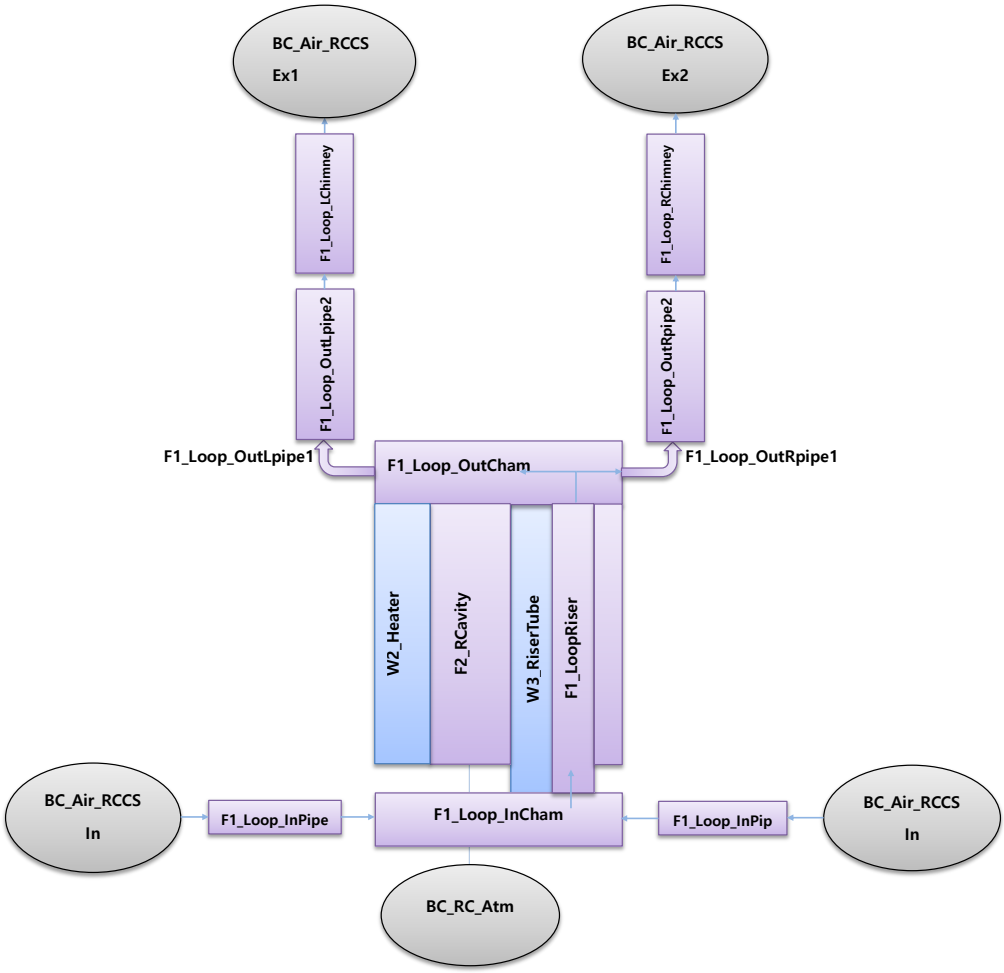

Figure 3.2-1. GAMMA+ model of the NACEF facility. (Khoza, 2015).

3.3 Frictional and minor/form losses

The ducts in the flow path are all considered to have a roughness of 10μm. The roughness is used to account for the pressure loss due to frictional forces resisting the flow.

The minor losses are accounted for in the GAMMA+ NACEF model, since there is a non-negligible loss over the junctions in the system.

The forward (k_f) and backward flow loss (k_r) coefficients are shown in Table 3.3-1.

Table 3.3-1. Coefficients for the form losses.

Junction in the system	k_f	k_r
Boundary condition/Inlet pipe	0.5	1.0
Inlet pipe/Inlet chamber	1.0	0.5
Inlet chamber/Riser tubes	0.5	1.0

Riser tubes/Outlet chamber	1.0	0.5
Outlet chamber/Outlet pipe 1 (right)	0.5	1.0
Outlet chamber/Outlet pipe 1 (left)	1E30	1E30
Outlet pipe 1/Outlet pipe 2 (right)	0	0
Outlet pipe 1/Outlet pipe 2 (left)	0	0
Outlet pipe 2/Chimney	0	0

The loss coefficient over the junction between the outlet chamber and left outlet pipe is selected as very large to restrict the flow to one of the chimneys. The model is simplified by this method by allowing a mass flow in only one of the two chimneys.

3.4 Thermal radiation view factors

The GAMMA+ model`s thermal radiation view factors were calculated by using SINDA/FLUENT (Khoza, 2015). The surfaces of the heated cavity of the NACEF are numbered as shown in Figure 3.4-1. The heated wall was numbered 1, the left side wall 2, the right side wall was numbered 3 and the reflective wall was numbered 4. The numbering of the riser tube surfaces is as follows: the outer tube surfaces are numbered 5 through 8 and the inner tube surfaces are numbered 9 through 12. The numbering convention should be used to interpret the radiation view factors shown in Table 3.4-1.

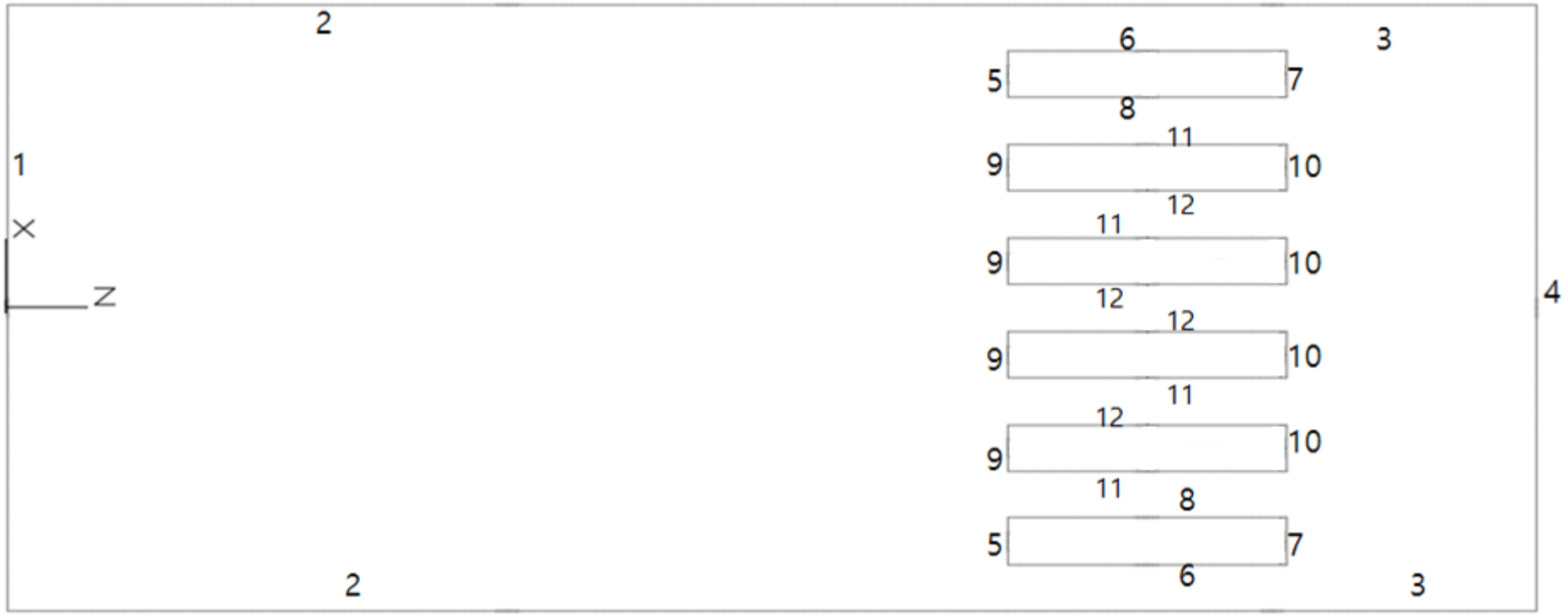

Figure 3.4-1. Numbering convention for the cavity surfaces. (Khoza, 2015).

The view factor matrix for the cavity surfaces is given in Table 3.4-1 using the numbering convention shown in Figure 3.4-1. These view factors were also implemented into the Flownex model as shown in Figure 6.2-7.

Table 3.4-1. Thermal radiation view factor matrix for the cavity surfaces.

	1	2	3	4	5	6	7	8	9	10	11	12
1	0.0	0.7306950	0.0323560	0.0333630	0.0400150	0.0003180	0.0	0.0263380	0.0889910	0.0	0.0126500	0.0352740
2	0.2578457	0.5154127	0.0104250	0.0002346	0.0364690	0.0255620	0.0	0.0115840	0.0682720	0.0	0.0421760	0.0320190
3	0.0221850	0.0202562	0.1253298	0.2314580	0.0	0.4703790	0.0348850	0.0036600	0.0	0.0358810	0.0410680	0.0148980
4	0.0333630	0.0006648	0.3375726	0.0614606	0.0	0.0039130	0.0885770	0.0606660	0.0	0.2259470	0.0749440	0.1128920
5	0.2600984	0.6717614	0.0	0.0	0.0681401	0.0	0.0	0.0	0.0.	0.0	0.0	0.0
6	0.0004134	0.0941703	0.8918376	0.0050869	0.0	0.0084919	0.0	0.0	0.0	0.0	0.0	0.0
7	0.0	0.0	0.3307229	0.5757733	0.0	0.0	0.0935038	0.0	0.0	0.0	0.0	0.0
8	0.0342391	0.0426751	0.0069393	0.0788651	0.0	0.0	0.0	0.0211274	0.0	0.0	0.816154	0.0
9	0.2892218	0.6287874	0.0	0.0	0.0	0.0	0.0	0.0	0.0819908	0.0	0.0	0.0
10	0.0	0.0	0.1700827	0.7343569	0.0	0.0	0.0	0.0	0.0	0.0955605	0.0	0.0
11	0.0082225	0.0776881	0.0389324	0.0487135	0.0	0.0	0.0	0.4080799	0.0	0.0	0.0107775	0.4075860
12	0.0229279	0.0589785	0.0141232	0.0733792	0.0	0.0	0.0	0.0	0.0	0.0	0.4075831	0.4230081

The thermal radiation view factors associated with the riser tube inner surfaces are shown in Table 3.4-2. These view factors were applied in Flownex as shown in Figure 6.2-8.

Table 3.4-2. Thermal radiation view factors for the inner surfaces of the riser tubes.

Surface	Front	Side	Side	Rear
Front	0	0.45049	0.45049	0.09902
Side	0.090098	0	0.819804	0.090098
Side	0.090098	0.819804	0	0.090098
Rear	0.09902	0.45049	0.45049	0

3.5 Convection heat transfer coefficients

The convection heat transfer coefficients for the cavity surfaces, as calculated by GAMMA+ are shown in Table 3.5-1 and Table 3.5-2. The former lists the coefficients for the baseline model, while the latter lists the coefficients for the modified case.

Table 3.5-1. Convection heat transfer coefficients for the cavity surfaces for the baseline case.

	Convection heat transfer coefficients (W/m^2-K)											
Elevation (m)	Heater wall	Left side wall	Right side wall	Reflective wall	Outer tubes				Inner tubes			
					Front	Left	Rear	Right	Front	Left	Rear	Right
1.29	5.270	3.664	2.156	1.689	2.709	4.197	4.384	4.371	2.829	4.436	4.468	4.427
1.49	5.228	3.585	2.353	2.194	2.541	4.086	4.275	4.258	2.678	4.327	4.364	4.319
1.69	5.199	3.551	2.410	2.257	2.564	4.069	4.253	4.236	2.696	4.304	4.341	4.297
1.89	5.175	3.533	2.425	2.298	2.576	4.054	4.235	4.219	2.704	4.286	4.322	4.279
2.09	5.153	3.521	2.425	2.358	2.571	4.035	4.214	4.198	2.697	4.265	4.299	4.258
2.29	5.132	3.510	2.420	2.467	2.557	4.012	4.190	4.175	2.683	4.242	4.275	4.235
2.49	5.112	3.501	2.414	2.512	2.538	3.989	4.165	4.151	2.664	4.218	4.250	4.211
2.69	5.092	3.490	2.409	2.501	2.518	3.966	4.140	4.127	2.645	4.193	4.224	4.186
2.89	5.071	3.478	2.407	2.469	2.496	3.942	4.115	4.102	2.623	4.168	4.199	4.162
3.09	5.049	3.465	2.408	2.462	2.475	3.918	4.091	4.078	2.602	4.144	4.174	4.138
3.29	5.026	3.451	2.410	2.515	2.454	3.895	4.066	4.054	2.582	4.120	4.149	4.114
3.49	5.002	3.436	2.413	2.518	2.436	3.872	4.043	4.031	2.564	4.097	4.125	4.091
3.69	4.977	3.421	2.417	2.478	2.418	3.850	4.020	4.008	2.547	4.074	4.102	4.068
3.89	4.951	3.405	2.421	2.410	2.405	3.830	3.998	3.987	2.533	4.052	4.080	4.047
4.09	4.924	3.388	2.428	2.381	2.395	3.810	3.977	3.966	2.522	4.032	4.058	4.026
4.29	4.894	3.367	2.440	2.633	2.383	3.790	3.955	3.946	2.511	4.011	4.037	4.006
4.49	4.860	3.341	2.464	2.661	2.374	3.771	3.935	3.926	2.501	3.991	4.016	3.986
4.69	4.821	3.302	2.512	2.615	2.352	3.749	3.912	3.904	2.480	3.968	3.993	3.964
4.89	4.769	3.230	2.613	2.571	2.370	3.740	3.902	3.893	2.494	3.957	3.982	3.952
5.09	4.682	3.051	2.842	2.583	2.515	3.781	3.936	3.926	2.623	3.988	4.013	3.983

Table 3.5-2. Convection heat transfer coefficients for the cavity surfaces for the modified case.

	Convection heat transfer coefficients (W/m^2-K)											
Elevation (m)	Heater wall	Left side wall	Right side wall	Reflective wall	Outer tubes				Inner tubes			
					Front	Left	Rear	Right	Front	Left	Rear	Right
1.29	4.989	3.416	0.505	1.905	3.926	4.193	4.27	4.285	4.010	4.340	4.350	4.337
1.49	4.931	3.280	1.753	0.653	3.696	3.984	4.065	4.079	3.790	4.140	4.153	4.137
1.69	4.896	3.210	1.971	1.929	3.573	3.87	3.952	3.963	3.667	4.024	4.039	4.021
1.89	4.867	3.172	2.053	2.138	3.483	3.788	3.87	3.879	3.576	3.940	3.956	3.937
2.09	4.837	3.143	2.097	2.220	3.407	3.72	3.801	3.81	3.500	3.870	3.886	3.867
2.29	4.804	3.116	2.132	2.239	3.337	3.658	3.739	3.747	3.430	3.807	3.824	3.804
2.49	4.769	3.087	2.166	2.249	3.275	3.602	3.684	3.69	3.368	3.750	3.767	3.747
2.69	4.732	3.056	2.197	2.259	3.218	3.55	3.632	3.638	3.311	3.697	3.715	3.694
2.89	4.694	3.026	2.222	2.275	3.163	3.501	3.583	3.588	3.255	3.647	3.665	3.644
3.09	4.657	2.999	2.241	2.293	3.108	3.451	3.534	3.538	3.200	3.596	3.615	3.594
3.29	4.622	2.974	2.251	2.292	3.051	3.401	3.483	3.487	3.143	3.545	3.564	3.542
3.49	4.588	2.954	2.255	2.292	2.99	3.348	3.431	3.433	3.082	3.492	3.511	3.489
3.69	4.557	2.936	2.253	2.311	2.924	3.291	3.375	3.377	3.016	3.435	3.455	3.432
3.89	4.528	2.921	2.249	2.307	2.852	3.231	3.315	3.317	2.946	3.375	3.396	3.373
4.09	4.500	2.905	2.247	2.266	2.775	3.168	3.254	3.254	2.871	3.313	3.335	3.311
4.29	4.472	2.884	2.257	2.244	2.696	3.104	3.191	3.191	2.794	3.250	3.272	3.248
4.49	4.442	2.850	2.291	2.448	2.615	3.04	3.129	3.127	2.714	3.186	3.210	3.184
4.69	4.406	2.792	2.361	2.490	2.537	2.98	3.07	3.067	2.639	3.127	3.151	3.124
4.89	4.359	2.687	2.486	2.466	2.48	2.936	3.026	3.021	2.582	3.081	3.106	3.078
5.09	4.280	2.454	2.707	2.470	2.545	2.978	3.064	3.058	2.638	3.114	3.139	3.111

3.6 Representative riser tubes

In order to simplify the model the riser tubes were grouped together into two representative riser tubes for the purposes of simulating the heat transfer. The two outer riser tubes were grouped into a single representative riser tube and the four inner tubes into a single representative inner tube. In each case the outside and inside surface areas of the representative tube were equal to the combined respective outside and inside areas of the original riser tubes. This was to ensure that the radiation and convection heat transfer would be simulated correctly. To simulate the conduction heat transfer correctly the wall thickness of the representative riser tubes was the same as that of the original riser tubes. In order to simplify the modelling of the flow path all six riser tubes were grouped into a single representative riser tube with cross sectional area equal to the combined cross sectional areas of the original riser tubes and a wetted perimeter equal to the combined wetted perimeter of the original riser tubes. The convection heat transfer associated with the inside surfaces of the representative outer and inner riser tubes were linked to the fluid temperature of the representative flow riser tube.

3.7 Summary

The NACEF has been described in this chapter. The important details concerning the physical model have been described. The GAMMA+ model and its boundary conditions have also been listed. The convection heat transfer coefficients of the cavity surfaces are of particular importance, since the coefficients are also used as is in Flownex. The thermal radiation view factors described in this chapter are also used in the Flownex model.

Chapter 4 - Theoretical background

The equations necessary to simulate the NACEF are discussed in this chapter.

4.1 Fluid mechanics theory

Flownex uses the conservation of mass, momentum and energy equations to solve fluid flows (M-Tech Industrial, 2015). The conservation equations in question are given in Equations 4.1-1, 4.1-2 and 4.1-4.

Conservation of mass (Rousseau, 2013):

$$\forall \frac{\partial \rho}{\partial t} + \dot{m}_e + \dot{m}_i = 0 \qquad \textbf{(4.1-1)}$$

Where:

$\forall$: Volume [m^3].

$\frac{\partial \rho}{\partial t}$: change in density over time $\left[\frac{kg}{m^3 - s}\right]$.

$\dot{m}_e$: mass flow rate at exit $\left[\frac{kg}{s}\right]$.

$\dot{m}_i$: mass flow rate at inlet $\left[\frac{kg}{s}\right]$.

Conservation of momentum (Rousseau, 2013):

$$\rho L \frac{\partial V}{\partial t} + \frac{P}{P_0}(P_{0e} - P_{0i}) + 0.5\rho V^2 \frac{1}{T_0}(T_{0e} - T_{0i}) + \rho g(z_e - z_i) + \Delta p_{0L} = 0 \qquad \textbf{(4.1-2)}$$

Where:

ρ : density $\left[\frac{kg}{m^3}\right]$.

L : flow path length [m].

$\frac{\partial V}{\partial t}$: change in velocity with respect to time $\left[\frac{m^3}{s}\right]$.

P : static pressure [kPa].

P_0 : stagnation pressure [kPa].

P_{0e} ; P_{0i} : stagnation pressure at outlet and inlet [kPa].

V : velocity $\left[\frac{m}{s}\right]$.

T_0 : stagnation temperature [K].

T_{0i} ; T_{0e} : stagnation temperature at inlet and outlet [K].

g : gravitational acceleration $\left[\frac{m}{s^2}\right]$.

z_i ; z_e : elevation at inlet and outlet [m].

Δp_{0L} : pressure loss attributed to frictional and minor losses $\left[\frac{kg}{m - s}\right]$.

The pressure loss in Equation 4.1-2 is calculated by (Rousseau, 2013):

$$\Delta \boldsymbol{p_{0L}} = \left(\frac{\boldsymbol{fL}}{\boldsymbol{D_h}} + \sum \boldsymbol{K}\right)\frac{|\dot{\boldsymbol{m}}|\dot{\boldsymbol{m}}}{\boldsymbol{2\rho A^2}} \qquad \textbf{(4.1-3)}$$

Where:

$\boldsymbol{f}$: Darcy − Weisbach friction factor $[-]$.

$\boldsymbol{K}$: secondary loss factor $[-]$.

$\boldsymbol{A}$: flow area $[\mathrm{m}^2]$.

$\boldsymbol{D_h}$: hydraulic diameter $[\mathrm{m}]$.

$\boldsymbol{L}$: flow length $[m]$.

Conservation of energy (Rousseau, 2013):

$$\boldsymbol{Q + W = \cancel{V}\frac{\partial}{\partial t}(\rho h_0 - P) + \dot{m}_e h_{0e} - \dot{m}_i h_{0i} + \dot{m}_e g z_e - \dot{m} g z_i} \qquad \textbf{(4.1-4)}$$

Where:

$\boldsymbol{Q}$: heat energy added to control volume $[\mathrm{W}]$.

$\boldsymbol{W}$: work done on control volume $[\mathrm{W}]$.

$\frac{\partial}{\partial t}$: change in the properties with respect to time.

$\boldsymbol{h_{0i}}$; $\boldsymbol{h_{0i}}$: enthalpy at inlet and outlet of control volume $\left[\frac{\mathrm{J}}{\mathrm{kg-K}}\right]$.

Note that the term $\cancel{V}\frac{\partial}{\partial t}(\rho h_0 - P)$ represents the change over time of the total stored energy within a control volume.

Equations 4.1-1, 4.1-2 and 4.1-4 are solved for a number of inter-linked control volumes.

The mass flow rate is related to the velocity by the following equation (Munson, et al., 2010):

$$\dot{\boldsymbol{m}} = \boldsymbol{\rho A V} \qquad \textbf{(4.1-5)}$$

Where:

$\dot{\boldsymbol{m}}$: mass flow rate $\left[\frac{\mathrm{kg}}{\mathrm{s}}\right]$.

$\boldsymbol{V}$: flow velocity $\left[\frac{\mathrm{m}}{\mathrm{s}}\right]$.

It is also necessary to calculate the Nusselt number, which is the ratio of convection to conduction and is given by (Incropera, et al., 2013):

$$\boldsymbol{Nu} = \frac{\boldsymbol{hD_h}}{\boldsymbol{k}} \qquad \textbf{(4.1-6)}$$

Where:

$\boldsymbol{Nu}$: Nusselt number $[-]$.

$\boldsymbol{h}$: convection heat transfer coefficient $\left[\frac{\mathrm{W}}{\mathrm{m^2-K}}\right]$.

$\boldsymbol{k}$: thermal conductivity coefficient $\left[\frac{\mathrm{W}}{\mathrm{m-K}}\right]$.

The Grashof number is an important parameter when natural convection is considered.
The Grashof number is the ratio of buoyancy forces to viscous forces (Incropera, et al., 2013):

$$\boldsymbol{Gr} = \frac{\boldsymbol{g\beta(T_s - T_\infty)D_h}^{\boldsymbol{3}}}{\boldsymbol{\nu^2}} \qquad \textbf{(4.1-7)}$$

Where:

$\boldsymbol{Gr}$: the Grasshof number $[-]$.

$\boldsymbol{\beta}$: expansion coefficient $\left[\frac{1}{\mathrm{K}}\right]$.

$\boldsymbol{\nu}$: kinematic viscosity $\left[\frac{\mathrm{m^2}}{\mathrm{s}}\right]$.

The Prandtl number is the ratio of momentum and thermal diffusivity (Incropera, et al., 2013):

$$\boldsymbol{Pr} = \frac{\boldsymbol{C_p \mu}}{\boldsymbol{k}} \qquad \textbf{(4.1-8)}$$

Where:

$\mathbf{Pr}$: Prandtl number $[-]$.

$\boldsymbol{C_p}$: specific heat capacity $\left[\frac{\mathrm{J}}{\mathrm{kg-K}}\right]$.

$\boldsymbol{\mu}$: dynamic viscosity $\left[\frac{\mathrm{Ns}}{\mathrm{m^2}}\right]$.

The Reynolds number is the ratio of the inertial and the viscous forces working on a fluid. The Reynolds number is given by:

$$\boldsymbol{Re} = \frac{\dot{\boldsymbol{m}}\, \boldsymbol{D_h}}{\mu \boldsymbol{A}} \qquad \textbf{(4.1-9)}$$

If the Reynolds number is below 2300, the flow is considered laminar. If the Reynolds number is larger than 5000, the flow is considered to be turbulent. If the Reynolds number is between 2300 and 5000, the flow falls within the transitional zone between the laminar and turbulent regimes.

Flow instabilities may occur in free convection, as in forced convection. The parameter used as a measure of turbulence in free convection is the Rayleigh number, which must therefore also be calculated and is given by (Incropera, et al., 2013):

$$\boldsymbol{Ra_L = Gr * Pr} \qquad \textbf{(4.1-10)}$$

If $Ra_L \leq 10^9$ then the regime, in terms of free convection, is regarded to be laminar.

4.2 Mixed convection theory

In calculating the mixed convection heat transfer, the fluid properties were evaluated at the film temperature, which was taken as the average of the film and fluid bulk temperatures.

The Aicher criterion was used to determine the flow regime of the air (Aicher & Martin, 1996):

$$\boldsymbol{Aicher_{criterion} = \frac{Ra^{1/3}}{Re^{0.8} * Pr^{0.4}}} \qquad \textbf{(4.2-1)}$$

The regime is as follows:
Forced convection if the Aicher criterion < 0.05.
Mixed convection if 0.05 < Aicher criterion < 0.2.
Free convection if the Aicher criterion > 0.2.

A further criterion on the regime map is based on the Richardson number (KAERI, 2014):

$$\boldsymbol{Ri = \frac{Gr}{Re^2}} \qquad \textbf{(4.2-2)}$$

From Equation 4.2-2, the Burmeister criterion (of which the function is shown in Figure 4.2-1) follows; where the Richardson number is equal to 1.

By using Equations 4.2-1 and 4.2-2, the graph in Figure 4.2-1 is obtained. The graph is similar to the graph in Figure 2.3-1. The flow falls under the mixed convection regime if Re vs. Gr Pr falls between the limits specified.

The Nusselt number for mixed convection is calculated by (Celata, et al., 1998):

$$\boldsymbol{Nu_{mixed} = \left(\left|Nu_{forced}^3 - Nu_{free}^3\right|\right)^{\frac{1}{3}}} \qquad \textbf{(4.2-3)}$$

Note that the sign in Equation 4.2-3 is negative since in the NACEF the forced and natural convection operate in the same direction (upward) in the turbulent regime. This is referred to as aiding flow.

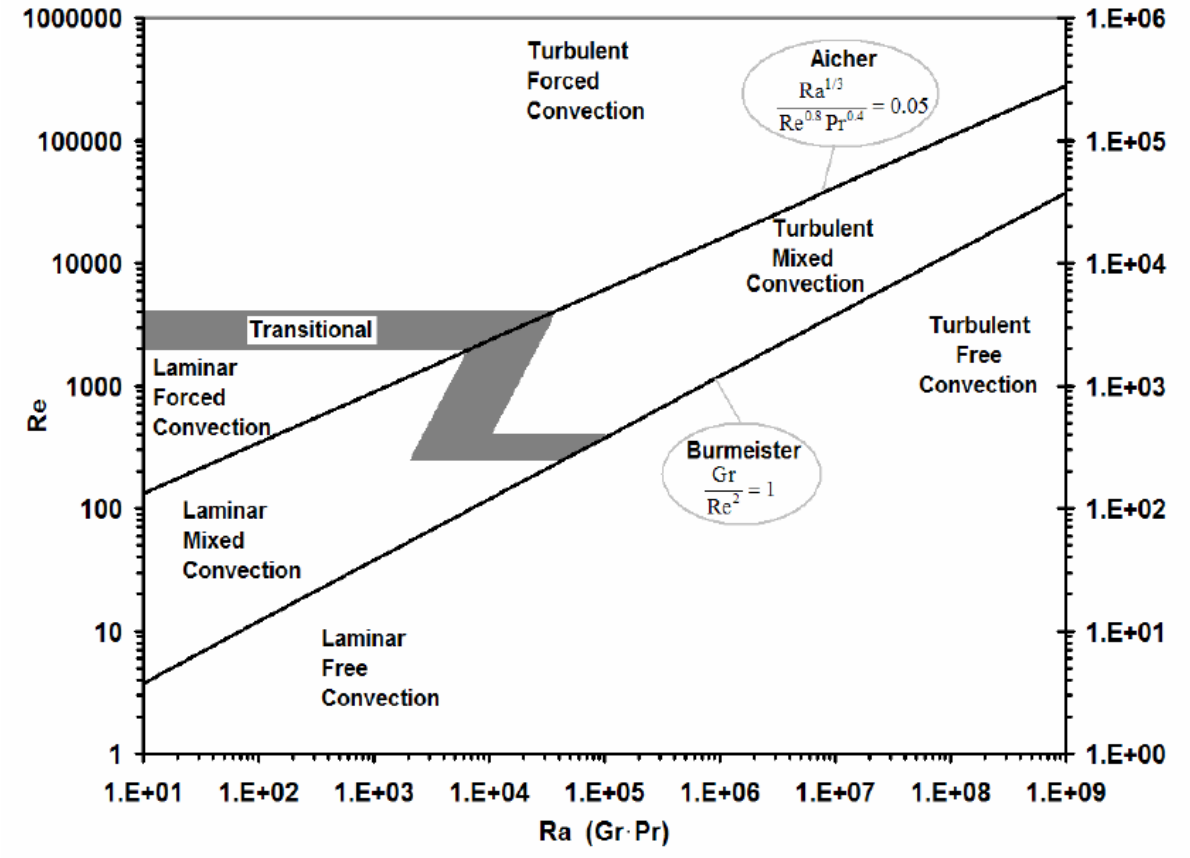

Figure 4.2-1. Mixed convection regime limits. (KAERI, 2014).

The correlation by Churchill and Chu was used to calculate the Nusselt number for free convection (Incropera, et al., 2013):

$$\mathbf{Nu_{free}} = \left(\mathbf{0.825} + \frac{\mathbf{0.387 * Ra^{1/6}}}{\left(\mathbf{1+\left(\frac{0.492}{Pr}\right)^{\frac{9}{16}}}\right)^{\mathbf{8/27}}} \right)^{\mathbf{2}} \qquad \textbf{(4.2-4)}$$

The forced convection can be either laminar, turbulent or in the transition between laminar and turbulent. A modified Dittus Boelter equation was used to calculate the Nusselt number for turbulent forced convection (Incropera, et al., 2013), (KAERI, 2014), (Kawaji, 2015):

$$\boldsymbol{Nu_{forced_{Turbulent}} = 0.021 Re^{0.8} Pr^{0.4} \eta} \qquad \textbf{(4.2-5)}$$

Where the property index for gasses are defined as (KAERI, 2014):

$$\boldsymbol{\eta = \left(\frac{T_{fluid}}{T_{wall}}\right)^{0.5}} \qquad \textbf{(4.2-6)}$$

The Prandtl number in Equation 4.2-5 is raised to the power 0.4, as opposed to 0.3, because in all cases in this study, the fluid was being heated.

The Nusselt number for the laminar forced convection was taken as a constant value which is a function of the given width to length ratio of the riser tube. (Incropera, et al., 2013), (KAERI, 2014):

$$\boldsymbol{Nu_{forced_{Laminar}} = 5.91\eta} \qquad \textbf{(4.2-7)}$$

The Nusselt number for forced transitional flow is calculated by linearly interpolating between the Nusselt numbers in Equations 4.2-5 and 4.2-7 in the following manner:

$$\boldsymbol{Nu_{forced} = Nu_{forced_{Turbulent}} * f_r + Nu_{forced_{Laminar}}(1 - f_r)} \qquad \textbf{(4.2-8)}$$

Where:

$$\boldsymbol{f_r = \frac{Re-2300}{5000-2300}} \qquad \textbf{(4.2-9)}$$

After the Nusselt number for mixed convection has been calculated, the mixed convection heat transfer coefficient can be calculated by rewriting Equation 4.1-6 as:

$$\boldsymbol{h = \frac{Nu_{mixed}\, k}{D_h}} \qquad \textbf{4.2-10}$$

4.3 Thermal radiation heat transfer theory

Thermal radiation heat transfer occurs between the cavity surfaces and within the riser tubes.

Where there is a surface, surface i, emitting heat to a surface j, the relation for the view factors is (Incropera, et al., 2013):

$$\boldsymbol{A_i * F_{ij} = A_j * F_{ji}} \qquad \textbf{(4.3-1)}$$

Where:

$\boldsymbol{A_i, A_j}$: surface area of surface i and j respectively [m^2].

$\boldsymbol{F_{ij}}$: radiation heat transfer view factor from surface i to surface j [−].

$\boldsymbol{F_{ji}}$: radiation heat transfer view factor from surface j to surface i [−].

The total emissive power of a surface is given by (Incropera, et al., 2013):

$$E_{bi} = \sigma T^4 \quad \textbf{(4.3-2)}$$

Where:

E_{bi} : emissive power of the surface $\left[\frac{\mathrm{W}}{m^2}\right]$.

σ : Stefan − Boltzmann constant $\left[\frac{\mathrm{W}}{\mathrm{m}^2 \ -\mathrm{K}^4}\right]$.

The net radiative heat transfer from a surface is given by (Incropera, et al., 2013):

$$q_i = \frac{E_{bi} - J_i}{\frac{(1-\varepsilon_i)}{A_i \varepsilon_i}} \quad \textbf{(4.3-3)}$$

Where:

q_i : heat transferred from surface [W].

J_i : radiosity of the surface $\left[\frac{\mathrm{W}}{\mathrm{m}^2}\right]$.

ε_i : emissivity of the radiating surface $[-]$.

The nett radiative heat transfer from surface i to all surfaces j it interacts (exchanges radiative heat) with, is given by (Incropera, et al., 2013):

$$q_i = \sum_{j=1}^{N} \frac{J_i - J_j}{(A_i F_{ij})^{-1}} \quad \textbf{(4.3-4)}$$

The radiation between the surfaces enclosed in the cavity (cavity and riser tube walls) needs to be solved using a network approach. Therefore combining Equation 4.3-3 and 4.3-4 to yield (Incropera, et al., 2013):

$$\frac{E_{bi} - J_i}{\frac{(1-\varepsilon_i)}{A_i \varepsilon_i}} = \sum_{j=1}^{N} \frac{J_i - J_j}{(A_i F_{ij})^{-1}} \quad \textbf{(4.3-5)}$$

4.4 Conduction heat transfer

The conduction heat transfer in the cavity walls and riser tube walls can be calculated as follows (Incropera, et al., 2013):

$$q_{conduction} = -kA_{surface} \frac{dT}{dx} \quad \textbf{(4.4-1)}$$

Where:

$A_{surface}$: area perpendicular to the heat transfer $direction$ $[\mathrm{m}^2]$.

$\frac{dT}{dx}$: temperature gradient in the direction of the conduction heat transfer [m].

4.5 Conclusion

The fundamental equations and important parameters that need to be calculated have been discussed. The conservation equations are important in the calculation of the fluid dynamics in the flow path. The mixed convection theory important to this study has been described. The radiation heat transfer, especially radiation heat exchange between surfaces was described. Lastly, the method for calculating the conduction heat transfer was given.

Chapter 5 - Verification exercises

Various simulations were performed to verify that the relevant parameters and the methodology were implemented correctly in the Flownex model. The verification exercises are described in this chapter. It includes a verification exercise concerning the thermal radiation view factors (Section 5.1), the use of mixed convection theory (Section 5.2) and thermal radiation heat transfer (Section 5.3). Section 5.4 compares results of a simplified model which was set up in EES and Flownex, while section 5.5 investigates the influence of the tangential conduction in the Flownex model.

5.1 Thermal radiation view factors

The view factors used in the GAMMA+ model were verified by using STAR CCM+, which in turn had to be verified by an exercise of which the analytical solution could be calculated.

5.1.1 Simplified view factor comparison

The thermal radiation view factors applicable in the cavity were calculated by using STAR CCM+. It was necessary to perform a verification exercise on the STAR CCM+ results by comparing them with analytical results. A test case was set up of which the view factors could be calculated analytically.

The test case geometry is shown in Figure 5.1-1. The view factor from the bottom surface ("i" in the figure) to the top surface ("j" in the figure) was calculated. The lengths of X, Y and L were chosen as 1.

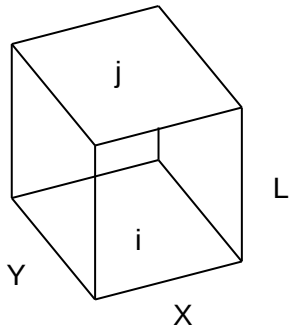

Figure 5.1-1. Simple geometry for the test case.

The analytical results were obtained by using (Incropera, et al., 2013):

$$F_{ij} =$$

$$\frac{2}{\pi XY}\left\{\ln\left[\frac{(1+X^2)(1+Y^2)}{1+X^2+Y^2}\right]^{0.5} + X\left(1+Y^2\right)^{0.5}\tan^{-1}\left(\frac{X}{(1+Y^2)^{0.5}}\right) + Y\left(1+X^2\right)^{0.5}\tan^{-1}\left(\frac{Y}{(1+X^2)^{0.5}}\right) - X\,tan^{-1}X - Y\tan^{-1}Y\right\} \quad \textbf{(5.1-1)}$$

Equation 5.1-1 was solved by using Engineering Equation Solver (EES). The solutions window is shown in Figure 5.1-2.

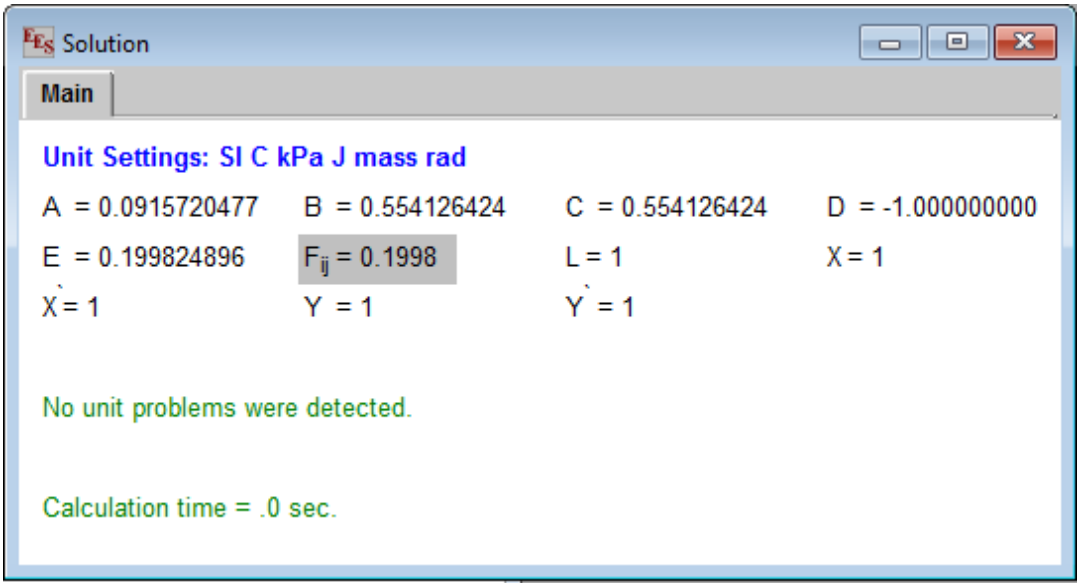

Figure 5.1-2. EES view factor calculation.

The STAR CCM+ model is shown in Figure 5.1-3. The grey surface in Figure 5.1-3 represents the same as the top surface, or "j" from Figure 5.1-1. Surface "i' is located similarly to the bottom surface in Figure 5.1-1. The other surfaces were specified as "free stream" surfaces in STAR CCM+.

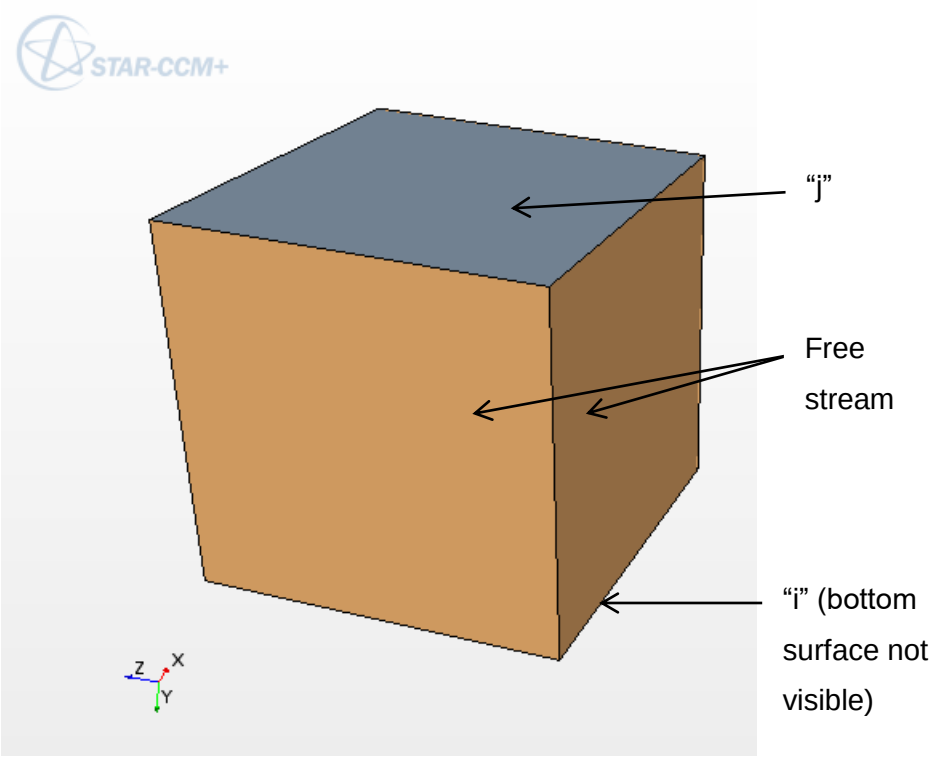

Figure 5.1-3. STAR CCM+ model.

The input values shown in Table 5.1-1 were adjusted to investigate the effect on the accuracy of the solution.

Table 5.1-1. Different input values for the STAR CCM+ simulation.

	First revision STAR	Second revision STAR	Third revision STAR
Tessellation	Medium	Very fine	Very fine
Verbosity	low	High	High
Number of beams	1024	5000	10000
Reciprocity tolerance	0.001	0.0001	0.0001

The results for the three different revisions are compared with the analytical results in Table 5.1-2.

Table 5.1-2. Comparison of the results between STAR CCM+ and EES.

	View factor	% difference with analytical solution
EES	0.1998	0
First revision STAR	0.2059	2.96
Second revision STAR	0.201976	1.08
Third revision STAR	0.201094	0.643

The third revision simulation shows the best correlation, as it differs only by 0.643 % from the analytical solution, but it also requires the longest computational time. The second revision needs less computational time, but is still provides a solution which differs only 1.08 % from the analytical solution. It was therefore decided that the inputs specified in the second revision simulation, would be used in further simulations.

5.1.2 Star CCM+ view factors for NACEF

5.1.2.1 Introduction

The thermal radiation view factor matrix was calculated by using Star CCM+. The numbering convention used to number the cavity surfaces is shown in Figure 3.4-1. The optimised mesh conditions, as calculated in section 5.1.1 was used.

5.1.2.2 Results

The view factor matrix as calculated in Star CCM+ is shown in Table 5.1-3.

Table 5.1-3. View factor matrix as calculated in Star CCM+.

	1	2	3	4	5	6	7	8	9	10	11	12
1	0.0000	0.6704	0.0401	0.0450	0.0485	0.0005	0.0000	0.0315	0.1045	0.0000	0.0153	0.0443
2	0.2462	0.5076	0.0119	0.0025	0.0387	0.0251	0.0000	0.0138	0.0746	0.0000	0.0451	0.0344
3	0.0274	0.0222	0.0870	0.2404	0.0000	0.4763	0.0397	0.0042	0.0000	0.0449	0.0425	0.0154
4	0.0450	0.0069	0.3515	0.0000	0.0000	0.0043	0.0959	0.0629	0.0000	0.2421	0.0759	0.1156
5	0.3154	0.6846	0.0000	0.0000	0.0000	0.0000	0.0000	0.0000	0.0000	0.0000	0.0000	0.0000
6	0.0006	0.0890	0.9048	0.0056	0.0000	0.0000	0.0000	0.0000	0.0000	0.0000	0.0000	0.0000
7	0.0000	0.0000	0.3770	0.6230	0.0000	0.0000	0.0000	0.0000	0.0000	0.0000	0.0000	0.0000
8	0.0410	0.0488	0.0080	0.0817	0.0000	0.0000	0.0000	0.0000	0.0000	0.0000	0.8205	0.0000
9	0.3396	0.6604	0.0000	0.0000	0.0000	0.0000	0.0000	0.0000	0.0000	0.0000	0.0000	0.0000
10	0.0000	0.0000	0.2132	0.7868	0.0000	0.0000	0.0000	0.0000	0.0000	0.0000	0.0000	0.0000
11	0.0100	0.0798	0.0403	0.0493	0.0000	0.0000	0.0000	0.4103	0.0000	0.0000	0.0000	0.4103
12	0.0288	0.0609	0.0146	0.0751	0.0000	0.0000	0.0000	0.0000	0.0000	0.0000	0.4103	0.4103

The view factor matrix calculated by KAERI is shown in Table 5.1-4.

Table 5.1-4. View factor matrix as calculated by KAERI in GAMMA+.

	1	2	3	4	5	6	7	8	9	10	11	12
1	0.0000	0.7307	0.0324	0.0334	0.0400	0.0003	0.0000	0.0263	0.0890	0.0000	0.0127	0.0353
2	0.2578	0.5154	0.0104	0.0002	0.0365	0.0256	0.0000	0.0116	0.0683	0.0000	0.0422	0.0320
3	0.0222	0.0203	0.1253	0.2315	0.0000	0.4704	0.0349	0.0037	0.0000	0.0359	0.0411	0.0149
4	0.0334	0.0007	0.3376	0.0615	0.0000	0.0039	0.0886	0.0607	0.0000	0.2259	0.0749	0.1129
5	0.2601	0.6718	0.0000	0.0000	0.0681	0.0000	0.0000	0.0000	0.0.	0.0000	0.0000	0.0000
6	0.0004	0.0942	0.8918	0.0051	0.0000	0.0085	0.0000	0.0000	0.0000	0.0000	0.0000	0.0000
7	0.0000	0.0000	0.3307	0.5758	0.0000	0.0000	0.0935	0.0000	0.0000	0.0000	0.0000	0.0000
8	0.0342	0.0427	0.0069	0.0789	0.0000	0.0000	0.0000	0.0211	0.0000	0.0000	0.8162	0.0000
9	0.2892	0.6288	0.0000	0.0000	0.0000	0.0000	0.0000	0.0000	0.0820	0.0000	0.0000	0.0000
10	0.0000	0.0000	0.1701	0.7344	0.0000	0.0000	0.0000	0.0000	0.0000	0.0956	0.0000	0.0000
11	0.0082	0.0777	0.0389	0.0487	0.0000	0.0000	0.0000	0.4081	0.0000	0.0000	0.0108	0.4076
12	0.0229	0.0590	0.0141	0.0734	0.0000	0.0000	0.0000	0.0000	0.0000	0.0000	0.4076	0.4230

The differences between the Star-CCM+ and KAERI view factors were calculated by:

$$Difference = |(Star - CCM+) - KAERI|$$

The average difference between the calculated view factors is 0.008, with the maximum being 0.0956. In the KAERI view factor matrix it is apparent that surfaces 4 through 11 each has a view factor of larger than zero to itself. The view factor from the surface to itself should be zero; however, the

view factor was calculated as larger than zero because of a normalization process that was done on the matrix.

5.1.2.3 Conclusion

Thermal radiation view factors were calculated in Star CCM+ and compared to the corresponding view factors calculated by KAERI. The results show good agreement (average difference of 0.008). Since the view factors are not calculated by either GAMMA+ or Flownex, it would be best to use the same matrix in Flownex as in GAMMA+. The Star CCM+ view factor matrix was thus not considered in further calculations. It did however serve as a verification exercise for the KAERI view factor matrix.

5.2 Convection heat transfer coefficient verification exercise

5.2.1 Model description.

A simplified model of the NACEF was simulated to verify that the mixed convection theory was correctly applied in Flownex. The simplified model consisted of a vertical riser tube with a length of 4 m. In its vertical length the tube was divided in to 20 increments of 0.2 m. A fixed heat input is specified on the wall of the vertical tube. The boundary conditions for the simulation are given in Table 5.2-1.

Table 5.2-1. Boundary conditions for the simplified NACEF model.

Property	Property value for specific case		
	Case 1	Case 2	Case 3
Mass flow rate at the inlet (kg/s)	0.18	0.3	0.4
Temperature at the inlet (C)	25	25	25
Heat input on riser wall per increment (kW)	0.800	1.380	1.790
Pressure at the outlet (kPa)	101.3	101.3	101.3

The mass flow rate and heat inputs specified in Table 5.2-1 were chosen such that forced- and mixed convection could be investigated independently as well as combined. In case 1, the flow regime was forced convection for the entire length of the tube. In case 2, the regime

was forced convection for the first half and mixed convection for the second half of the tube. In case 3 the regime was mixed convection for the entire length of the tube.

A single increment of the Flownex model is shown in Figure 5.2-1.

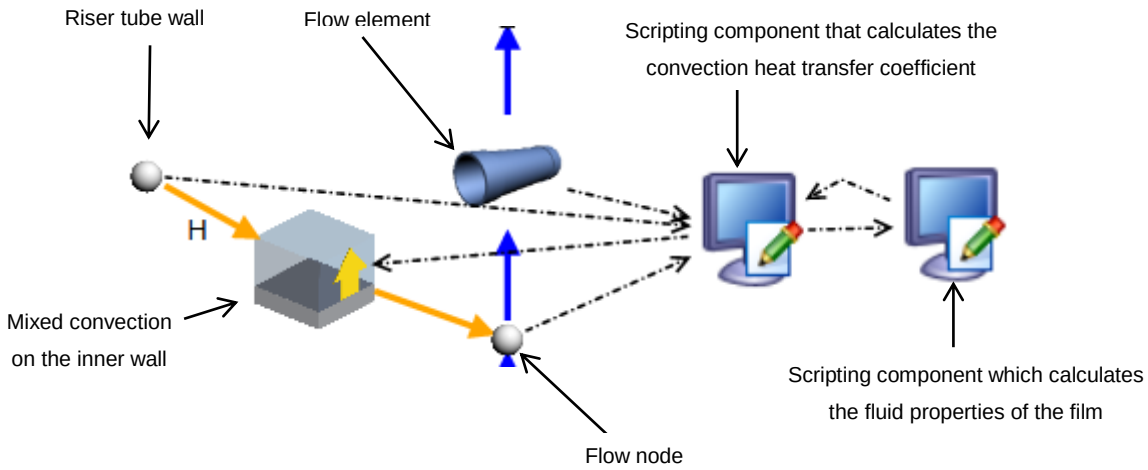

Figure 5.2-1. A single increment of the simplified NACEF model in Flownex.

A fixed heat input was specified at the riser tube wall (Figure 5.2-1). The scripting components were used to calculate the convection heat transfer coefficient for each increment. The fluid properties had to be calculated based on the film temperature; hence the need for the second scripting component. The film temperature is defined as the average between the wall and the bulk fluid temperatures. The second scripting component uses temperature, pressure and enthalpy inputs from the first scripting component to calculate the fluid properties applicable to the film.

An EES and GAMMA+ model was set up to also calculate the convection heat transfer coefficient, intended to verify the results obtained using Flownex. The GAMMA+ model was set up by Prof. C.G. du Toit. The EES model listed in Appendix C was verified against an EES model written by Prof. C.G. du Toit.

5.2.2 Results

The heat transfer coefficients as a function of axial position for the various cases are compared in Figure 5.2-2, Figure 5.2-3 and Figure 5.2-4. The graphs show an increase of the convection heat transfer coefficient with an increase of elevation. The coefficients calculated by Flownex and EES are lower than the coefficients calculated by GAMMA+. In

Figure 5.2-3 the discontinuity is apparent where the regime changes from mixed convection to forced convection. It is also apparent that the jump in the coefficient occurs one increment later in the EES model. The reason is the difference in the viscosity (differs 2.63% with GAMMA+) and the density (differs 0.95% with GAMMA+). These properties indirectly influence the value of the Aicher criterion (Equation 4.2-1). The Aicher criterion differs 1.38% with GAMMA+, resulting in the EES model calculating the coefficient for mixed convection, while GAMMA+ and Flownex calculate the coefficient for forced convection.

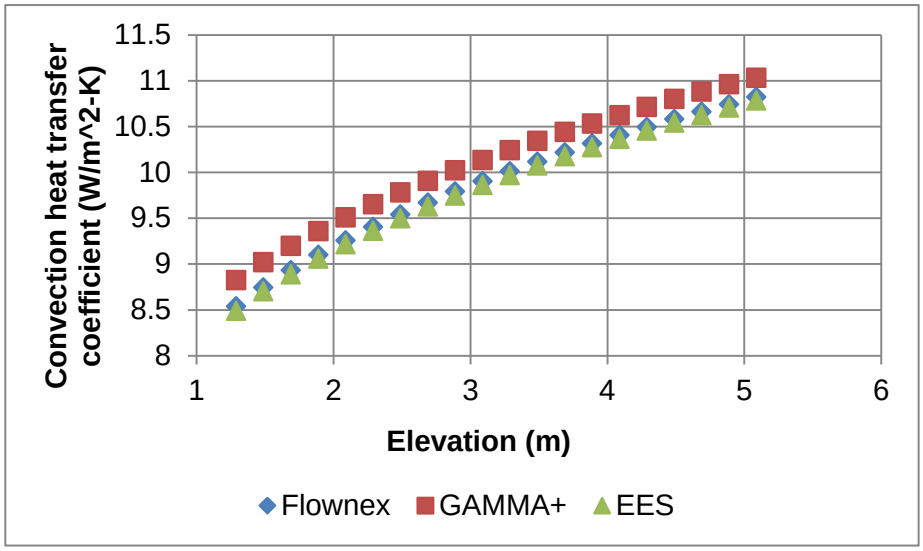

Figure 5.2-2. The convection heat transfer coefficient as a function of elevation for case 1.

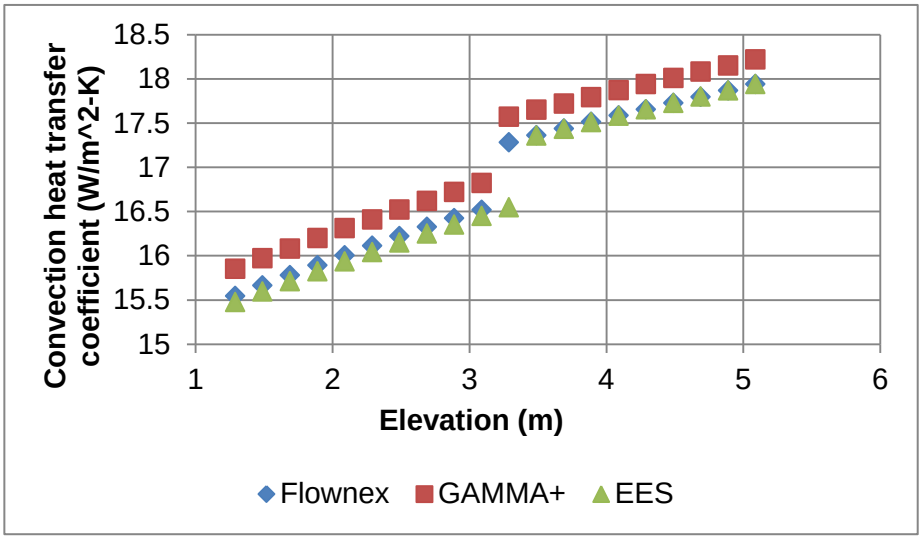

Figure 5.2-3. The convection heat transfer coefficient as a function of elevation for case 2.

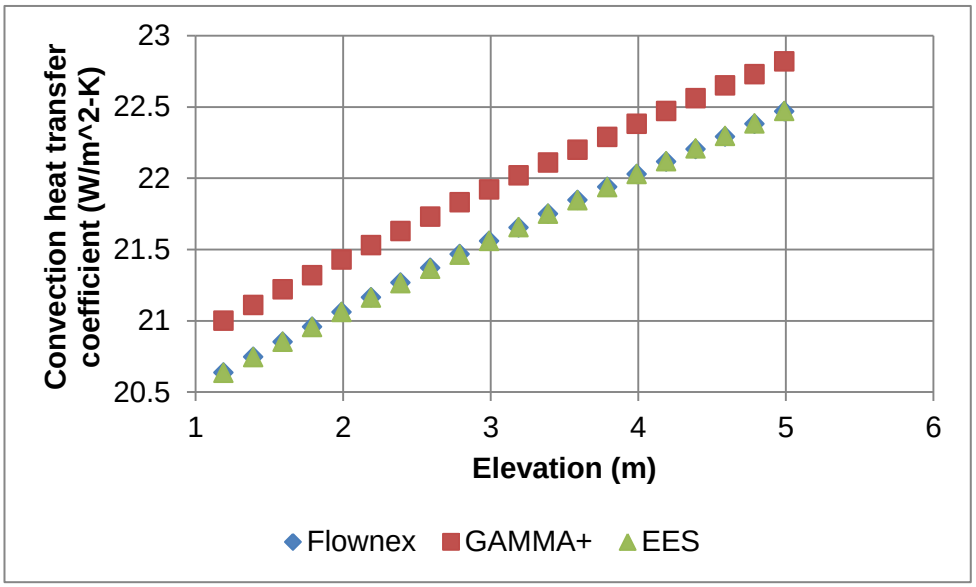

Figure 5.2-4. The convection heat transfer coefficient as a function of elevation for case 3.

The percentage difference between the coefficients at each elevation was calculated and then averaged over the entire elevation of the riser tube. The average value is used as a measure to infer the correlation between the results. The average values for the differences between the Flownex and GAMMA+ results are 2.37%, 1.72% and 1.64% for cases 1, 2 and 3 respectively.

The data from the three cases are plotted on the regime map in Figure 5.2-5. The Aicher criterion line and the Burmeister criterion line are also shown in the figure. In case 1, all of the data points for Re vs. Gr Pr D/L falls within the criterion lines, which means the regime is mixed convection. In case 2 half of the regime falls within mixed convection and the other half falls under forced convection. In Case 3 all the data points are above the Aicher criterion line, which means the regime is forced convection. The Reynolds number is larger than 5000 in all three cases, which means the flow is turbulent for all three cases. Note that the data points associated with the lowest elevation is at the far right of the graph. The Gr Pr D/L value associated with each increment decreases with an increase in elevation. In other words, the data points on the graph should be read from right to left.

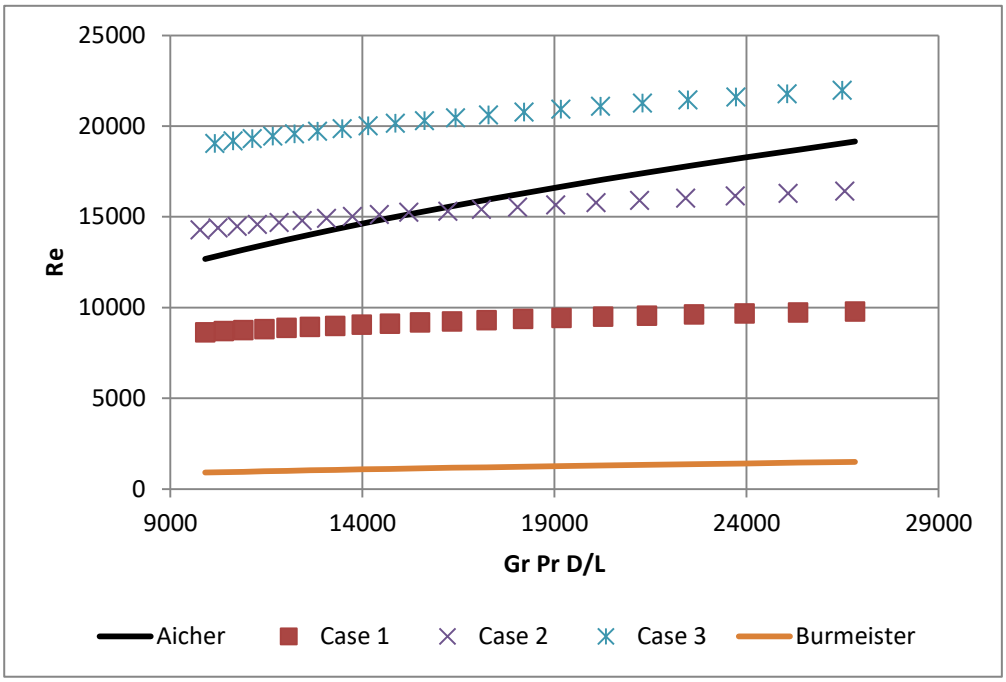

Figure 5.2-5. Data from the three cases plotted on the regime map.

5.2.3 Conclusion

The mixed convection theory described in Chapter 4 was implemented into Flownex by means of scripting components. A simplified model was simulated by using GAMMA+, Flownex and an EES code to compare the convection heat transfer coefficients obtained by the codes. The results show good agreement, which means that the theory is implemented in a similar manner in GAMMA+ and Flownex. Furthermore, it can be assumed that the scripting components can be used to calculate the heat transfer coefficients in the riser tubes for the complete NACEF model.

5.3 Radiation heat transfer verification exercise

An investigation was done to determine whether Flownex and GAMMA+ calculated thermal radiation in a similar manner. A sample problem was adapted from Incropera et al. (2013) and solved by using Flownex and GAMMA+. Engineering Equation Solver (EES) was also used to determine the analytical solution.

5.3.1 Simplified radiative heat transfer problem

The geometry and the numbering convention are shown in Figure 5.3-1. Walls 1 through 3 are referred to as the outer part of the walls. 4 through 7 are the inner parts of the walls and point 7 represents the air in the enclosure.

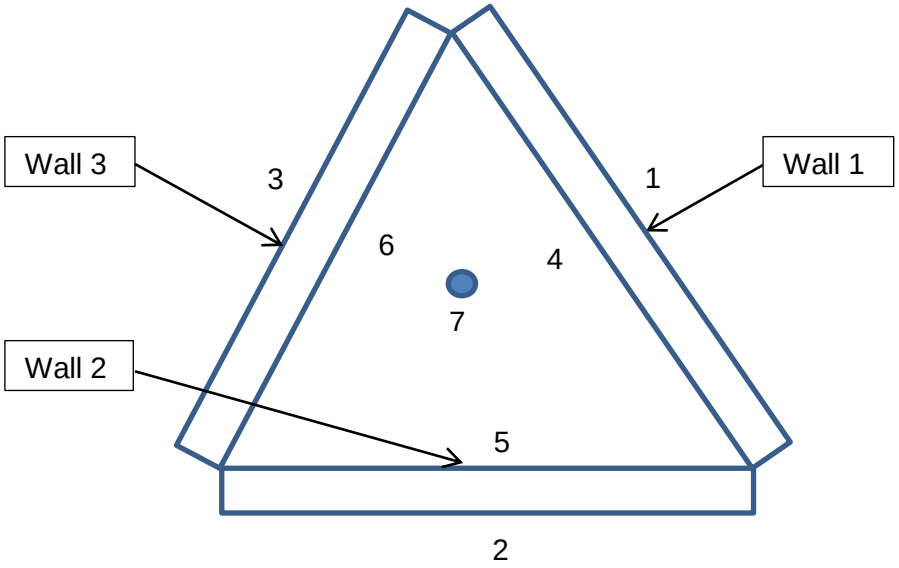

Figure 5.3-1. Simple geometry radiation and convection problem.

The boundary conditions for the problem are given in Table 5.3-1.

Table 5.3-1. Boundary conditions for the problem.

Property	Value
Temperatures	
Point 4 (K)	1200
Point 5 (K)	500
Point 6 (K)	1102.1734
Conductivity of walls (W/m-K)	15
Wall area (m^2)	1
Wall thickness (m)	0.001
Convection heat transfer coefficients	
Wall 1 inner surface (W/m^2-K)	4.087
Wall 2 inner surface (W/m^2-K)	5.53
Wall 3 inner surface (W/m^2-K)	3.744

Wall emissivity	
Wall 1	0.8
Wall 2	0.4
Wall 3	0.8
Radiation view factor	
F_12=F_13=F_23	0.5

5.3.2 Flownex model

The Flownex model of the simple problem is shown in Figure 5.3-2. The thermal radiation and convection and conduction heat transfer is accounted for as shown in the figure.

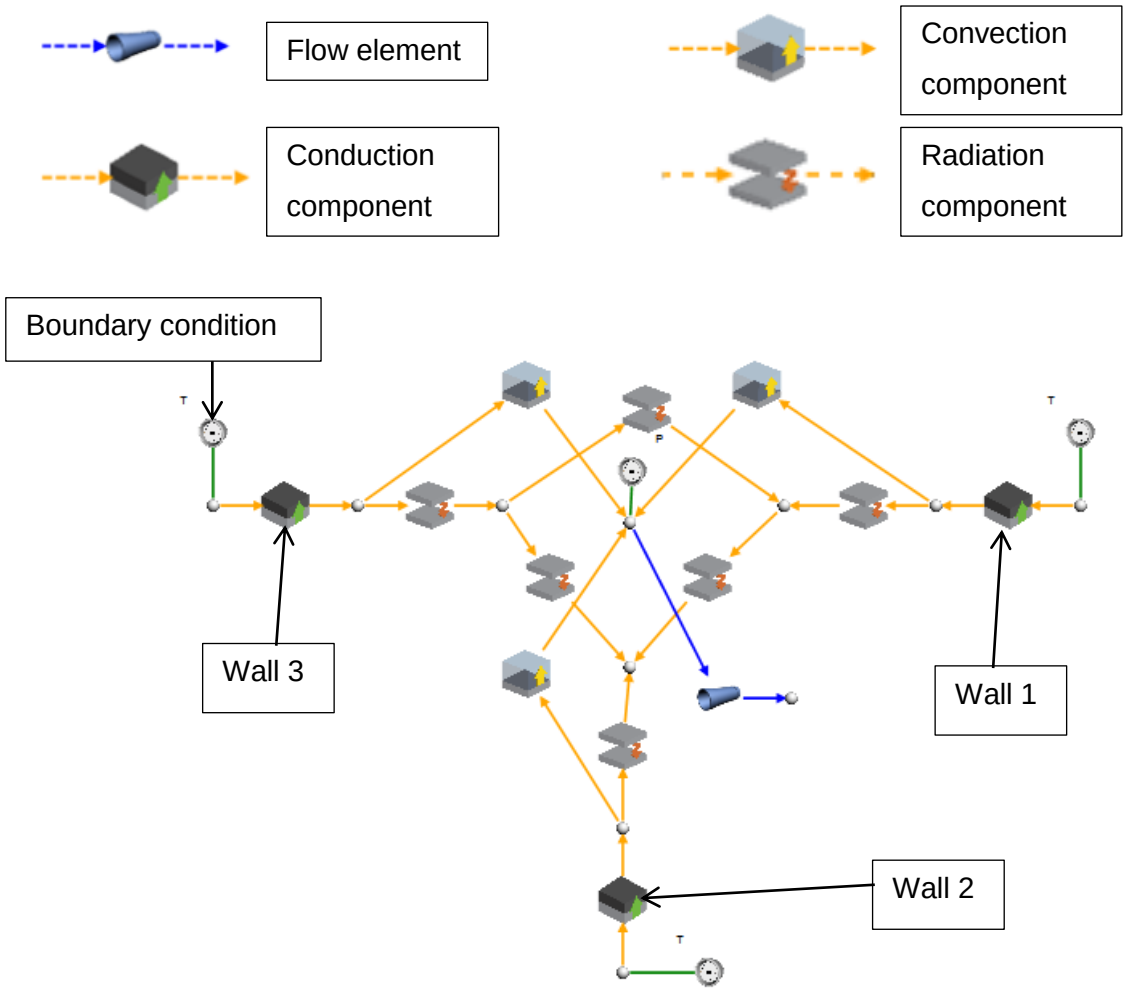

Figure 5.3-2. Flownex model of the simple problem.

Note that the placement of the flow element (in Figure 5.3-2) is necessary in Flownex when modelling the air enclosed in the space. The flow element is given arbitrary dimensions and

a zero mass flow rate is specified in the element. The convection heat transfer can then be calculated, since the convection heat transfer components need to be connected to a flow element.

5.3.3 Results comparison

The results are compared in Table 5.3-2. The GAMMA+ results were supplied by Prof. C.G. du Toit. The EES program was verified against another EES program, written by Prof. C.G. du Toit. The program code used in the EES program is given in Appendix D.

Table 5.3-2. Results comparison of the simplified problem.

	Flownex	EES	GAMMA+
Wall 1			
Radiation (W)	-36351.51	-36351.57	-36354.79
Convection (W)	-1284.73	-1284.73	-1284.71
Inside temperature (°C)	924.34	924.34	924.34
Outside temperature (°C)	926.85	926.85	926.85
Wall 2			
Radiation (W)	36762.80	36762.83	36766.12
Convection (W)	2104.46	2104.46	2104.48
Inside temperature (°C)	229.44	229.44	229.44
Outside temperature (°C)	226.85	226.85	226.85
Wall 3			
Radiation (W)	-441.29	-411.27	-411.34
Convection (W)	-819.73	-819.73	-819.77
Inside temperature (°C)	828.94	828.94	828.94
Outside temperature (°C)	829.02	829.02	829.02
Cavity air temperature (°C)	610.00	610.00	610.02

5.3.4 Conclusion

The results show very good agreement, with minimal difference in the results. This confirms that GAMMA+, Flownex and EES solve the radiation heat transfer in a similar manner.

5.4 Flownex/EES comparison of the single increment NACEF

5.4.1 Introduction

It was decided to compare a Flownex model with a model set up using Engineering Equation Solver (EES). The NACEF model was simplified for the sake of the comparison: the heated section with the riser tubes was isolated from the rest of the model. This leaves two riser tubes enclosed in a cavity, which is heated by specifying a fixed heat flux on one of the surfaces. Only a single increment of the heated cavity (of the possible twenty) was considered.

5.4.2 Model description

The boundary conditions were specified as shown in Table 5.4-1.

Table 5.4-1. Boundary conditions of the model.

Property	Value
Inlet temperature (°C)	50
Mass flow rate (kg/s)	0.19
Outlet pressure (kPa)	101.3

The boundary conditions were applied at the inlet and outlet positions as indicated in Figure 5.4-1. The model consists of two rectangular riser tubes enclosed in a rectangular cross section cavity. There are therefore eight elements in the model representing the surfaces of the riser tubes (outer and inner tube in Figure 5.4-1). There are four elements that represent the cavity walls (heater-, left-side-, right-side- and reflective wall in Figure 5.4-1). The thermal radiation heat transfer between the cavity walls, as well as the exchange between the inner surfaces of the riser tube has been accounted for.

The convection heat transfer elements are applied to each surface as shown in the figure. A single node was used to represent the cavity air. The tangential conduction heat transfer exchange between cavity walls and between riser tube walls has been neglected.

Note the flow element connected to the node representing the cavity air. This element is necessary in Flownex, since the convection heat transfer components need to be connected to a so-called flow node. The flow element can be given arbitrary dimensions and a zero mass flow rate is specified in the element, since no external pressure source exists in the cavity.

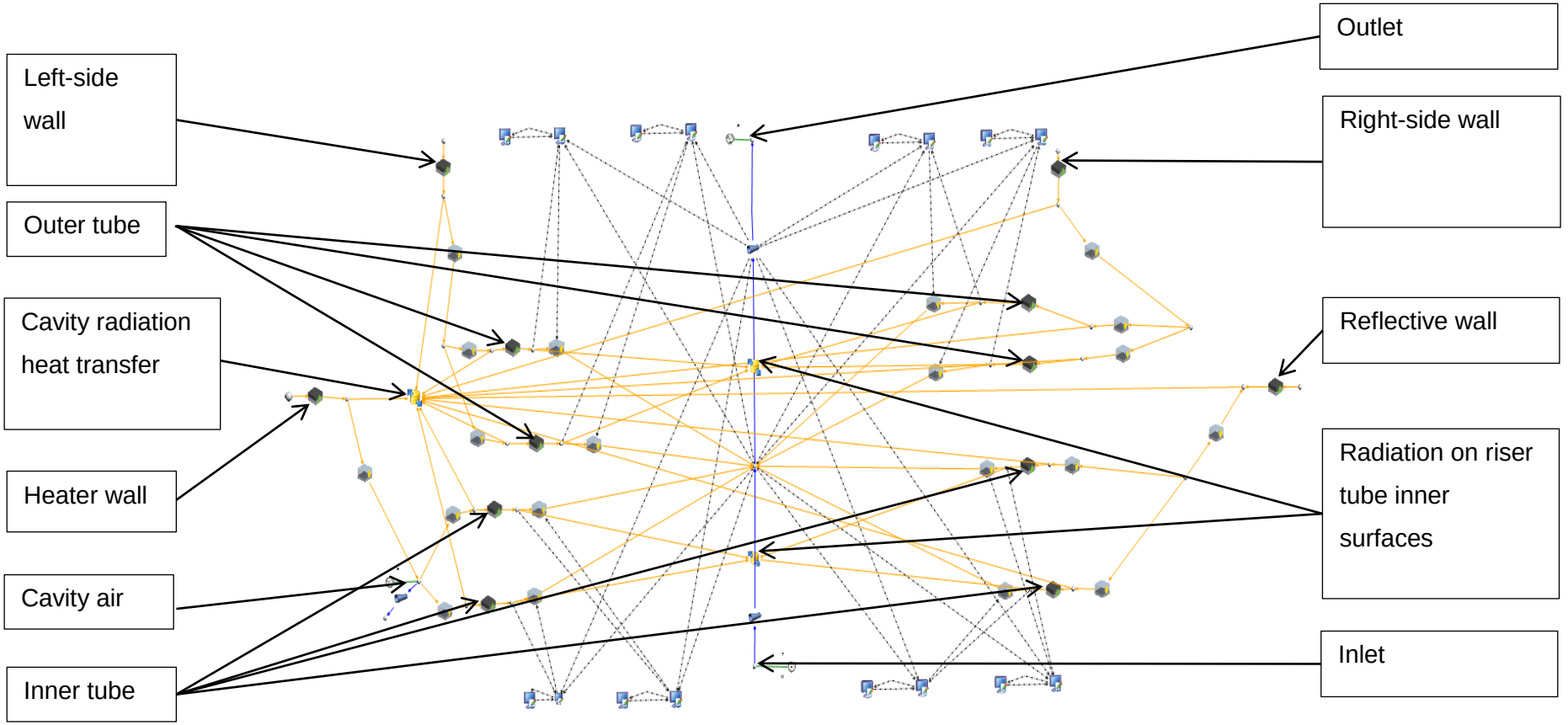

Figure 5.4-1. Single increment Flownex model for comparison with EES.

The EES model contained some of the equations described in Chapter 4. The mixed convection in the riser tubes was calculated by using the same correlations and the heat transfer by radiation was implemented in the model. The convection heat transfer coefficients on the cavity surfaces and the riser tubes outer surfaces were taken from Flownex and used as inputs in the EES program.

5.4.3 Results

The temperatures obtained by Flownex and EES are shown in Table 5.4-2. The Flownex model was refined by Prof. C.G. du Toit to obtain the results shown in the table. The EES results were supplied by Prof. C.G. du Toit and were verified against the EES model in Appendix E.

Table 5.4-2. Comparison of the temperatures obtained by Flownex and EES.

	EES	Flownex	% Difference
Heater wall temperature (°C)	354.23	354.22	0.003
Left side wall temperature (°C)	223.95	223.94	0.004
Right side wall temperature (°C)	168.89	168.88	0.006
Reflective wall temperature (°C)	167.98	167.97	0.006
Outer tube			
Front surface temperature (°C)	191.67	191.67	0.000
Left surface temperature (°C)	128.67	128.17	0.389
Right surface temperature (°C)	121.54	121.53	0.008
Rear surface temperature (°C)	121.33	121.33	0.000
Inner tube			
Front surface temperature (°C)	191.51	191.50	0.005
Left surface temperature (°C)	118.83	118.83	0.000
Right surface temperature (°C)	119.09	119.08	0.008
Rear surface temperature (°C)	119.92	119.91	0.008
Cavity air temperature (°C)	180.46	180.45	0.006

The results show good agreement, with a maximum difference of 0.389%.

5.4.4 Conclusion

A simplified model was simulated in Flownex and EES and the results have been compared. The results show good agreement. It can therefore be concluded that EES and Flownex solve the equations in a similar manner.

5.5 Flownex/GAMMA+ single increment model NACEF

5.5.1 Introduction

The effect of modelling the tangential conduction in Flownex was investigated. The tangential conduction accounts for the conduction heat transfer in the circumferential direction between the connected walls of each of the riser tubes. An increment of the NACEF model was considered in isolation to be studied in closer detail.

The geometric data and convection coefficients associated with each of the cavity walls are given in Table 5.5-1. Note that the riser tube inner surface areas are given in brackets.

Table 5.5-1. Input data concerning the cavity walls.

	Convection heat transfer coefficient (W/m^2-K)	Height (m)	Thickness (m)	Area (m^2)
Heater wall	5.069	0.2	0.025	0.13
Left-side wall	3.48	0.2	0.03	0.3684
Right-side wall	2.383	0.2	0.03	0.1896
Reflective wall	2.44	0.2	0.03	0.13
Inner tube				
Front wall	2.707	0.2	0.005	0.04 (0.032)
Left wall	4.211	0.2	0.005	0.2 (0.192)
Right wall	4.175	0.2	0.005	0.2 (0.192)
Rear wall	4.181	0.2	0.005	0.04 (0.032)
Outer tube				
Front wall	2.593	0.2	0.005	0.02 (0.016)
Left wall	3.963	0.2	0.005	0.1 (0.096)
Right wall	4.131	0.2	0.005	0.02 (0.016)

Rear wall	4.117	0.2	0.005	0.1 (0.096)

The input data important to the flow path is listed in Table 5.5-2.

Table 5.5-2. Input data for the flow path.

Parameter	Value
Riser tube area (m^2)	0.0576
Riser tube circumference (m)	3.36
Surface roughness of the riser tube (µm)	10

The boundary conditions of the model are listed in Table 5.5-3.

Table 5.5-3. Boundary conditions of the model.

Boundary condition	Value
Air inlet temperature (C)	50
Mass flow rate (kg/s)	0.19
Outlet pressure (kPa)	101.3
Difference in elevation between inlet and outlet (m)	0.2

5.5.2 Flownex model description

The model in Figure 5.5-1 is similar to the model described in section 5.4. The only difference is that the tangential conduction was added. The elements used to calculate the tangential conduction are shown in Figure 5.5-2.

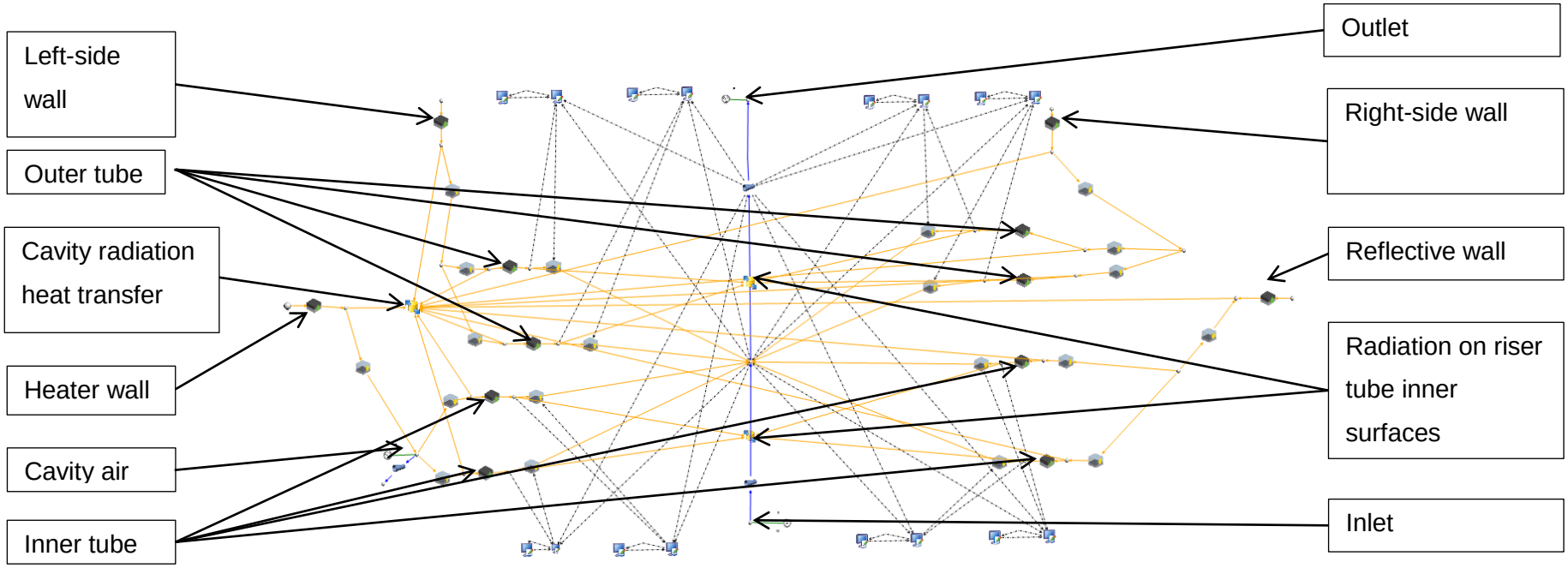

Figure 5.5-1. Single increment model in Flownex.

The elements used to calculate the tangential conduction are shown in Figure 5.5-2. The inner and outer nodes of each wall in Figure 5.5-1, connects to the nodes in Figure 5.5-2 as shown in the figure.

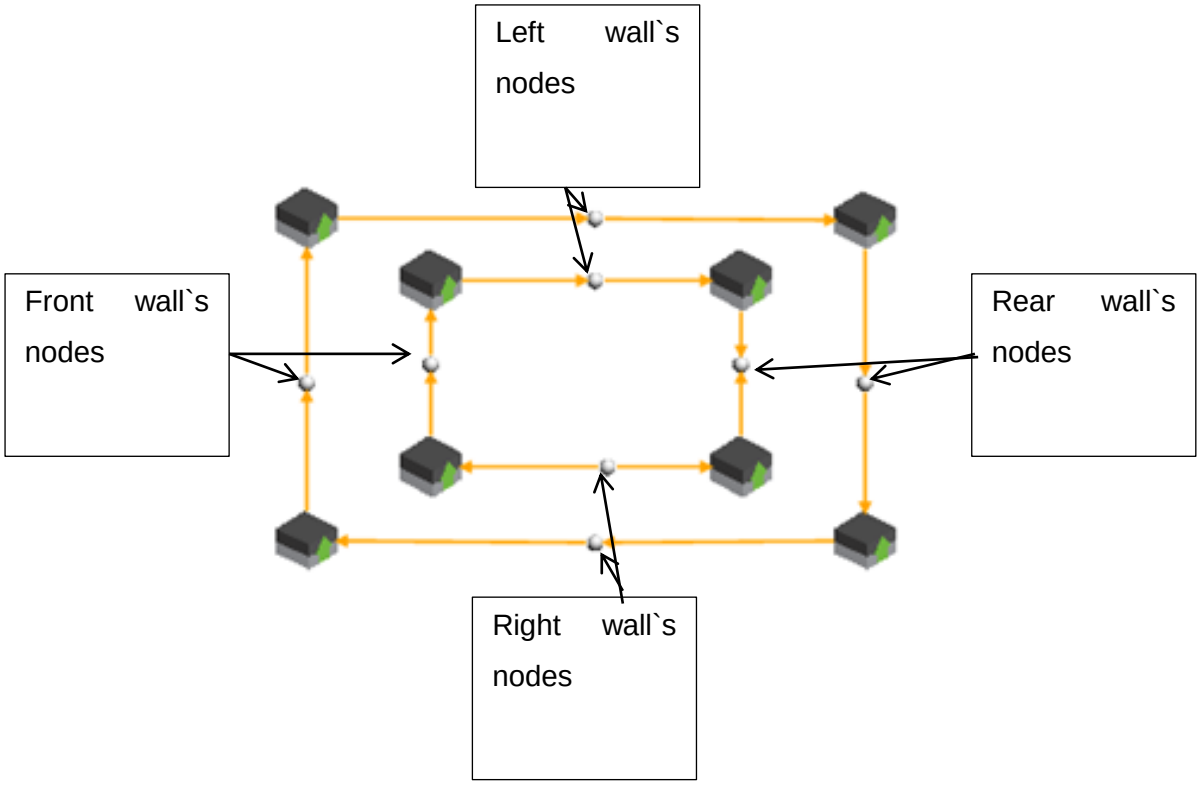

Figure 5.5-2. Tangential conduction in the single increment Flownex model.

5.5.3 Results

The results for the investigation are compared in Table 5.5-4. The GAMMA+ results were supplied by Prof. C.G. du Toit. The Flownex results were obtained by the Flownex model as described above, which was refined by Prof. C.G. du Toit.

Table 5.5-4. Results comparison; with and without tangential conduction.

	Flownex with tangential conduction (Case 1)	Flownex without tangential conduction (Case 2)	GAMMA+	% Difference (Case 1 and GAMMA+)	% Difference (Case 2 and GAMMA+)
Heater wall temperature (°C)	350.86	354.22	350.84	0.01	0.95
Left side wall (°C)	220.14	223.94	220.11	0.01	1.71

Right side wall (°C)	168.25	168.88	168.18	0.04	0.41
Reflective wall (°C)	167.40	167.97	167.34	0.04	0.38
Outer tube					
Front wall temperature (°C)	164.44	191.67	164.58	0.09	14.13
Left wall temperature (°C)	129.42	128.17	129.21	0.16	0.80
Right wall temperature (°C)	123.20	121.53	123.15	0.04	1.32
Rear wall temperature (°C)	123.52	121.33	123.66	0.11	1.88
Inner tube					
Front wall temperature (°C)	162.36	191.50	162.47	0.07	15.16
Left wall temperature (°C)	121.29	118.83	121.25	0.03	2.00
Right wall temperature (°C)	121.56	119.08	121.50	0.05	1.99
Rear wall temperature (°C)	120.17	119.91	120.10	0.06	0.16
Cavity air temperature (°C)	179.31	180.45	179.26	0.03	0.66

From the results in Table 5.5-4 it can be seen that adding the tangential conduction does have an effect on the temperature distribution in the cavity. The most notable is the difference in the outer and inner tubes` front surface temperatures.

5.5.4 Conclusion

The effect of the tangential conduction on the Flownex results was investigated. There is a notable difference in the calculated temperatures between the two Flownex models. The results from the two Flownex cases were compared to the results obtained by using GAMMA+. The agreement with GAMMA+ was better for the Flownex model in which tangential conduction was accounted for. Tangential conduction should therefore be included in the Flownex model of the NACEF.

5.6 Conclusion

Various verification exercises have been performed to confirm that the methodology used in Flownex was correct. The constituent parts of the Flownex model, including the thermal radiation, use of mixed convection and conduction heat transfer has been verified by using appropriate codes (EES, GAMMA+ and Star-CCM+).

Chapter 6 - Simulation Models

The Flownex models of the NACEF are described in this chapter. The important input values and boundary conditions are also given. Finally the different variations of the simulation model are also described.

6.1 Model simplifications

The geometry that was simulated is shown in Figure 6.1-1, which shows a single increment of the heated section of the NACEF. The GAMMA+ and Flownex models divide the heated section into 20 increments of equal height. A distinction is made between the air inside and outside of the six riser tubes. The air on the outside of the riser tubes is referred to as the cavity air and the air inside the riser tubes is referred to the riser air. The cavity and riser air never comes into direct contact at any point in the facility.

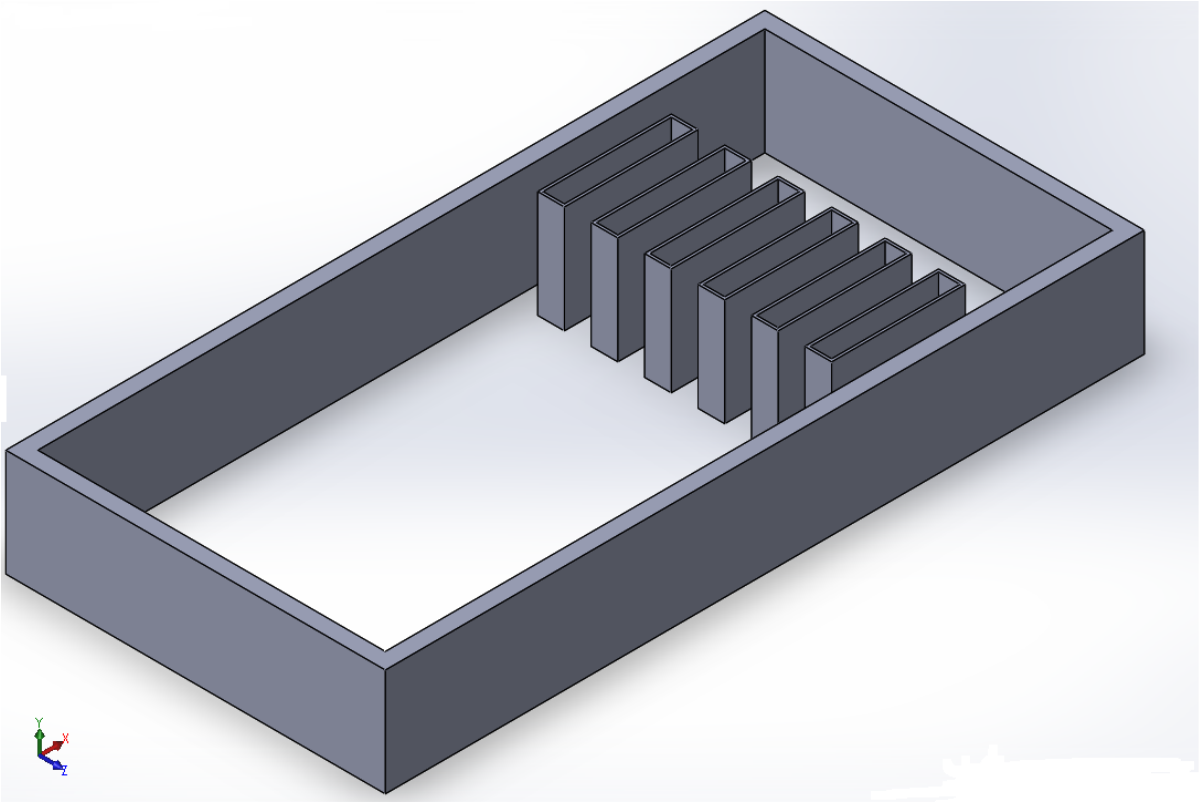

Figure 6.1-1. SolidWorks model of a single increment of the NACEF.

The GAMMA+ model was simplified by grouping the six riser tubes together to form two representative riser tubes namely the outer tubes and the inner tubes. The outer tubes represent the two tubes closest to the cavity walls and the inner tubes represent the four remaining tubes. The thermal radiation view factor matrix could therefore be simplified

considerably since there were 8 surfaces representing the riser tubes instead of 24. The two riser tubes are finally grouped into a single representative riser tube.

A further simplification was applied on the cavity side walls. The opposing walls were grouped together to form the left side wall and the right side wall (Figure 6.1-2). The cavity walls were thus represented by the heater wall, left side wall, right side wall and reflective wall (Figure 6.1-2).

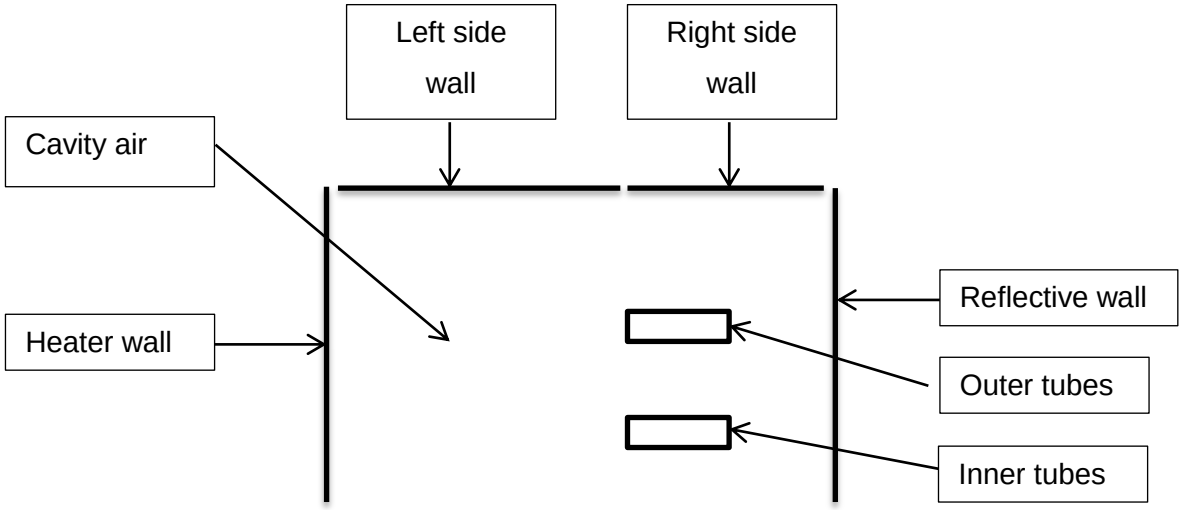

Figure 6.1-2. Simplifications made to the model.

No tangential conduction heat transfer was modelled between the cavity walls i.e. conduction heat transfer between the heater wall and left side wall or left side wall and reflective wall etc. was neglected. The axial conduction within the cavity walls was accounted for. The axial and tangential conduction was modelled in the riser tube walls.

6.2 Flownex

6.2.1 Frictional- and minor losses

The pressure losses due to friction in the flow path were accounted for in the Flownex model. The surface roughness was specified as 10µm, which is the same as in the GAMMA+ model.

The minor/secondary/form losses are accounted for differently in Flownex than in GAMMA+. GAMMA+ uses fluid blocks as control volumes, which are inter-connected by junction blocks. The form loss coefficients are assigned to the junction blocks. The pressure loss, due to the form losses, was then calculated over the junction block between two fluid blocks. The velocity associated with the smallest diameter inter-connected fluid block was used in the calculation of the pressure loss. The form losses calculated in this manner differ from

the losses calculated by using Flownex. A study by Du Toit (2016), investigated the difference in the philosophy when calculating the frictional and form losses. The result of the study, was that the smallest diameter flow element in the junction`s length had to be increased. The flow element length in Flownex was increased such that the length was equal to junction block`s length in the GAMMA+ model. The flow elements` (represented as pipes in Flownex) lengths used in the Flownex model are given in Appendix A. The form loss coefficients used in Flownex were however the same as in GAMMA+ and are listed in Table 3.3-1.

6.2.2 Cavity convection heat transfer coefficients

The convection heat transfer coefficients of the cavity air could not be calculated in Flownex. This is because Flownex is a one-dimensional simulation program. The convection heat transfer coefficients related to the natural circulation in the cavity must be calculated by a two or three dimensional program. The coefficients calculated by GAMMA+ were therefore used for the cavity surfaces. The convection heat transfer coefficients used on each surface at a given elevation in the cavity for the baseline model (described in section 6.3.1) is given in Table 3.5-1. The convection heat transfer coefficients of the cavity surfaces were different for the modified case (described in section 6.3.2). The coefficients for the modified case are listed in Table 3.5-2.

6.2.3 Mixed convection in the riser tubes

The mixed convection theory described in Chapter 4 had to be incorporated into Flownex. This was done by using scripting components to define the equations to be used for calculating various parameters. The most important parameter being the convection heat transfer coefficients on the inside surfaces of the riser tubes. The results were verified by simulating a simplified model in Flownex, EES and GAMMA+ and comparing the results. The verification exercise is explained in section 5.2. The results show good agreement and the scripting components could therefore be applied to the full NACEF Flownex model.

6.2.4 Thermal radiation view factor matrix

The same thermal view factors from GAMMA+ were applied in the Flownex model, since Flownex can`t calculate the thermal radiation view factor matrix. The GAMMA+ view factors were verified by using STAR CCM+. The verification exercises for the view factors are described in detail in section 5.

6.2.5 *Flownex model inlet*

The inlet of the Flownex model is shown in Figure 6.2-1. The temperature and pressure boundary conditions are implemented at the position shown in the figure. The two inlet pipes are divided into two increments, as is the inlet plenum. The node through which the inlet connects to the riser tube is also indicated in the figure. This figure corresponds to the "F1_Loop_inPip" and "F1_Loop_InCham" in Figure 3.2-1.

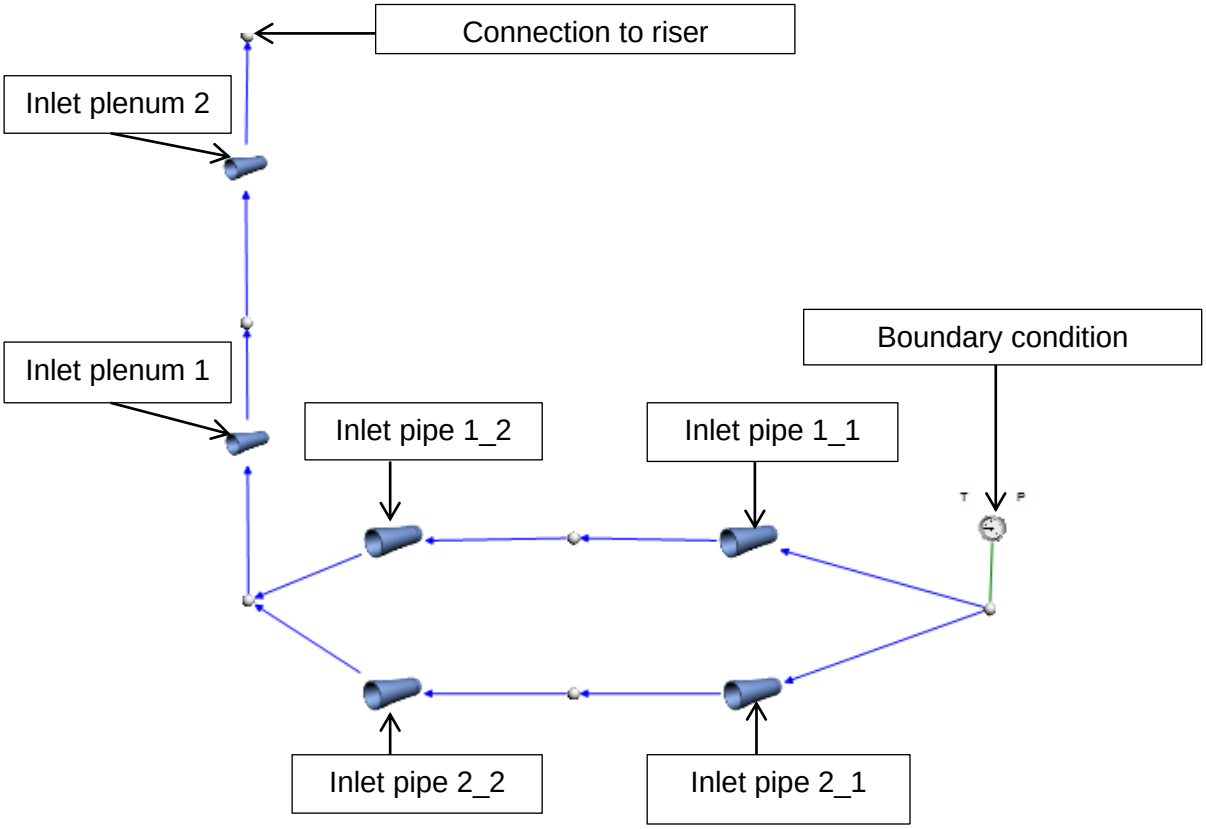

Figure 6.2-1. Inlet of the NACEF as modelled in Flownex.

6.2.6 *Unheated riser tube section*

One of the increments of the unheated section of the riser tube is shown in Figure 6.2-2. The increment shown in the figure connects to the second unheated increment as indicated. The second increment in turn connects to the heated section of the riser tube which is enclosed in the cavity. The outside surfaces of the riser tube in the unheated section are assumed to be adiabatic. The figure corresponds to the bottom most part of "W3_RiserTube" and "F1_LoopRiser" in the GAMMA+ model in Figure 3.2-1.

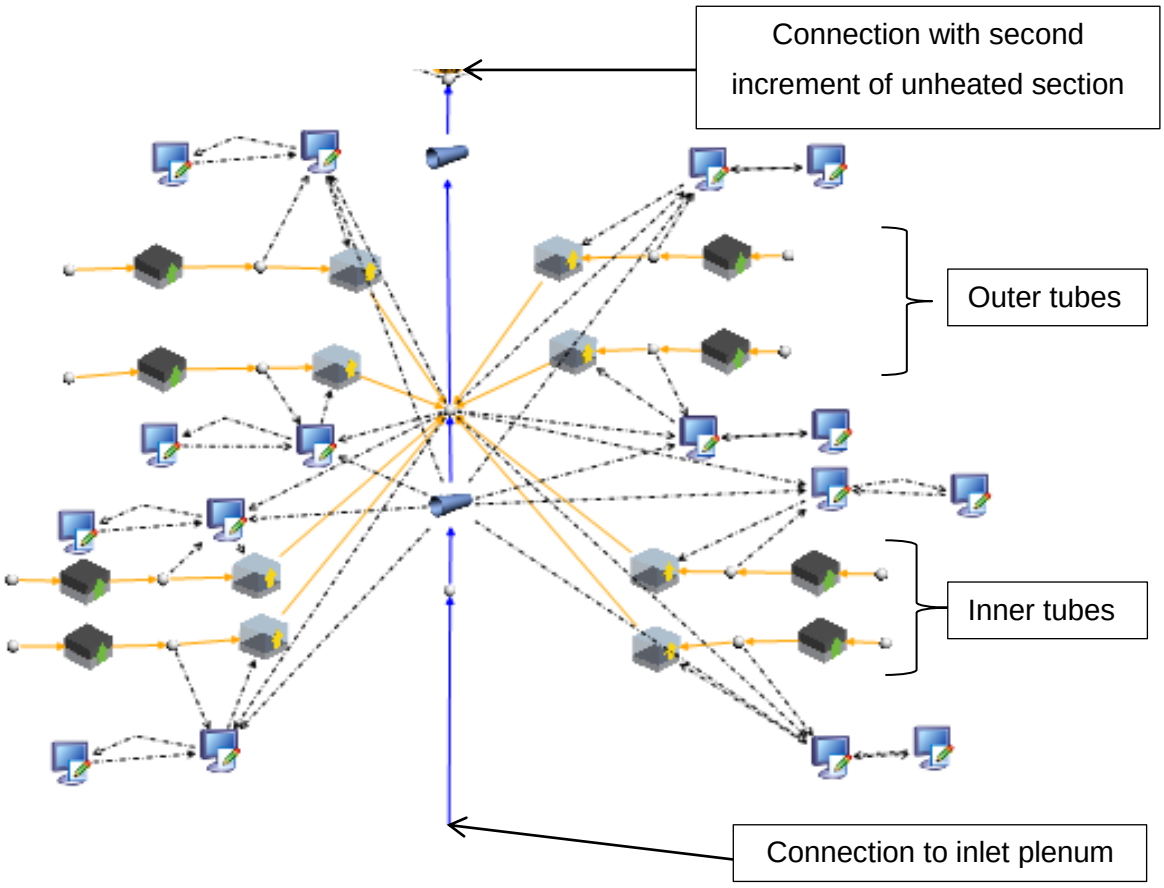

Figure 6.2-2. The unheated section of the riser tube of the NACEF in Flownex.

6.2.7 Heated riser tube section

A single increment of the heated section of the cavity is shown in Figure 6.2-3. The fluid flows of the outer and inner riser tubes are grouped together and represented by a single flow element (pipe in Figure 6.2-3). The representative tube has 8 surfaces and therefore there are 8 different flow paths for the heat transfer (all of which have been accounted for). The surface to surface radiation within the cavity, as well as within the riser tubes, has been accounted for as shown in Figure 6.2-3. Finally the axial conduction in the cavity walls and the riser tube walls has also been accounted for. The cavity air is represented by a single node (control volume) per increment, as opposed to four control volumes in the GAMMA+ model. The air properties in the cavity would therefore be represented by averaged values. Note that in the figure it appears as though there are four nodes, but they are in fact the same node. There are 20 increments like the one shown in Figure 6.2-3, with the bottom increment connecting to the unheated section (Figure 6.2-2) and the top increment connecting to the outlet plenum (Figure 6.2-6). The figure corresponds to “W2_Heater”, “F2_RCavity”, “W3_RiserTube” and “F1_LoopRiser” in the GAMMA+ model in Figure 3.2-1.

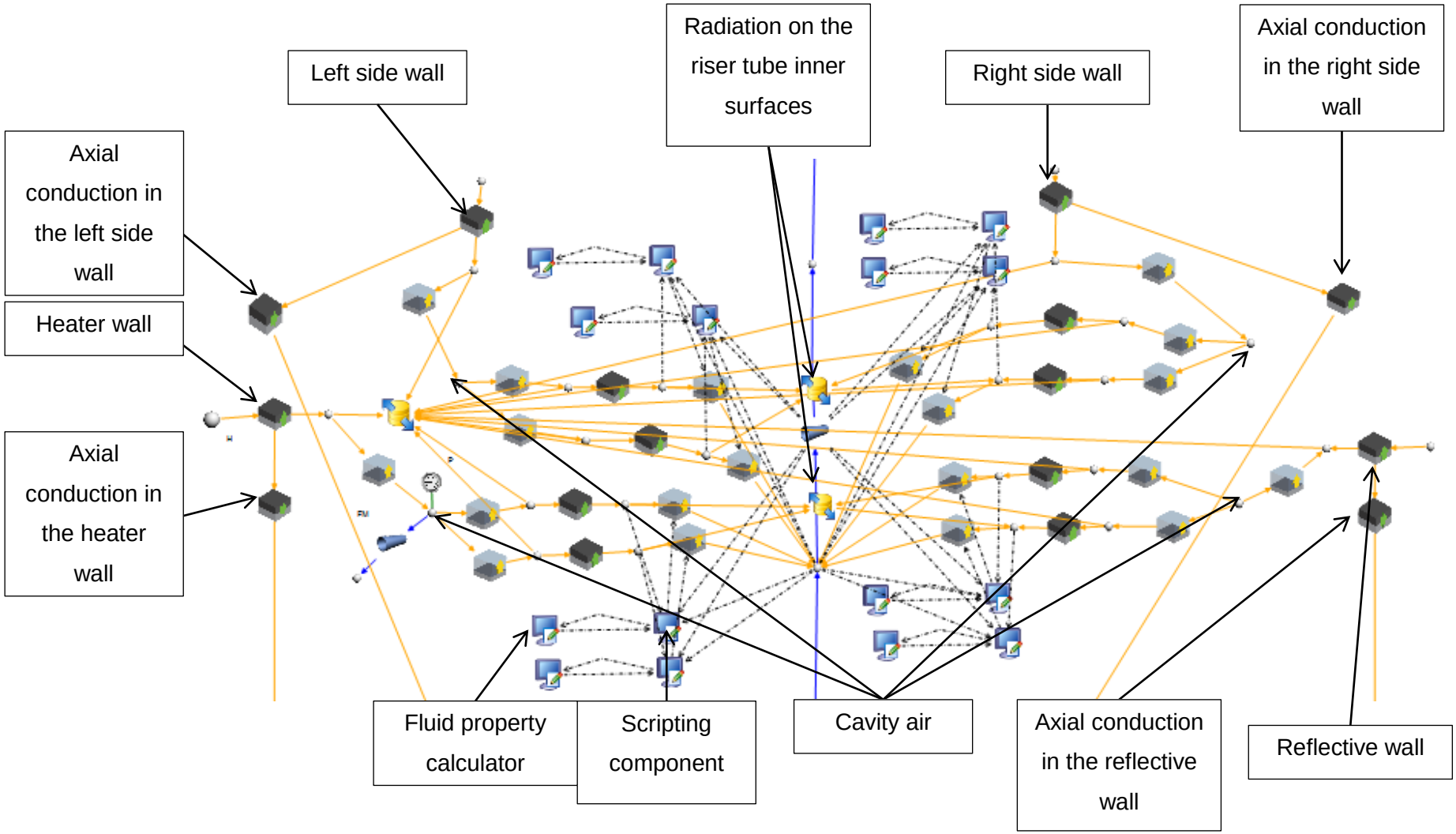

Figure 6.2-3. A single increment of the heated section of the NACEF model in Flownex.

The tangential conduction in the riser tubes was modelled as shown in Figure 6.2-4. The nodes represent a midpoint of the surface. The conduction elements model the heat transfer between the surfaces of the riser tubes. The four walls of the riser tube are represented by two nodes each.

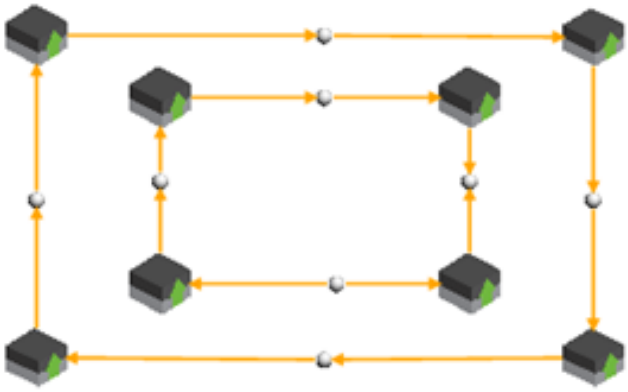

Figure 6.2-4. Modelling of the tangential conduction in Flownex.

The axial conduction in the riser tube is accounted for as shown in Figure 6.2-5. Similarly to the tangential conduction, each wall of the riser tube has two conduction elements (for the inner and outer part of each wall) for modelling the heat transfer. The axial conduction would account for the heat transfer between the vertically stacked increments.

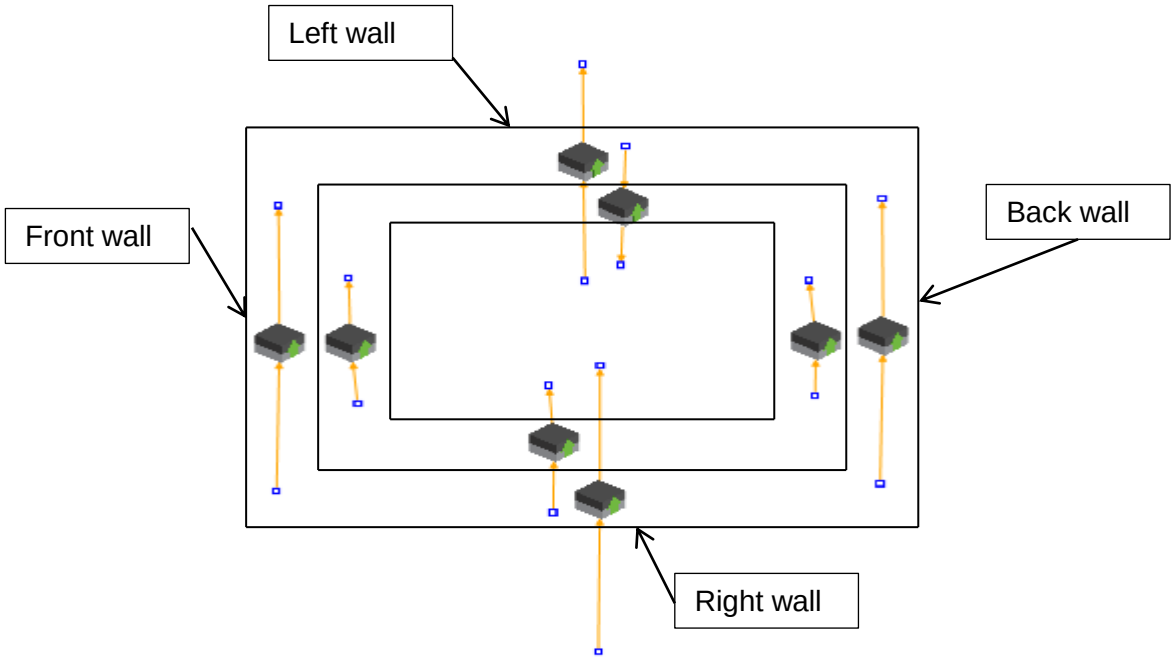

Figure 6.2-5. Axial conduction in the riser tube in Flownex.

The elements in Figure 6.2-4 and Figure 6.2-5 would then be connected to the applicable nodes in Figure 6.2-3.

6.2.8 Outlet of the facility

The outlet of the NACEF as modelled in Flownex is shown in Figure 6.2-6. The connection to the riser tubes is indicated in the figure. The outlet consists of outlet pipe 1, outlet pipe 2 and the chimney. All of which are divided into increments. One of the chimneys is choked for the purpose of the simulation. The pressure boundary condition was applied as shown in the figure. The figure corresponds to "F1_Loop_Outcham", "F1_Loop_OutPipe1", "F1_Loop_Outpipe2" and "F1_Loop_Chimney" in the GAMMA+ model in Figure 3.2-1.

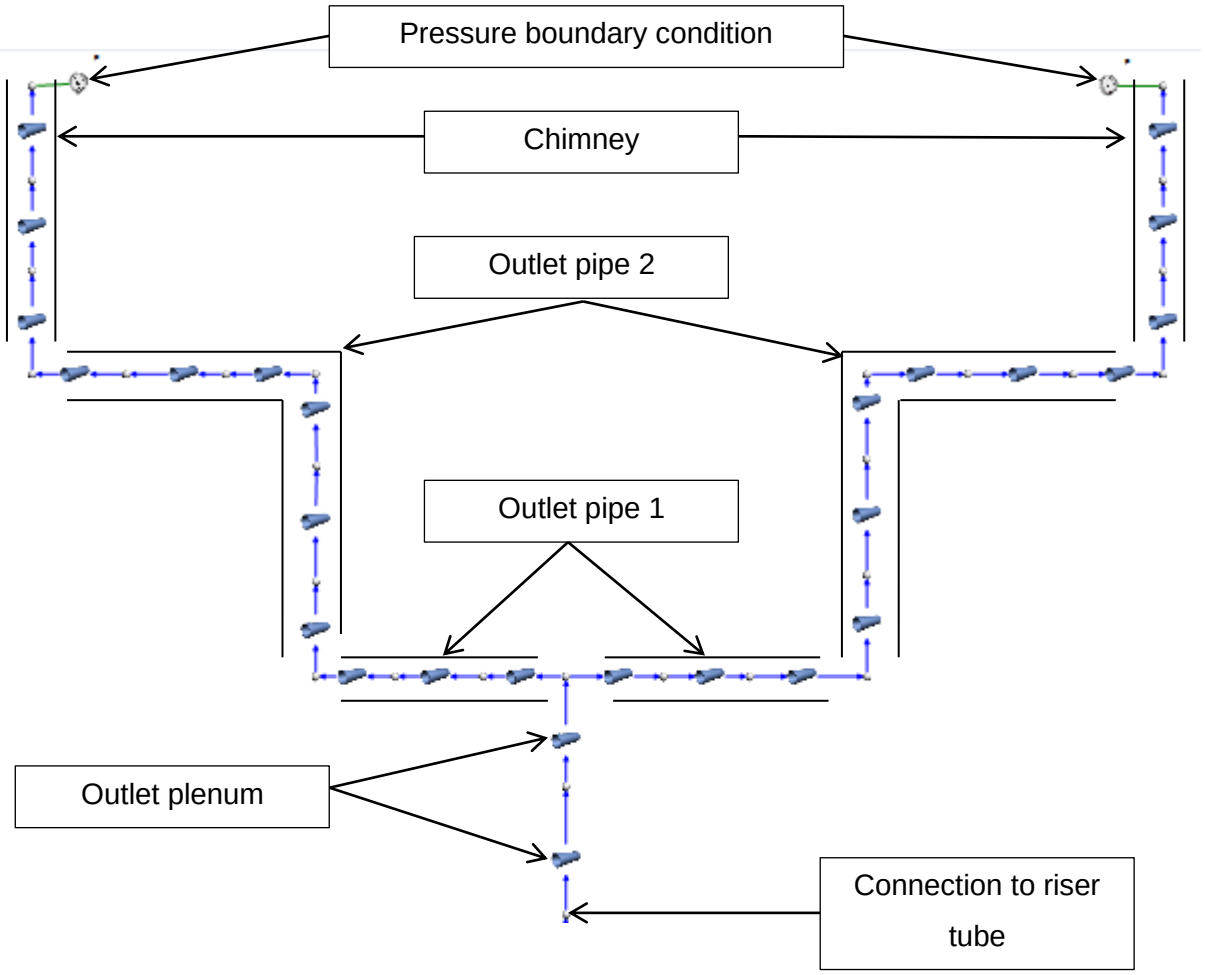

Figure 6.2-6. Outlet of the NACEF in Flownex.

6.2.9 Thermal radiation between the cavity surfaces

The thermal radiation between the cavity surfaces is modelled as shown in Figure 6.2-7. The walls are represented by surface radiation elements, which accounts for the surface emissivity. The radiation heat transfer between the surfaces is modelled by spatial radiation heat transfer elements, on which the specific view factor was applied.

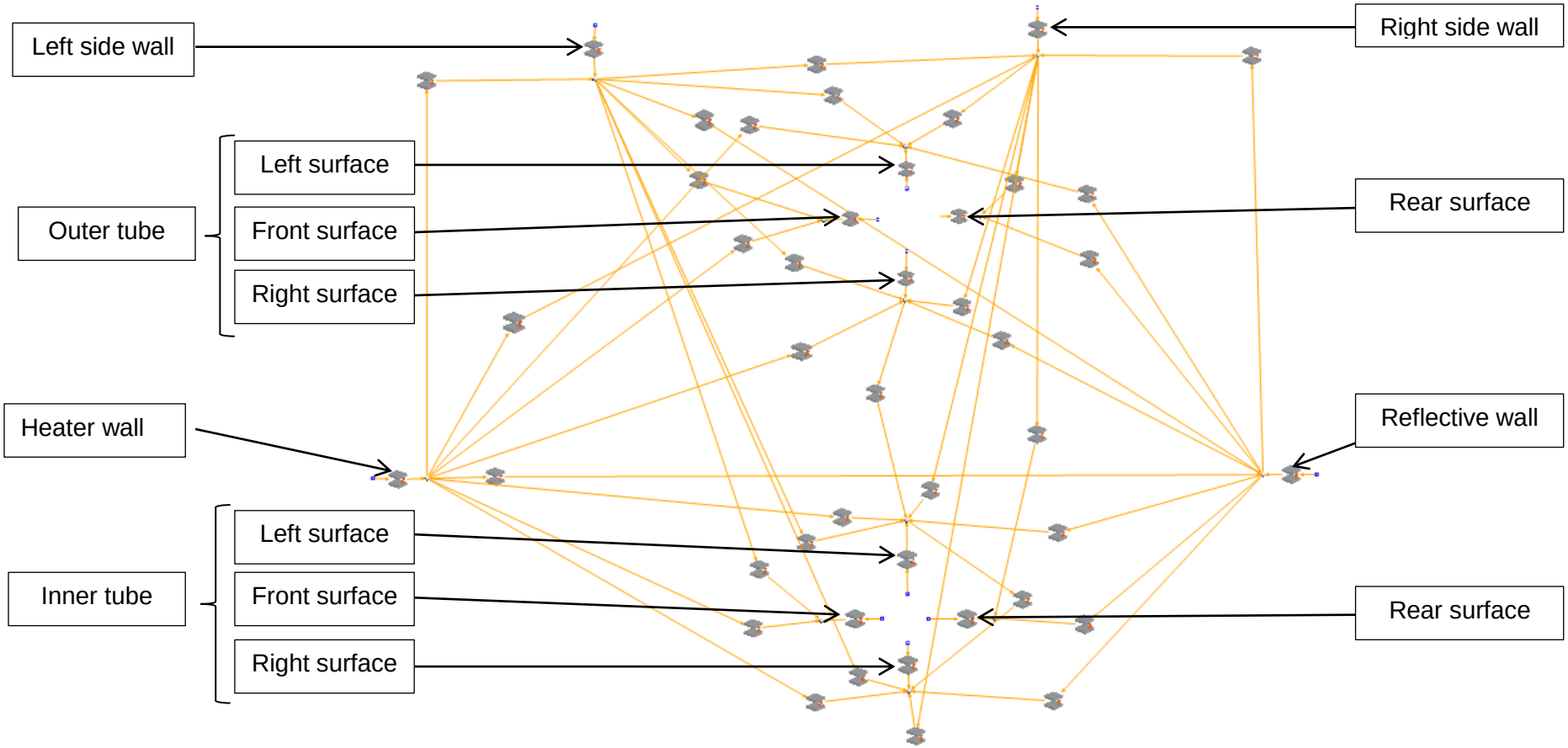

Figure 6.2-7. Thermal radiation network in Flownex.

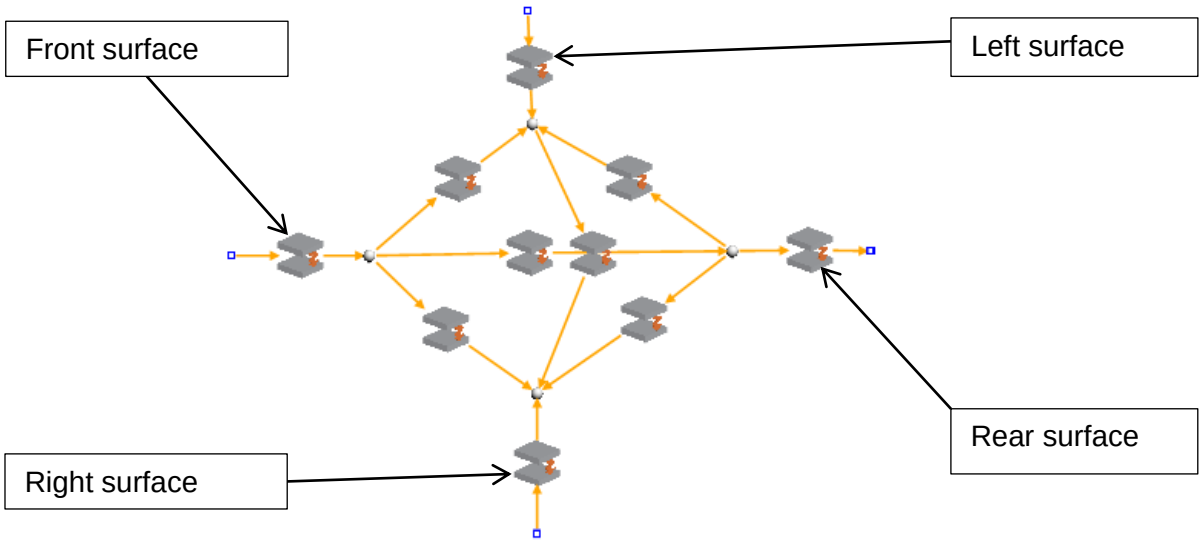

Figure 6.2-8. Thermal radiation heat transfer network for the riser tubes in Flownex.

Similarly to Figure 6.2-7, the riser tube inner surfaces are represented by surface radiation elements (indicated in Figure 6.2-8). The radiation exchange is modelled by spatial radiation elements, which account for the view factor.

The radiation networks in Figure 6.2-7 and Figure 6.2-8 were connected to each increment as shown in Figure 6.2-3. The radiation heat transfer was thus modelled in the horizontal direction only. The radiation heat transfer in the vertical direction between the increments was neglected.

Other input properties are given in Table 6.2-1.

Table 6.2-1. Input properties of the model.

Property	Value
Material	AISI 304 Stainless steel
Emissivity	
Heater wall	0.75
Left side wall	0.1
Right side wall	0.1
Reflective wall	0.1
Riser tube walls	0.8
Riser tube dimensions	
Wall thickness	0.005 m

Length (outer dimension)	0.25 m
Width (outer dimension)	0.05 m
Hydraulic diameter	0.0685714 m

The wall areas (cavity walls, as well as, riser tube walls) are the same as specified in Table 5.5-1. It is therefore not repeated here.

6.3 Simulation details

Several different variations of the model were simulated. The details of the simulations are given in sections 6.3.1 to 6.3.5. The main simulations of importance for the study were the baseline model and the modified inputs model. The other simulations were done to gauge the behaviour of the system under certain circumstances.

6.3.1 The baseline model

Firstly the model was simulated for the following boundary conditions:

Table 6.3-1. Boundary conditions of the baseline model.

Property	Value
Inlet pressure (kPa)	101.46
Outlet pressure (kPa)	101.3
Inlet temperature (°C)	24
Heat input (kW/m^2)	4.34

The inlet pressure boundary condition was chosen to reflect purely hydrostatic flow.

6.3.2 The modified model

Secondly, the boundary conditions were modified slightly. The boundary conditions are as follows:

Table 6.3-2. Boundary conditions of the modified model.

Property	Value
Inlet pressure (kPa)	101.466
Outlet pressure (kPa)	101.3
Inlet temperature (°C)	12
Heat input (kW/m^2)	2.65

The material of the solid parts in this model was changed from stainless steel to plain carbon steel.

6.3.3 Two-flow-path model

Third, the flow path was split and the inner and outer tubes` flow paths were modelled individually. The boundary conditions were the same as in the baseline model. The intention was to observe the system`s behaviour to verify the accuracy of the simplifying assumption of one representative flow path.

6.3.4 Unrestricted chimneys

Fourth, the flow restriction in the “left outlet pipe 1” in Figure 6.2-6 (“F1_Loop_OutLpipe1” in the GAMMA+ model in Figure 3.2-1) was removed. A mass flow rate could therefore develop in both chimneys. The minor loss coefficient for the junction (Table 3.3-1) was previously set very large. In this case the minor loss coefficient was set as the same value as the other outlet pipe (right side outlet pipe 1 in Figure 6.2-6). The boundary conditions were the same as in the baseline model.

6.3.5 Pressure pulse transient case study

Fifth, a transient study was done to determine the model`s sensitivity to flow reversals. The pressure boundary condition at the top of one of the chimneys was modified to reflect a temporary increase in pressure caused by meteorological conditions. The pulse was set to occur for 20 seconds where after the pressure would drop back to atmospheric pressure. This model is not intended to accurately predict the phenomena, but rather an attempt to see

the behaviour of the system under these conditions. This study has not been verified against GAMMA+, but the same correlations are implemented as in the verified simulations. One of the limiting factors is that the convection heat transfer coefficients on the cavity surfaces would change as a function of time during a transient. Since these coefficients are inserted into the model as inputs, it would be cumbersome to simulate an accurate case. The change in the coefficients on the cavity surfaces is assumed to be relatively small, which means that the model does possess some authority in predicting the phenomena.

Figure 6.3-1 shows the inlet plenum and outlet pipes of the NACEF.

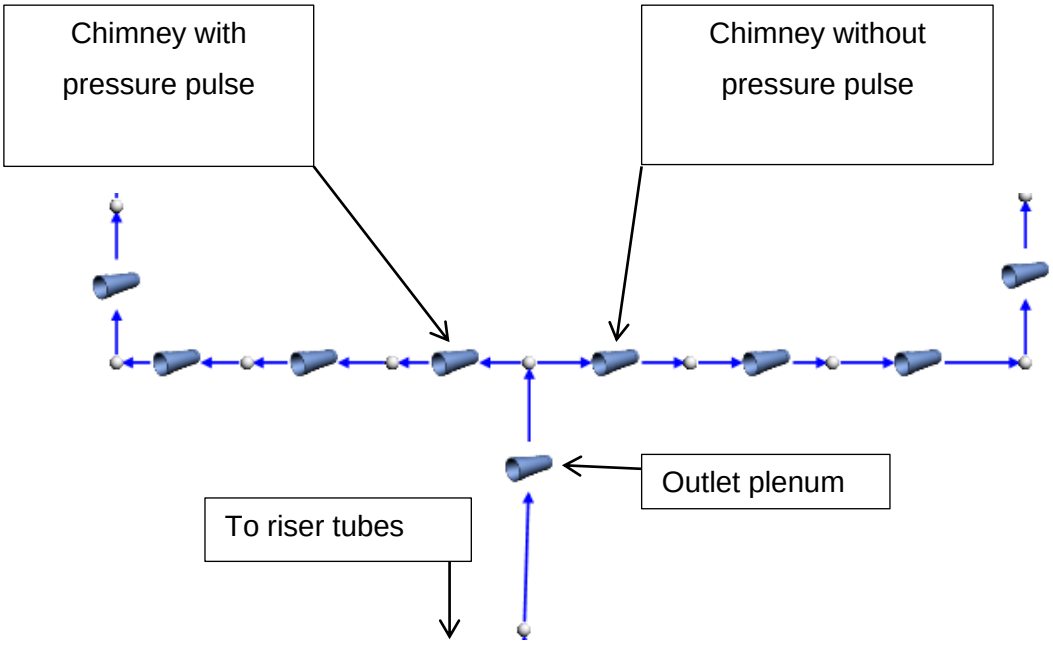

Figure 6.3-1. Inlet plenum and chimney of the NACEF in Flownex.

6.4 Conclusion

The details concerning the Flownex simulation models have been discussed. Several variations have been simulated. The baseline model and the modified model have been simulated to have exactly the same conditions as the corresponding GAMMA+ models. These simulations serve as the basis of the verification of this study. Subsequent simulations have not been verified and merely to get an indication of the system`s behaviour under the specified conditions. The results of the specified simulations are discussed in the next chapter.

Chapter 7 - Results and discussion

The results for the different simulations are discussed in this chapter. Section 7.1 contains the results for the baseline model, section 7.2 contains the results for the modified inputs model, sections 7.3 and 7.4 contain the results for the two-flow-path and unrestricted flow models respectively. Section 7.5 contains the results for a transient case study. The temperature distribution as a function of the elevation was used as a measure of the level of agreement between the results. Most of the graphs therefore represent a comparison between the temperatures as a function of elevation in the heated cavity as calculated in Flownex and GAMMA+. Note that the convergence criteria used in Flownex was 1E(-6).

7.1 Steady state results of the baseline model

The Flownex simulation described in section 6.3.1 yielded the following results. The riser tube air temperature is plotted as function of elevation in Figure 7.1-1. It is compared with the corresponding GAMMA+ results.

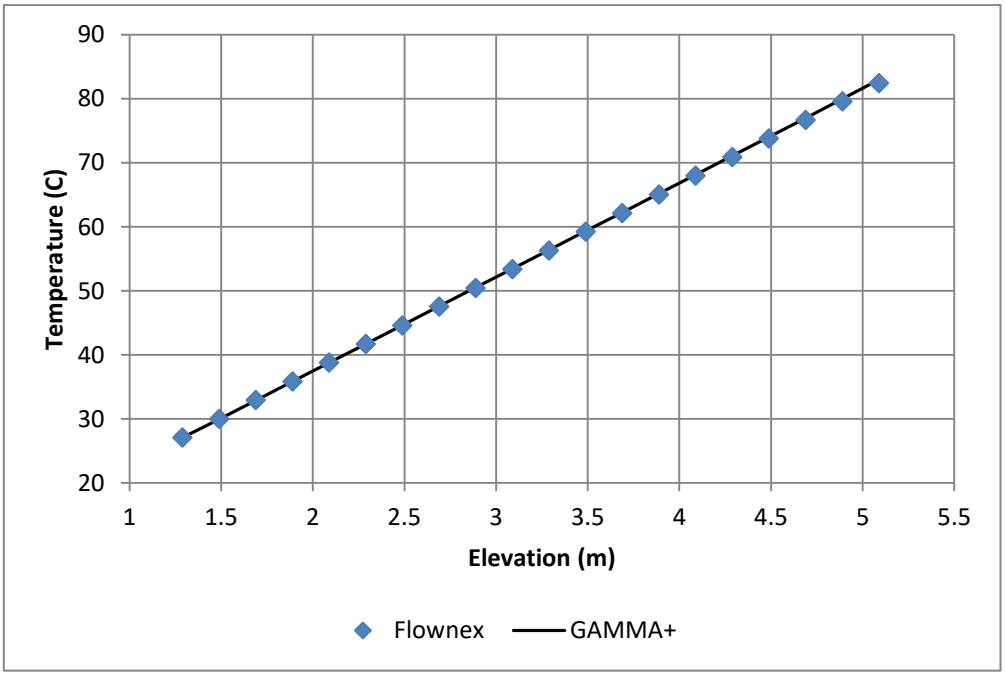

Figure 7.1-1. Riser tube air temperature as a function of elevation.

The percentage difference between the corresponding data points has been calculated which in turn was averaged over the spectrum of data points. The calculation yielded an average difference of 0.23%. This method was implemented for all the data shown in this chapter to

serve as a measure of the agreement between the results of the two codes. The results are in very good agreement.

A graph illustrating the percentage difference between results of Figure 7.1-1 is shown in Figure 7.1-2. The maximum percentage difference is at the highest elevation. The largest percentage difference is however relatively small.

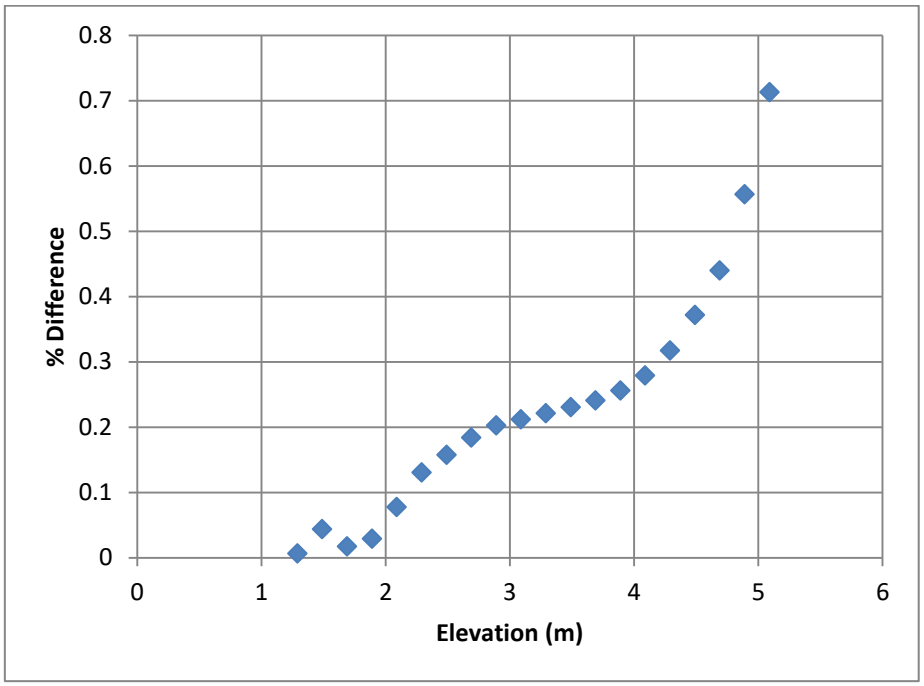

Figure 7.1-2. Percentage difference in the riser tube air temperature.

Figure 7.1-3 and Figure 7.1-4 show the cavity wall temperatures as function of elevation. The results show good agreement. The average difference between results is as follows: 1.23% for the heater wall, 1.41% for the reflective wall, 0.91% for the left side wall and 1.32% for the right side wall. The temperatures show a gradual increase with an increase in elevation. The difference in the calculated temperatures at the highest elevation most noticeable in Figure 7.1-4 is due to the difference in the values obtained for the fluid properties by the two codes.

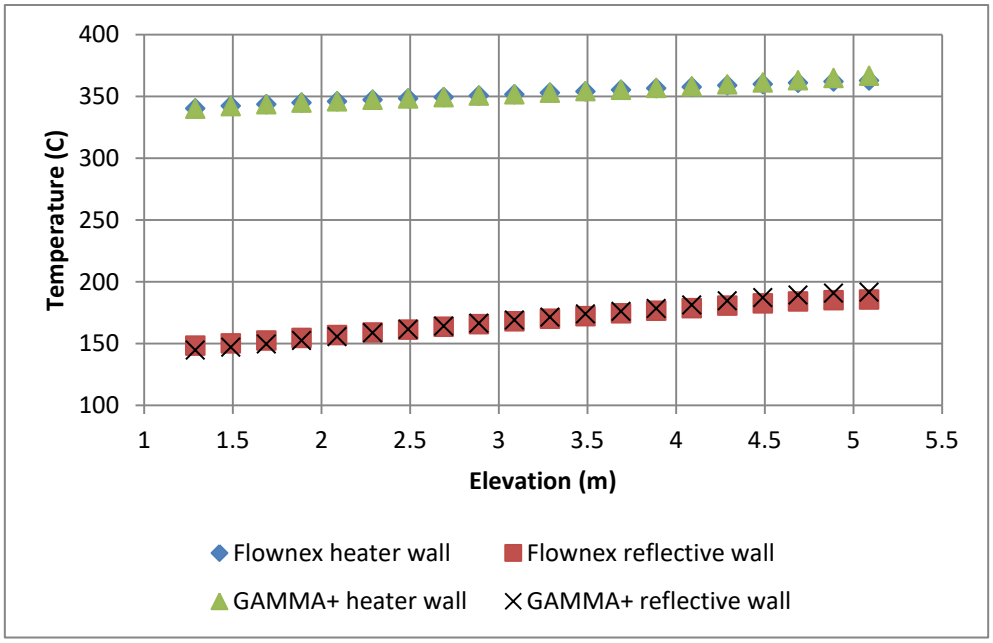

Figure 7.1-3. Heater and reflective wall temperatures as function of elevation.

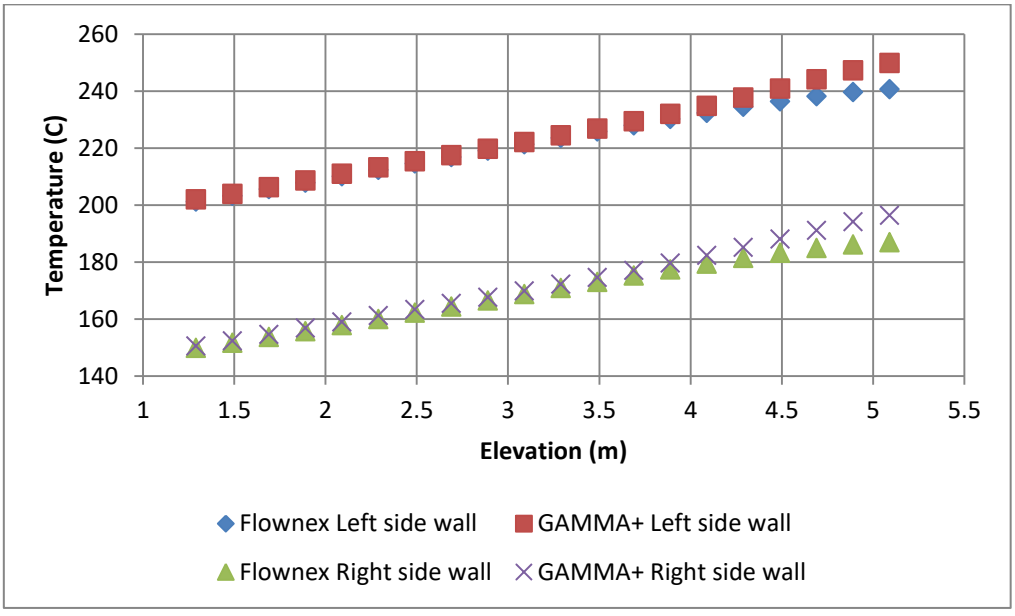

Figure 7.1-4. Left side and right side wall temperatures as function of elevation.

The convection heat transfer coefficient as calculated in GAMMA+ and Flownex are compared in Figure 7.1-5. The coefficient plotted in the graph represents the average of the coefficients on the eight riser tube walls at a given elevation. The results show good agreement with an average difference of 1.52%.

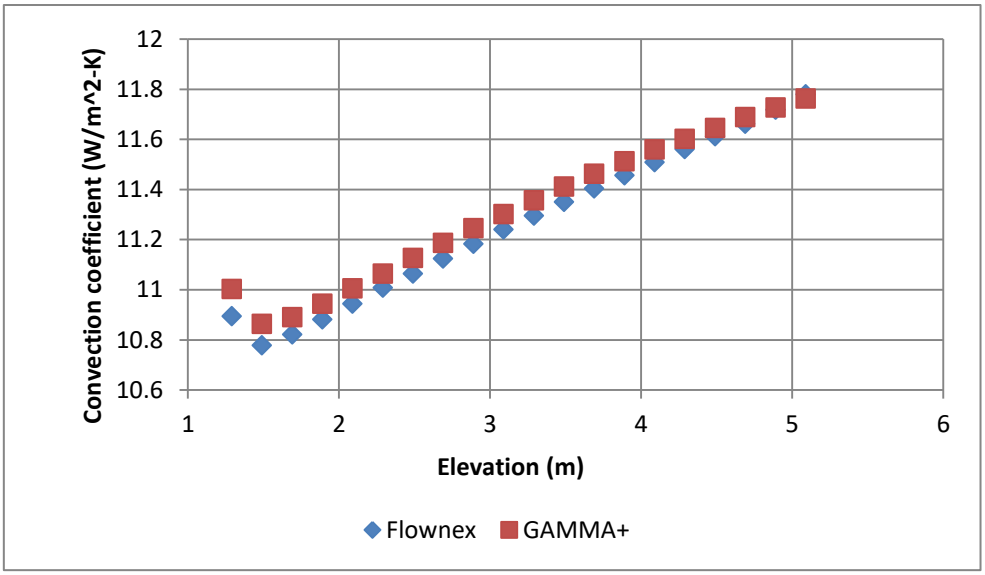

Figure 7.1-5. Convection heat transfer coefficient as a function of elevation.

Predictably, the temperatures show a gradual increase with an increase in elevation (Figure 7.1-1, Figure 7.1-3 Figure 7.1-4). The minimum temperatures are at the lowest elevation, while the maximum temperatures are reached at the top of the cavity i.e. the highest elevation.

The convection heat transfer coefficient plotted in Figure 7.1-5 also shows an overall gradual increase with elevation. The first data point is higher than the second, third and fourth data points. This is possibly due to the axial conduction in the riser tube wall. Heat escapes downward to the unheated section by mechanism of conduction, resulting in a lower temperature in the first increment of the heated section. The lower temperature causes a higher convection heat transfer coefficient to be calculated in the first increment. Another reason can be explained through Equation 4.2-3, which is repeated for convenience:

$$\boldsymbol{Nu} = \left(\left|\boldsymbol{Nu}_{\boldsymbol{forced}}^{\boldsymbol{3}} - \boldsymbol{Nu}_{\boldsymbol{free}}^{\boldsymbol{3}}\right|\right)^{\frac{\boldsymbol{1}}{\boldsymbol{3}}}$$

The forced convection Nusselt number dominates the free convection Nusselt number in the equation, since air is just entering the heated section and the density gradient is still small. As the air travels higher into the riser tube, the heater induces an ever increasing density gradient in the air, increasing the free convection Nusselt number. The overall Nusselt number is therefore larger than for the second increment, leading to a larger convection heat transfer coefficient to be calculated at that location.

The regime of the flow is plotted on the regime map proposed by Metais & Eckert (1964) in Figure 7.1-6. The regime falls within the mixed convection regime, since it falls between the Aicher criterion line (from Equation 4.2-1), and the Burmeister line (from Equation 4.2-2). The Reynolds number for the forced convection sub component is larger than 5000, which means the regime is turbulent mixed convection. Note that the data point corresponding to the lowest elevation is located at the very right of the graph.

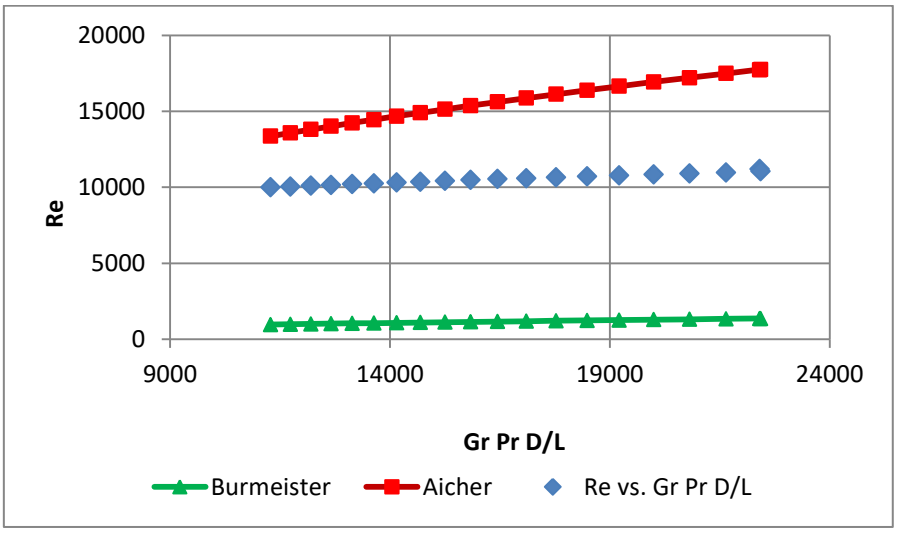

Figure 7.1-6. Regime map of the flow in the riser tube.

7.2 Steady state results of the modified inputs model

The modified case consisted of a decreased heat input, different material for the solids and a lower air temperature at the inlet. The model`s inputs are described in section 6.3.2. The riser tube air temperature as calculated by GAMMA+ and Flownex is compared in Figure 7.2-1. The temperature at the riser outlet (highest elevation in the graph, is higher than is the case in the baseline model. The reason is that the mass flow rate was higher in the baseline model, meaning the air was exposed to the heater for a shorter time than in the modified input model.

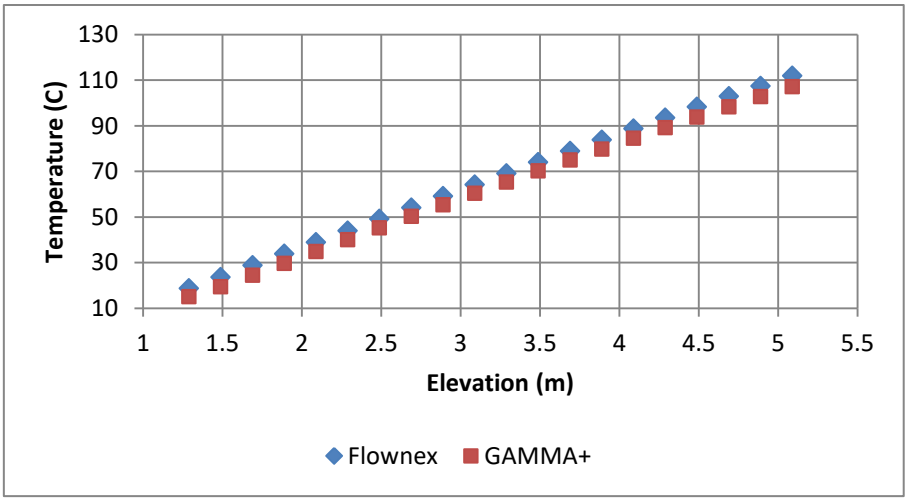

Figure 7.2-1. Riser tube air temperature as a function of elevation.

Figure 7.2-2 shows the percentage difference between GAMMA+ and Flownex for the riser tube air temperatures from Figure 7.2-1. Conversely to the baseline model case, the highest deviation is at the lowest elevation.

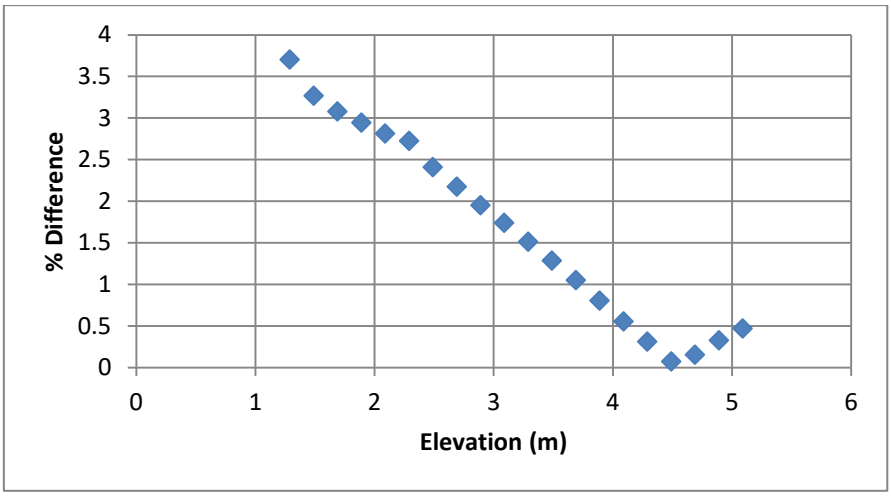

Figure 7.2-2. Percentage difference between GAMMA+ and Flownex in the riser tube air temperature at a given elevation.

The explanation for the difference in trend in Figure 7.1-2 and Figure 7.2-2 is as follows: since the fluid properties are different in the two codes, the largest difference would be where the influence of the fluid properties is the highest. In calculating the mixed convection, the forced- and free convection subcomponents are important. The dimensionless parameter important to free convection is the Grashof number, calculated in Equation 4.1-7, repeated here for convenience:

$$Gr = \frac{g\beta(T_s - T_\infty){D_h}^3}{\nu^2}$$

Since the fluid property (kinematic viscosity) is squared in the equation, a small difference in the fluid property in the codes has a notable effect in the results. In the case of the forced convection subcomponent, the Reynolds number equation does not contain any squared parameters. Therefore, where the free convection dominates, the larger difference between the results from the two codes will be obtained.

The heater- and reflective wall temperatures are compared in Figure 7.2-3. The average difference is 0.52% and 1.3% respectively. Similar to the baseline model, the maximum temperatures are at the highest elevation.

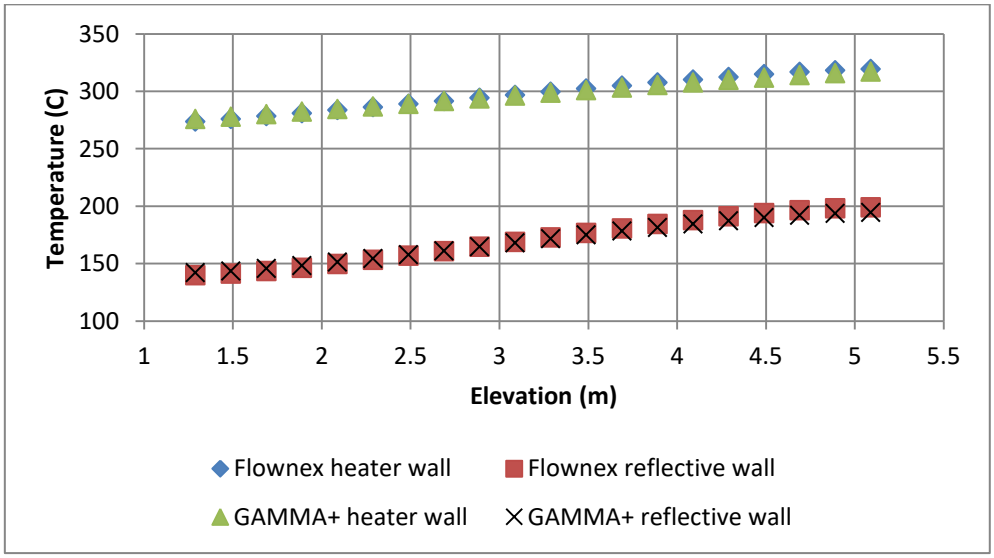

Figure 7.2-3. Heater wall and reflective wall temperature as a function of elevation.

The left-side and right-side wall temperatures are compared in Figure 7.2-4. The average difference in the results is 1.38% and 1.28% respectively.

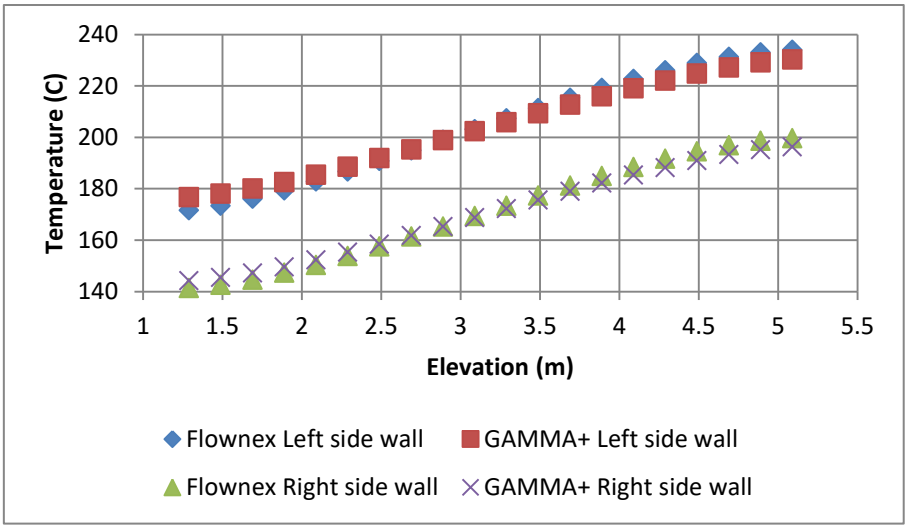

Figure 7.2-4. Left-side and right-side wall temperature as a function of elevation.

The convection heat transfer coefficient on the inner surfaces of the riser tubes are compared in Figure 7.2-5. The average difference in the results is 1.02%.

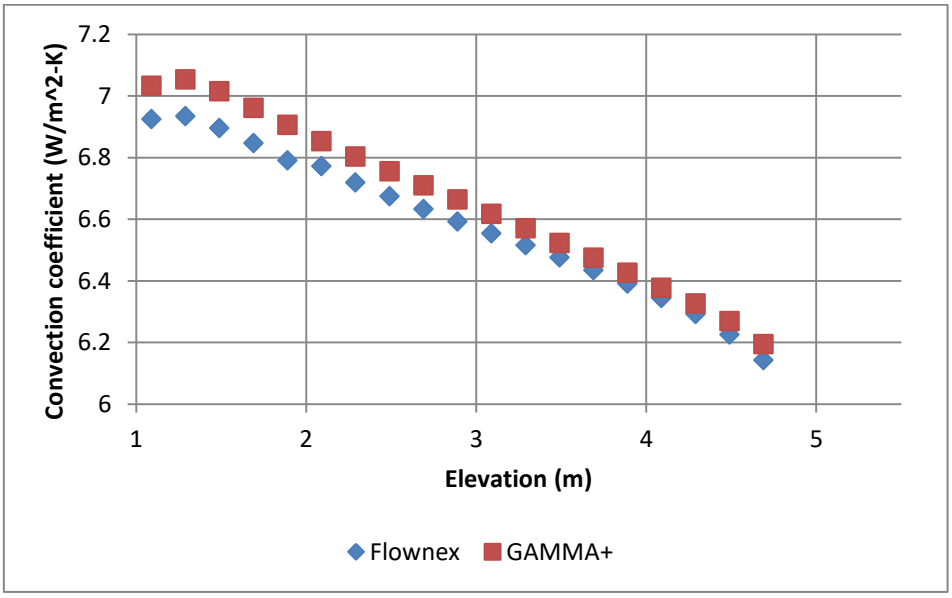

Figure 7.2-5. Convection heat transfer coefficient as a function of elevation.

The convection heat transfer coefficient in the modified case exhibits the opposite behaviour to that in the baseline case. The coefficient decreases with an increase in elevation. This occurrence is owed to laminarizational effects in the flow path. The Reynolds number decreases with an increase in elevation, which means that the forced convection subcomponent moves closer towards laminar flow. The free convection Nusselt number in

Equation 4.2-3 (repeated here for convenience) is comparable in magnitude to the forced convection Nusselt number.

$$\boldsymbol{Nu = \left(\left|Nu_{forced}^3 - Nu_{free}^3\right|\right)^{\frac{1}{3}}}$$

The Nusselt number therefore deceases. The heat transfer coefficient is calculated by Equation 4.1-6 rewritten as:

$$\boldsymbol{h = \frac{Nu * D_h}{k}}$$

The convection coefficient is also a function of k, the conductivity. The conductivity increases as a function of elevation, which means the convection coefficient decreases.
The combined effect of the Nusselt number decreasing and the fluid conductivity increasing means that the convection heat transfer coefficient decreases with an increase in elevation.

The regime map of the flow in the riser tube is shown in Figure 7.2-6. The flow falls under the mixed convection regime, since Re vs. Gr*Pr*D/L lies between the Aicher and Burmeister lines. In this case, the forced convection subcomponent falls within the transitional flow regime, since the Reynolds number lies between 3200 and 5000.

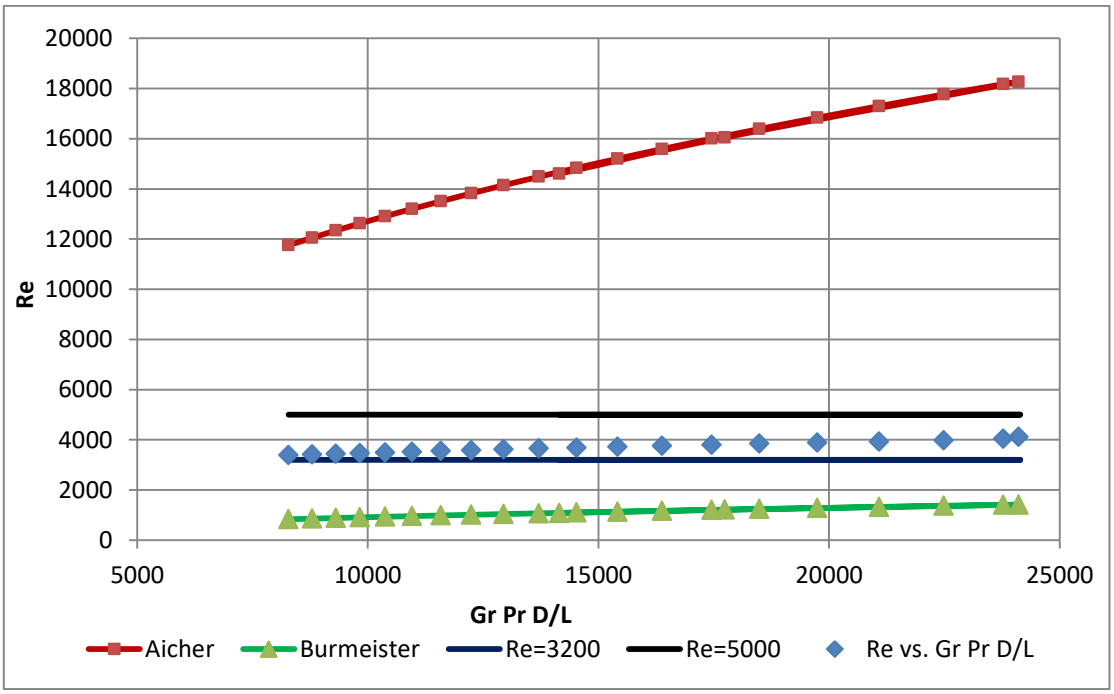

Figure 7.2-6. Regime map of the flow in the riser tube.

7.3 Steady state results of the two-flow-path model

The baseline model was adjusted by splitting the flow path into two paths. The riser tube air temperatures are compared in Figure 7.3-1. The temperatures show very little difference between the two different approaches. The average percentage difference between the temperatures was 0.90%.

The mass flow rate in the inner tube was 0.128 kg/s and the mass flow rate in the outer tube was 0.0638 kg/s. The total mass flow rate in the two-flow path system was 0.192 kg/s, which is the same mass flow rate as in the baseline model. The temperature distribution in the cavity is slightly different, with an average difference of 2% between the baseline model and two-flow path model. The temperatures are slightly higher in the latter model. The result implies that the simplifying approach was valid, since the results are in very good agreement. The simplified model does however underestimate the maximum temperatures

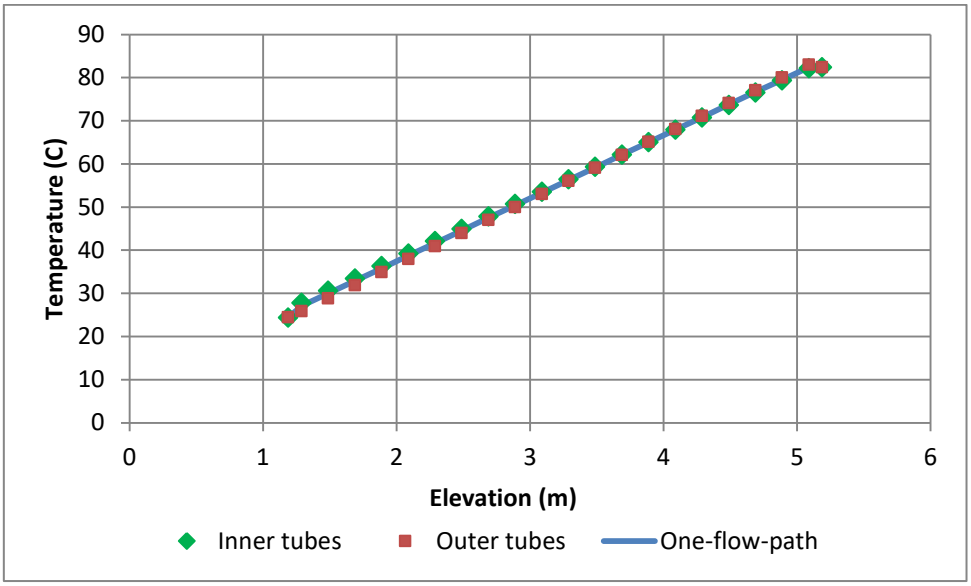

Figure 7.3-1. Riser tube air temperature as a function of elevation.

7.4 Steady state results of the unrestricted flow path model

A next approach was to remove the restriction in one of the chimneys. A very large minor loss coefficient was previously applied to the component labelled “outlet pipe 1” in Figure 6.2-6 which is the same component as “F1_loop_outLPipe1” in Figure 3.2-1. In this simulation the minor loss coefficient was set to the same value as in the case of the other outlet pipe. This change allowed an airflow rate to develop in both chimneys. The total mass flow rate in the unrestricted flow path system is 0.196 kg/s as opposed to 0.192 kg/s for the

restricted flow path system. The air temperature at the outlet of the restricted flow path system is higher, at 82.40 °C versus 81.17 °C for the unrestricted flow path system.

The riser air temperature is compared in Figure 7.4-1 for the restricted vs. unrestricted flow path system. The temperatures show very little difference, with a maximum difference of 1.06%. The restricted flow path system has slightly higher temperatures, owing to the longer duration that the air is exposed to the heater in this configuration, due to the lower mass flow rate.

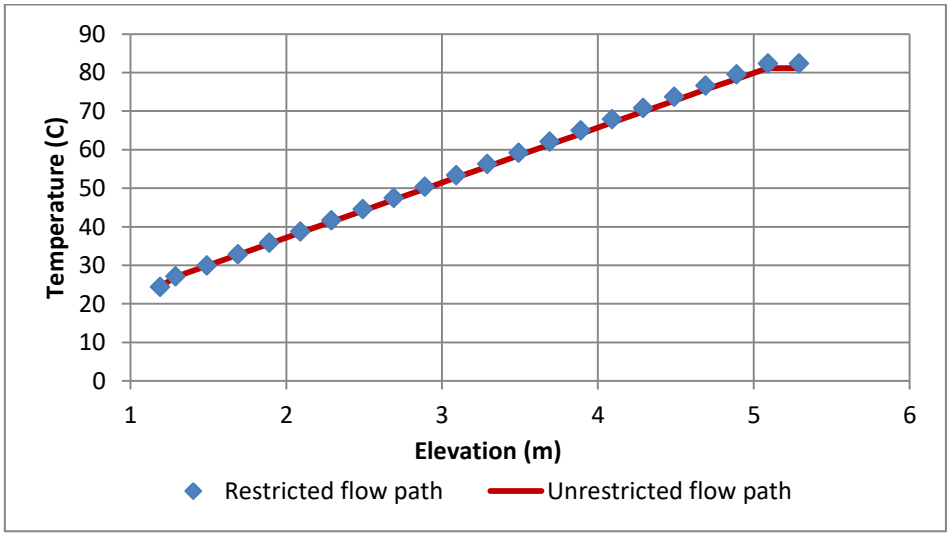

Figure 7.4-1. Riser tube air temperature comparison for a restricted and unrestricted flow path.

7.5 Pressure pulse transient case study

The system was run at steady state for 50 seconds, where after a pressure pulse was specified for 20 seconds. The system`s vulnerability against flow reversals was thereby investigated.

Three different pulses were investigated, namely 101.302 kPa, 101.303 kPa and 101.4 kPa. The mass flow rates in the outlet plenum and the two chimneys are plotted as a function of time in Figure 7.5-1, Figure 7.5-2 and Figure 7.5-3 for the three pressure pulses.

The mass flow rate response following a pressure pulse of 101.302 kPa is shown in Figure 7.5-1. The pulse resulted in stagnant air in the chimney in which the pressure pulse occurred. The mass flow rate eventually returned to the original direction after the pulse was removed (in the chimney that experienced the pulse). The chimney in which no pulse occurred had an increase in mass flow rate for the duration of the pulse, where after the

mass flow rate returned to the initial rate. The mass flow rate in the outlet plenum decreased slightly for the duration of the pulse.

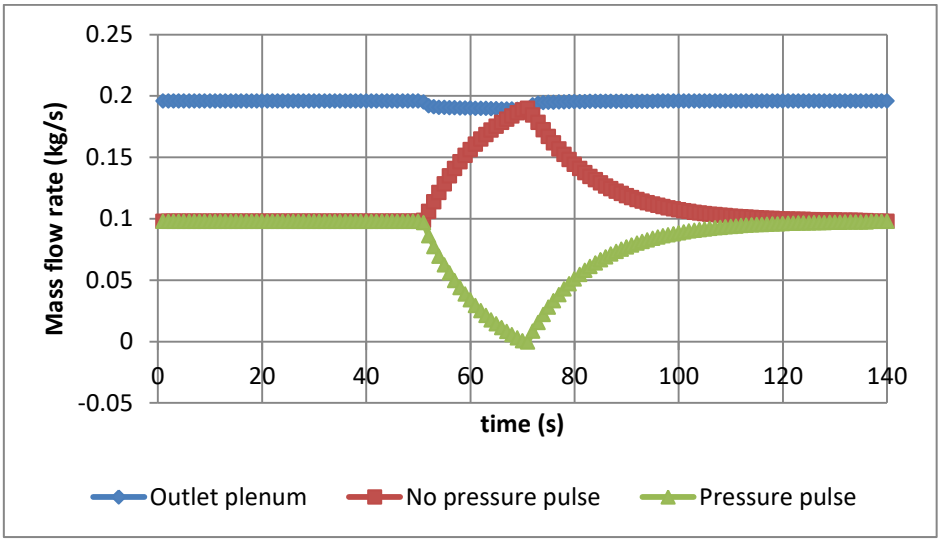

Figure 7.5-1. Mass flow rate as function of time with pressure pulse of 101.302 kPa.

The mass flow rate response after a pressure pulse of 101.303 kPa is shown in Figure 7.5-2. The pulse results in a flow reversal (in the chimney subjected to the pressure pulse). After the pulse was removed, the direction of the mass flow rate did not return to the original flow direction and this chimney became a secondary inlet. The chimney in which no pressure pulse occurred, experienced an increase in mass flow rate which stabilised at 0.282 kg/s. The mass flow rate of the outlet plenum decreased to 50% of its original value.

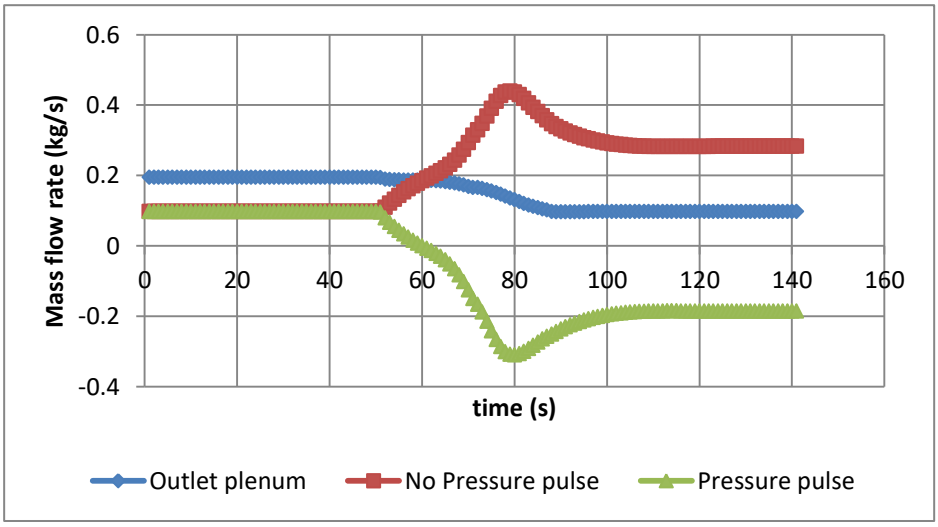

Figure 7.5-2. Mass flow rate as a function of time with a pressure pulse of 101.303 kPa.

When a pressure pulse of 101.4 kPa was specified (Figure 7.5-3), the behaviour was similar to the previous case. The mass flow rates showed a faster response time to the pulse being applied and removed than in the previous cases. The mass flow rate in the inlet and riser section also reversed when the pressure pulse was applied, but recovered to the original flow direction after the pulse was removed.

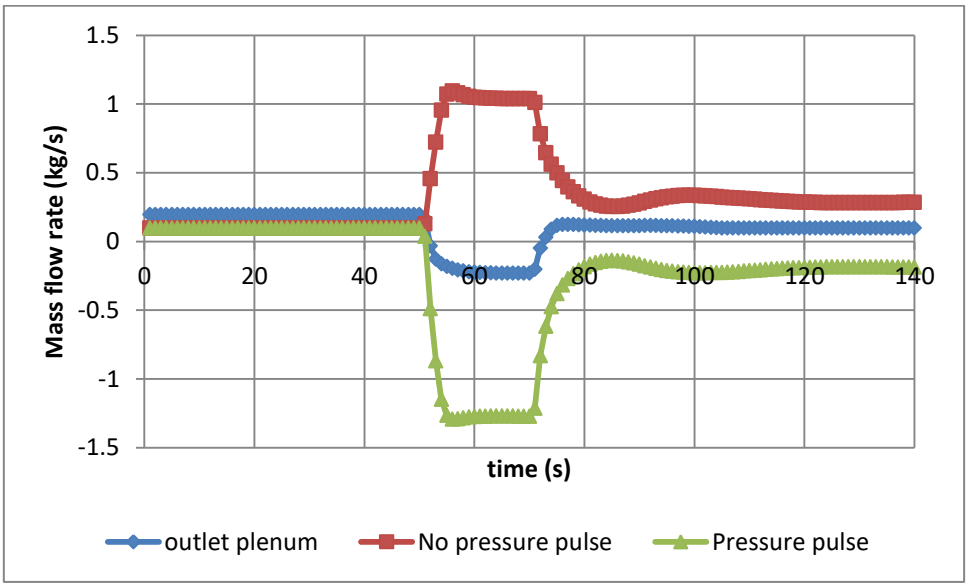

Figure 7.5-3. Mass flow rate as a function of elevation with a pressure pulse of 101.4 kPa.

7.6 Conclusion

The various simulation results have been compared and discussed. The results from Flownex were compared with the GAMMA+ results for the baseline and modified cases. The steady state results show very good agreement which implies both programs solve the system in a similar manner. A transient case study was done to determine the behaviour of the system under the condition that a pressure pulse occurred in one of the chimneys.

Chapter 8 - Conclusion and recommendations

The natural cooling experimental facility (NACEF) was constructed by the Korea Atomic Energy Research Institute (KAERI). The facility is a ¼ scale model of the reactor cavity cooling system (RCCS) of the PMR200 nuclear reactor design. The facility aids in validating the multi-dimensional system code, GAMMA+, for being used to simulate the thermal-hydraulic phenomena in a RCCS.

The NACEF has been modelled using the simulation code Flownex. The flow regime within the riser tube falls under the mixed convection regime. The Nusselt numbers were therefore interpolated between the forced convection- and free convection Nusselt numbers. Flownex does not account for flow in the mixed convection regime. The correlations used in GAMMA+ were therefore incorporated in Flownex.

The mixed convection regime has some peculiarities which influences heat transfer. For the turbulent regime, if the forced- and free convection is in the same direction (aiding flow), the Nusselt number decreases and heat transfer is impaired. The reason is that a laminarization occurs in the flow in the boundary layer.

The important surface and fluid temperatures obtained by using the two codes have been compared. The results show very good agreement, which indicates that the two codes solve the relevant phenomena in a similar manner. The small differences between the results are attributed to the following:

- Differences in the calculation of fluid properties.
- Different methodology in calculating frictional and minor losses.
- The capability of GAMMA+ to model the recirculating flow in the cavity with a 3D approach. Flownex can only model convection and conduction heat transfer between stationary flow nodes in the cavity.

The steady state results of the models described in section 6.3.1 and 6.3.2 form the basis of the study. These models have been verified, since the Flownex and GAMMA+ results are in agreement. The other simulations have not been explicitly verified due to the unavailability of corresponding GAMMA+ results. However, since the flow falls within the scope of the verified cases, the results can be seen as a representation of the possible behaviour of the system.

A recommendation for further study is to investigate the difference in the results if all six flow paths were to be considered individually.
Consideration should be given to couple Flownex with an appropriate code that is capable of calculating the convection heat transfer coefficients on the cavity surfaces.
A further possible investigation is the effect of the elevation of the outlet. The change in the hydrostatic pressure at the inlet could cause the system to behave differently.

A further recommendation in terms of the design of the RCCS is, to modify the geometry so as to induce turbulence on the surfaces of the riser ducts. The laminarizational effect caused by the aided mixed convection is undesirable for the operation of the RCCS. The surface of the riser duct can be made to have a higher roughness, have dimples, or have other turbulence inducing geometry to ensure turbulent flow. A recommendation for further study would therefore be to model these proposed solutions to investigate the system`s behaviour and performance.

References

Aicher, T. & Martin, H. 1996. New correlations for mixed turbulent natural and forced convection heat transfer in vertical tubes. *International journal for heat and mass transfer*, 40(15): 3617-3626.

Allan, T., Busby, J., Meyer, M. & Petti, D. 2010. Materials challenges for nuclear systems. *Materials today*, 13(12): 14-23.

Argonne National Laboratory. 2015. The NSTF at Argonne: Passive Safety and Decay Heat Removal for Advanced Nuclear Reactor Designs. http://www.ne.anl.gov/capabilities/rsta/nstf/index.shtml. Date of access: 2015/07/24.

Bae, Y., Hong, S. & Kim, Y. 2012. Scaling analysis of reactor cavity cooling system for PMR200. Proceedings of the HTR 2012. Tokyo, Japan, October 28 – November 1, 2012.

Celata, G.P., D'Annibale, F., Chiaradia, A. & Cumo, M. 1998. Upflow turbulent mixed convection heat transfer in vertical pipes. *International journal of heat and mass transfer,* 41(1998): 4037-4054.

Chapin, D., Kiffer, S. & Nestell, J. 2004. The very high temperature reactor: a technical summary. www.mpr.com/uploads/news/very-high-temperature-reactor.pdf. Date of Access: 2016/09/13.

Du Toit, C.G. 2016. Comparison of the GAMMA+ and Flownex philosophies. Doc. No.: CNE-2016-002, North-West University.

Du Toit, C.G., Rousseau, P.G., Jun, J.S. & Noh, J.M. 2014. 1D and 3D numerical simulation of the reactor cavity cooling system of a very high temperature reactor. Proceedings of the 15th international heat transfer conference, IHTC-15. August 10-15, Kyoto, Japan.

Frisani, A., Hassan, Y.A. & Ugaz, V.M. 2010. Computational dynamics analysis of very high temperature gas-cooled reactor cavity cooling system. *Nuclear technology*, 176 :238-259. http://www.osti.gov/scitech/servlets/purl/1044181. Date of access: 2015/07/20.

General Atomics. 1996. Gas turbine-modular helium reactor (GT-MHR) conceptual design description report. pbadupws.nrc.gov/docs/ML0224/ML022470282.pdf. Date of access: 2015/08/30.

Hall, W.B. & Jackson, J.D. 1969. Laminarization of a turbulent pipe flow by buoyancy forces. *ASME* 69-HT-55.

IAEA. 2008. Accident analysis for nuclear power plants with modular high temperature gas cooled reactors. http://www-pub.iaea.org/MTCD/Publications/PDF/pub1318_web.pdf. Date of access: 2015/07/22.

Incropera, F.P., Dewitt, D.P., Bergman, T.L. & Lavine, A.S. 2013. Principles of heat and mass transfer. 7th ed. Hoboken, NJ: Wiley.

Kawaji,M., Valentin, F., Artoun, N., Banarjee, S., Sohal, M., Schultz, R., & McEligot, D. 2015. Investigation of abnormal heat transfer and flow in a VHTR reactor core. Doc. No.: Project No. 11-3218.

Kim, J., Bae, Y., Hong, S., Kim, C., Cho, B. & Kim, M. 2014. Results of the preliminary test in the ¼ scale RCCS of the PMR200 VHTR. Transactions of the Korean nuclear society autumn meeting, Pyeongchang, Korea, October 30-31.

Kim, S.H., Tak, N. & Kim, M. 2008. Comparison of axisymmetric and 3D simulations of the heat transfer in RCCS. Transactions of the Korean nuclear society autumn meeting, PyeongChang, Korea, October 30.

Khoza, S. 2015. Preliminary analysis of KAERI RCCS experiment using GAMMA+. Nuclear hydrogen project calculation note. Doc. No.: NHDD-RD-CA-14-009, KAERI.

Khoza, S., Tak, N., Lim, H., Lee, S., Cho, B. & Kim, J. 2015. Preliminary analysis of the KAERI RCCS experiment using GAMMA+. Transactions of the Korean Nuclear Society Spring Meeting, Jeju, Korea, May 7-8.

Korea Atomic Energy Research Institute. 2014. Transient gas multicomponent mixture analysis code for analysing the thermo-fluid transients in an VHTR; Vol. 2 GAMMA+ Theory Manual. Doc. No.: NHDD-RD-CA-13-035, Rev.00.

Lamarsh, J.R. & Baratta, A.J. 2014. Introduction to nuclear engineering. 3rd ed. Harlow, Essex: Pearson.

Lee, J., No, H. & Hejzlar, P. 2009. Evaluation of system codes for analysing naturally circulating gas loop. *Nuclear engineering and design*, 239: 2931-2941.

Lisowski, D.D. & Farmer, M.T. 2014. Experimental observations of natural circulation flow in the NSTF at steady-state conditions. Proceedings of the HTR 2014. Weihai, China, October 27-31.

Lomperski, S., Ponter, W.D., Tzanos, C.P., Wei, T.Y.C. & Krauss, A.R. 2011. Generation IV nuclear energy system initiative: Air cooled option RCCS studies and NSTF preparation. www.ipd.anl.gov/anlpubs/2012/11/71292.pdf. Date of access: 2015/07/18.

McEligot, D.M., McCreery, G.E., Schultz, R.R.. Lee, J., Hejzlar,P., Stahle, P. & Saha, P. 2006. Investigation of fundamental thermal-hydraulic phenomena in advanced gas-cooled reactors. Doc. No.: INL/EXT-06-11801.

Metais, B. & Eckert, E.R.G. 1964. Forced, mixed and free convection regimes. *Journal of heat transfer* 86(2), 295-296.

Minhwan, K. 2015. Status of VHTR thermo-fluid experimental researches in KAERI. https://www.iaea.org/NuclearPower/Downloadable/Meetings/2015/2015-01-12-01-15-NPTDS/21_Minhwan_Kim_KAERI_Experiments.pdf. Date of access: 2015/07/24.

Mei, D., Xing, F., Wen, M., Lei, P. & Fang, Z. 2015. Numerical simulation of mixed convection heat transfer of galvanized steel sheets in the vertical alloying furnace. *Applied thermal engineering*, 93(2016):500-508.

M-Tech Industrial. 2015. Flownex simulation environment. Flownex library theory manual.

Munson, B.R., Young,D.F., Okiishi, T.H. & Huebsch, W.W. 2010. Fundamentals of Fluid Mechanics. 6th ed. Wiley.

Park, R.J., Ha, K.S., Kim, S.B. & Kim, H.D. 2006. Two-phase natural circulation flow of air and water in a reactor cavity model under an external vessel cooling during a severe accident. *Nuclear engineering and design*, 236 (2006): 2424-2430.

Rousseau, P.G., du Toit, C.G., Jun, J.S. & Noh, J.M. 2015. Code-to-code comparison for analysing the steady-state heat transfer and natural circulation in an air-cooled RCCS using GAMMA+ and Flownex. *Nuclear engineering and design*, 291:71-89. http://www.sciencedirect.com/science/article/pii/S0029549315001910. Date of access: 2015/09/28.

Travis, B.W. & El-Genk, M.S. 2013. Numerical simulation and turbulent convection heat transfer correlation for coolant channels in a very-high-temperature reactor. *Heat transfer and engineering*, 34(1):1-14.

Tzanos, C.P. & Farmer, M.T. 2006. Feasibility study for use of the natural convection shutdown heat removal test facility (NSTF) for initial VHTR water-cooled RCCS shutdown. www.osti.gov/scitech/servlets/purl/932941. Date of access: 2015/08/30.

Appendix A - Node elevations and pipe lengths of Flownex model

The geometry in the Flownex model is built up out of nodes and pipe elements. The same discretization for the flow path was used than in GAMMA+ (described in section 3.2). The pipe lengths of the Flownex model (described in section 6.2) were adjusted to account for the difference in the calculation of the frictional losses.

The model is broken up into three sub parts for the purpose of the discussion. The inlet part is shown in Figure A-1. The figure lists the lengths of the pipes (solid lines) and the elevations of the nodes (circles).

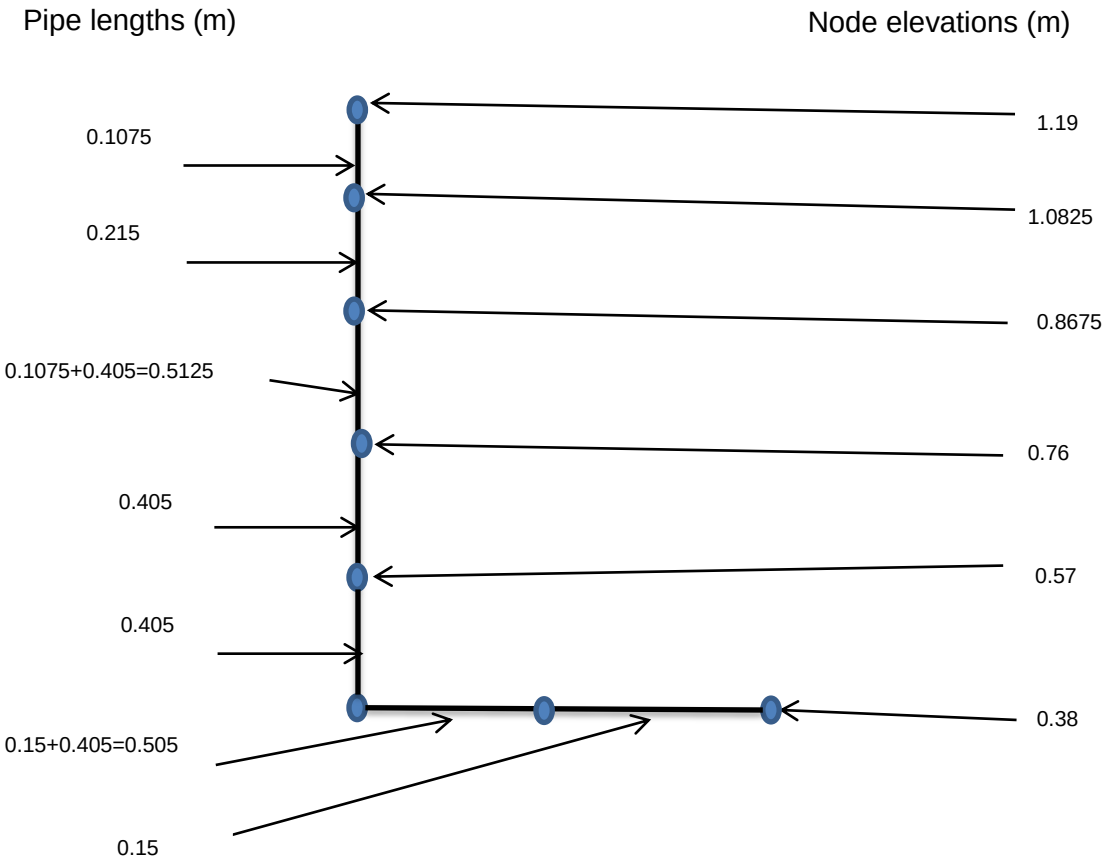

Figure A – 1. Node elevations and pipe lengths at the inlet of the Flownex model.

Similarly, the node elevations and pipe lengths of the riser tube are shown in Figure A-2.

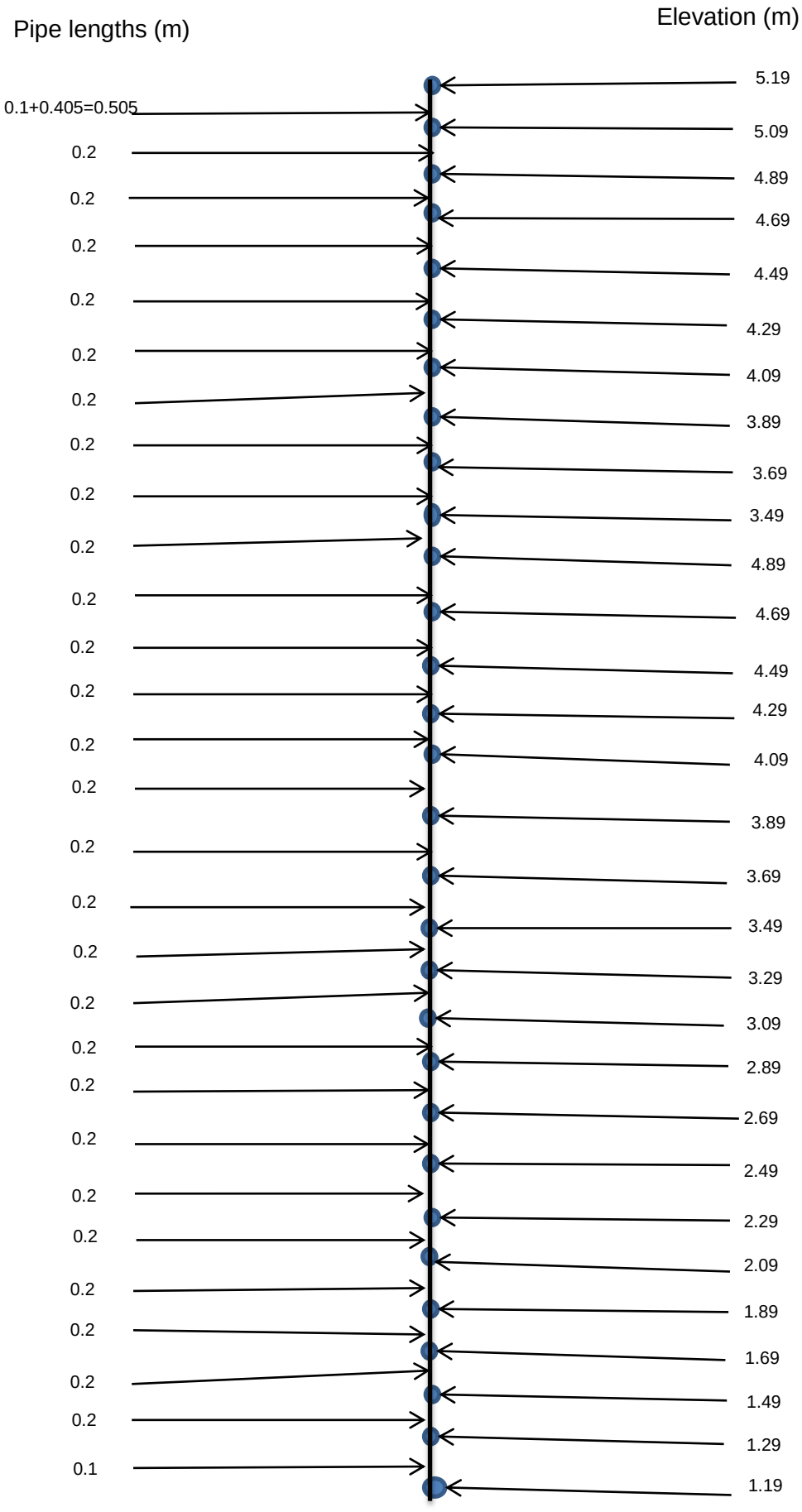

Figure A – 2. Riser tube pipe lengths and node elevations.

The node elevations and pipe lengths of the NACEF outlet are specified in Figure A-3

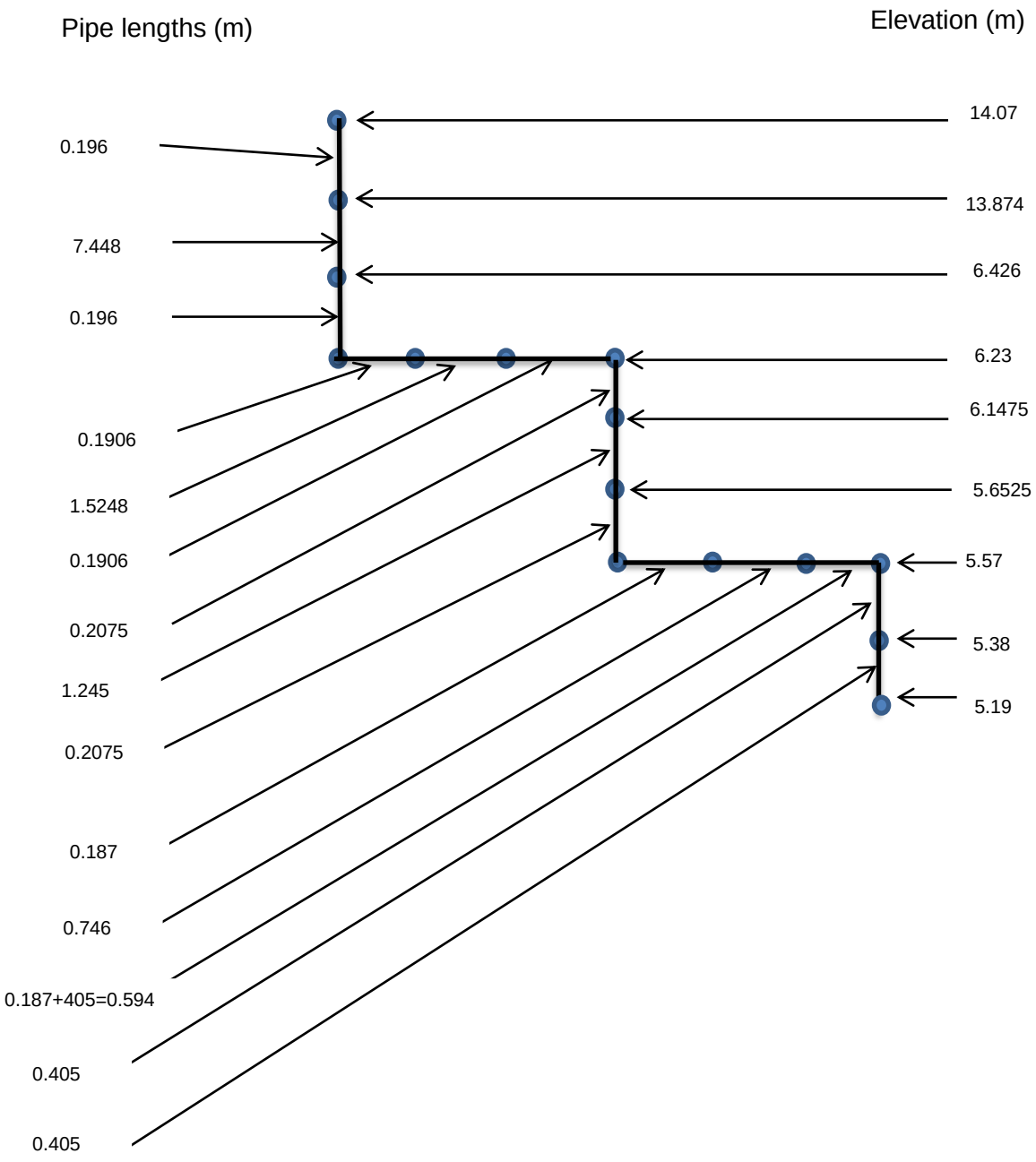

Figure A – 3. Outlet pipe lengths and node elevations in the Flownex model.

Appendix B - Flownex scripting component description

The programming code used in the Flownex scripting component to calculate the mixed convection heat transfer coefficient (based on the equations in section 4.2) is given in this section.

Programming in the script

```
double g = 9.806;

D_h.Value=4*A/P_w;
T_film.Value=0.5*(T_wall+T_fluid);
Bheta.Value=1/(T_film);
Gr.Value = Math.Pow(rho_calc,2) * g * Bheta * Math.Pow(D_h,3) * Math.Abs(T_wall-
T_fluid) / (Math.Pow(mu_calc,2));
Ra.Value = Gr * Pr_calc;
Re.Value= m_dot*D_h/(A*mu_calc);
eta.Value=Math.Pow(((T_fluid)/(T_wall)),0.5);

//Aicher criterion
Ai.Value= Math.Pow(Ra,0.333333)/( Math.Pow(Re,0.8)*Math.Pow(Pr_calc,0.4));

//Nusselt number for the transitional zone
if (Re < 5000)
{
 Nu_laminar.Value=5.91*eta;
  if (Re > 2300)
   {
     Nu_turbulent.Value=0.021* Math.Pow(5000,0.8)*Math.Pow(Pr_calc,0.4)*eta;

     //Fraction onf turbulent flow in transitional zone
     fr.Value=(Re-2300)/(5000-2300);
     Nu_forced.Value=Nu_turbulent*fr+Nu_laminar*(1-fr);
   }
}
```

```
//Nusselt number for laminar flow
if (Re < 2300)
{
 Nu_laminar.Value=5.91*eta;
 Nu_forced.Value=Nu_laminar;
}
//Nusselt number for turbulent flow
if (Re > 5000)
{
  Nu_turbulent.Value=0.021* Math.Pow(Re,0.8)*Math.Pow(Pr_calc,0.4)*eta;
  Nu_forced.Value=Nu_turbulent;
}

//Aicher criterion for forced convection
if (Ai < 0.05)
{
  Nu.Value=Nu_forced;
}
//Aicher criterion for mixed convection
if (Ai > 0.05)
{
  if (Ai < 0.2)
  {
  //interpolation for mixed convection
  Nu_free.Value=Math.Pow( 0.825+ (0.387 * Math.Pow(Ra,0.166667)) / (    Math.Pow(1+Mat
h.Pow(0.492/Pr_calc,0.5625)  ,  0.296296  )        )            ,2 );
  Nu_forced_cubed.Value=Math.Pow(Nu_forced,3);
  Nu_free_cubed.Value= Math.Pow(Nu_free,3);
  Nu.Value= Math.Pow(Math.Abs(Nu_forced_cubed  -  Nu_free_cubed),(0.333333));
  }
}
//Aicher criterion for free convection
if (Ai > 0.2)
{
 Nu_free.Value=Math.Pow( 0.825+          (0.387 * Math.Pow(Ra,0.166667))     /    (    Math.P
ow(1+Math.Pow(0.492/Pr_calc,0.5625)  ,  0.296296  )        )            ,2 );
 Nu.Value=Nu_free;
```

```
}

h.Value=Nu * k_calc / D_h;
```

Appendix C - EES code for calculating the convection heat transfer coefficient.

The EES code to solve the simplified riser in section 5.2 is listed in this section. The code is intended to calculate the convection heat transfer coefficient for comparison with the coefficients calculated using GAMMA+ and Flownex.

EES code

```
Function Nusselt (Aicher_criterion,Nuss_forced,Nuss_free)
IF (Aicher_criterion < 0.05 ) THEN
Nusselt:=Nuss_forced

ELSE
Nusselt:=(abs(Nuss_forced^3-Nuss_free^3))^(0.333)

ENDIF
END

//constants
D_h= 0.068571 [m]
g=9.81
A=0.0576
L=0.2
A_2=0.66
ebs=10*10**(-6)

q={800}  {1380} 1790
t=0.005

//boundary conditions
m_[0]={0.18} {0.3}  0.4

T_0[1] =29.42 +273.15

P_0[21]=101.3*10**3

z_[0]=1.09
z_[21]=5.29

duplicate j = 1,20
m_[j]=m_[j-1]
m_[j]=rho_[j]*A*V_el_[j]
z_[j]=z_[j-1]+L

Q=m_[j]*Cp_[j]*(T_0[j+1]-T_0[j])
Q=h_convCoef_[j]*A_2*(T_wall_[j]-T_0[j])

//fluid properties
Cp_[j]=cp(air_ha,t=t_0[j],p=p_0[j])
rho_[j]=density(air_ha,t=t_0[j],p=p_0[j])
mu_[j]=viscosity(air_ha,P=P_0[j],T=T_0[j])

//Reynolds numbers
Re_bulk[j]=m_[0]*D_h/(mu_[j]*A)
```

```
Re_[j]=m_[0]*D_h/(mu_film_[j]*A)

//Bernoulli
P_0[j]+rho_[j]*V_el_[j]^2/2+rho_[j]*g*z_[j]=P_0[j+1]+rho_[j+1]*V_el_[j+1]^2/2+rho_[j+1]*g*Z_[j+1]+rho_[
j+1]*f_[j]*L*V_el_[j]^2/(2*D_h)

//friction factor
f_[j]=0.25*(log10(0.27*ebs/d_h+5.74/Re_bulk[j]^0.9))^(-2)

end

//Fluid mechanics
duplicate j=1,20

//fluid properties
  //Prandtl number
Pr_[j]=Prandtl(air_ha,T=T_film_[j],P=P_0[j])

  //Conductivity
k_[j]=conductivity(air_ha,T=T_film_[j],P=P_0[j])

{k_steel[j]=19.8 [W/m-K] {Incropera @ 600 K}}

  //viscosity
mu_film_[j]=viscosity(air_ha,t=t_film_[j],p=p_0[j])

Bheta_[j]=1/T_film_[j]

  //Film temperature
T_film_[j]=0.5*(T_wall_[j]+T_0[j])

  //density
rho_film[j]=density(air_ha,t=t_film_[j],p=p_0[j])

//specific heat
  Cp_film[j]=cp(air_ha,t=t_film_[j],p=p_0[j])

//Grashof number
Grashof_[j]=(rho_film[j]^2*g*Bheta_[j]*D_h^3*abs(T_wall_[j]-T_0[j]))/(mu_film_[j]^2)

//Rayleigh number
Rayleigh_[j]=Grashof_[j]*Pr_[j]

//Aicher criterion
Aicher_criterion_[j]=Rayleigh_[j]^(1/3)/(Re_[j]^(0.8)*Pr_[j]^(0.4))

//Dittus Boelter
Nuss_forced_[j]=0.021*Re_[j]^0.8*Pr_[j]^0.4*eta_[j]

//Churchill and Chu correlation (free convection)
Nuss_free_[j]=(0.825+(0.387*Rayleigh_[j]^(1/6))/(1+(0.492/Pr_[j])^(9/16))^(8/27))**2

//interpolation between free and forced convection Nusselt numbers
eta_[j]=sqrt(abs(T_0[j]/T_wall_[j]))

Nusselt[j]=Nusselt(aicher_criterion_[j],Nuss_forced_[j],Nuss_free_[j])

//Calculation of convection coefficient
h_convCoef_[j]=Nusselt[j]*k_[j]/D_h
```

```
end
rho_[21]=density(air_ha,t=t_0[21],p=p_0[21])
V_el_[21]=m_[0]/(rho_[21]*A)
```

Appendix D - Flownex/EES surface radiation calculation verification exercise.

The EES code for the simple radiative heat transfer problem in section 5.3.1 is listed in this chapter.

EES code

The EES code that was used:

```
//wall surface areas
A_1=1
A_2=1
A_3=1

//view factor
F_12=0.5

//conductivity of wall
k_1=15
k_2=15
k_3=15

//convection heat transfer coefficient
h_1=4.087
h_2=5.53
h_3=3.744

//inner wall surface temperatures
T_4=1200
T_5=500
T_6=1102.1734

//emissivities
ebsilon_1=0.8
ebsilon_2=0.4
ebsilon_3=0.8

//Stefan-Boltzmann constant
sigma=5.67*10**(-8)

//Wall thickness
l=0.001 [m]

//external heat input
q_ext=0

//wall 1 heat transfer
E_1=sigma*T_1^4
q_ext=q_cond_1+q_conv_1+q_rad_1
q_rad_1=F_12*A_1*(J_2-J_1)+F_12*A_1*(J_3-J_1)

//wall 2 heat transfer
E_2=sigma*T_2^4
q_ext=q_cond_2+q_conv_2+q_rad_2
q_rad_2=F_12*A_2*(J_1-J_2)+F_12*A_2*(J_3-J_2)
```

//wall 3 heat transfer
E_3=sigma*T_3^4
q_ext=q_cond_3+q_rad_3+q_conv_3
q_rad_3=F_12*A_3*(J_1-J_3)+F_12*A_3*(J_2-J_3)

//cavity convection
h_1*A_1*(T_1-T_7)+h_2*A_2*(T_2-T_7)+h_3*A_3*(T_3-T_7)=0

//convection heat transfer on walls
q_conv_1=h_1*A_1*(T_7-T_1)
q_conv_2=h_2*A_2*(T_7-T_2)
q_conv_3=h_3*A_3*(T_7-T_3)

//radiation heat transfer from walls
q_rad_1=(J_1-E_1)/((1-ebsilon_1)/(ebsilon_1*A_1))
q_rad_2=(J_2-E_2)/((1-ebsilon_2)/(ebsilon_2*A_2))
q_rad_3=(J_3-E_3)/((1-ebsilon_3)/(ebsilon_3*A_3))

//conduction heat transfer through walls
q_cond_1=-k_1*A_1/l*(T_1-T_4)
q_cond_2=-k_2*A_2/l*(T_2-T_5)
q_cond_3=-k_3*A_3/l*(T_3-T_6)

//energy balance
q_Eb1=Q_conv_1+q_rad_1
q_Eb2=q_conv_2+q_rad_2
q_Eb3=q_conv_3+q_rad_3

q_EB=q_Eb1+q_Eb2+q_Eb3

//Temperatures to Celcius
T_abs=273.15 [K]
T_1C=T_1-T_abs
T_2C=T_2-T_abs
T_3C=T_3-T_abs
T_4C=T_4-T_abs
T_5C=T_5-T_abs
T_6C=T_6-T_abs
T_7C=T_7-T_abs

Appendix E - Flownex/EES comparison of a single increment model

The EES code used to solve the one increment model in section 5.4 is listed in this chapter.

EES model program

The EES program that solves a single increment of the NACEF model is as follows:

```
//Single increment NACEF

//heat transfer areas
A_1=0.13 [m^2]
A_2=0.3684 [m^2]
A_3=0.1896 [m^2]
A_4=0.13 [m^2]

A_5=0.02 [m^2]
A_6=0.1 [m^2]
A_7=0.02 [m^2]
A_8=0.1 [m^2]

A_9=0.04 [m^2]
A_10=0.04 [m^2]
A_11=0.2 [m^2]
A_12=0.2 [m^2]

//view factors from surface 1
F_12=0.730695
F_13=0.032356
F_14=0.033363
F_15=0.040015
F_16=0.000318
F_17=0
F_18=0.026338
F_19=0.088991
F_110=0
F_111=0.01265
F_112=0.035274

//View factors from surface 2
F_23=0.010425
F_24=0.0002346
F_25=0.036469
F_26=0.025562
F_27=0
F_28=0.011584
F_29=0.068272
F_210=0
F_211=0.042176
F_212=0.032019

//View factors from surface 3
F_35=0
F_36=0.470379
F_37=0.034885
F_38=0.00366
```

F_39=0
F_310=0.035881
F_311=0.041068
F_312=0.014898

//View factors from surface 4
F_43=0.337573
F_45=0
F_46=0.00391
F_47=0.088577
F_48=0.060666
F_49=0
F_410=0.22547
F_411=0.074944
F_412=0.112892

//View factros from surface 8
F_811=0.816154

//view factors from surface 11
F_1112=0.407586

//convection heat transfer coefficients on outer cavity surfaces
h_1=5.069
h_2=3.48
h_3=2.383
h_4=2.44
h_5=2.593
h_6=3.963
h_7=4.117
h_8=4.131
h_9=2.707
h_10=4.181
h_11=4.211
h_12=4.175

//emissivity
ebsilon_1=0.75
ebsilon_2=0.8
ebsilon_3=0.1

//Stefann Boltzmann
sigma=sigma#

//Boundary conditions
m=0.19 [kg/s]
g=9.81 [m/s^2]

q=564.2 [W]

//Radiative heat transfer
E_1=sigma*T_1^4
E_2=sigma*T_2^4
E_3=sigma*T_3^4
E_4=sigma*T_4^4
E_5=sigma*T_5^4
E_6=sigma*T_6^4
E_7=sigma*T_7^4
E_8=sigma*T_8^4
E_9=sigma*T_9^4

E_10=sigma*T_10^4
E_11=sigma*T_11^4
E_12=sigma*T_12^4

//radiation on surface 1
(E_1-J_1)/((1-ebsilon_1)/(ebsilon_1*A_1))=A_1*F_12*(J_1-J_2)+A_1*F_13*(J_1-J_3)+A_1*F_14*(J_1-J_4)+A_1*F_15*(J_1-J_5)+A_1*F_16*(J_1-J_6)+A_1*F_17*(J_1-J_7)+A_1*F_18*(J_1-J_8)+A_1*F_19*(J_1-J_9)+A_1*F_110*(J_1-J_10)+A_1*F_111*(J_1-J_11)+A_1*F_112*(J_1-J_12)

//radiation on surface 2
F_21*A_2=F_12*A_1

(E_2-J_2)/((1-ebsilon_3)/(ebsilon_3*A_2))=A_2*F_21*(J_2-J_1)+A_2*F_23*(J_2-J_3)+A_2*F_24*(J_2-J_4)+A_2*F_25*(J_2-J_5)+A_2*F_26*(J_2-J_6)+A_2*F_27*(J_2-J_7)+A_2*F_28*(J_2-J_8)+A_2*F_29*(J_2-J_9)+A_2*F_210*(J_2-J_10)+A_2*F_211*(J_2-J_11)+A_2*F_212*(J_2-J_12)

//radiation on surface 3
A_3*F_31=A_1*F_13
A_3*F_32=A_2*F_23
(E_3-J_3)/((1-ebsilon_3)/(ebsilon_3*A_3))=A_3*F_31*(J_3-J_1)+A_3*F_32*(J_3-J_2)+A_3*F_34*(J_3-J_4)+A_3*F_35*(J_3-J_5)+A_3*F_36*(J_3-J_6)+A_3*F_37*(J_3-J_7)+A_3*F_38*(J_3-J_8)+A_3*F_39*(J_3-J_9)+A_3*F_310*(J_3-J_10)+A_3*F_311*(J_3-J_11)+A_3*F_312*(J_3-J_12)

//radiation on surface 4
A_1*F_14=A_4*F_41
A_2*F_24=A_4*F_42

A_4*F_43=A_3*F_34
F_410*A_4=F_104*A_10
(E_4-J_4)/((1-ebsilon_3)/(ebsilon_3*A_4))=A_4*F_41*(J_4-J_1)+A_4*F_42*(J_4-J_2)+A_4*F_43*(J_4-J_3)+A_4*F_45*(J_4-J_5)+A_4*F_46*(J_4-J_6)+A_4*F_47*(J_4-J_7)+A_4*F_48*(J_4-J_8)+A_4*F_49*(J_4-J_9)+A_4*F_410*(J_4-J_10)+A_4*F_411*(J_4-J_11)+A_4*F_412*(J_4-J_12)

//radiation on surface 5
A_5*F_51=A_1*F_15
A_5*F_52=A_2*F_25
(E_5-J_5)/((1-ebsilon_2)/(ebsilon_2*A_5))=A_5*F_51*(J_5-J_1)+A_5*F_52*(J_5-J_2)

//radiation on surface 6
F_61*A_6=A_1*F_16
F_62*A_6=A_2*F_26
F_63*A_6=A_3*F_36
F_64*A_6=A_4*F_46
(E_6-J_6)/((1-ebsilon_2)/(ebsilon_2*A_6))=A_6*F_61*(J_6-J_1)+A_6*F_62*(J_6-J_2)+A_6*F_63*(J_6-J_3)+A_6*F_64*(J_6-J_4)

//radiation on surface 7
F_37*A_3=F_73*A_7
F_47*A_4=F_74*A_7
(E_7-J_7)/((1-ebsilon_2)/(ebsilon_2*A_7))=A_7*F_73*(J_7-J_3)+A_7*F_74*(J_7-J_4)

//radiation on surface 8
F_84*A_8=F_48*A_4
F_83*A_8=F_38*A_3
F_82*A_8=F_28*A_2
F_81*A_8=F_18*A_1

(E_8-J_8)/((1-ebsilon_2)/(ebsilon_2*A_8))=A_8*F_81*(J_8-J_1)+A_8*F_82*(J_8-J_2)+A_8*F_83*(J_8-J_3)+A_8*F_84*(J_8-J_4)+A_8*F_811*(J_8-J_11)

//radiation on surface 9
A_1*F_19=A_9*F_91
A_2*F_29=A_9*F_92
(E_9-J_9)/((1-ebsilon_2)/(ebsilon_2*A_9))=A_9*F_91*(J_9-J_1)+A_9*F_92*(J_9-J_2)

//radiation on surface 10
F_103*A_10=F_310*A_3
(E_10-J_10)/((1-ebsilon_2)/(ebsilon_2*A_10))=A_10*F_103*(J_10-J_3)+A_10*F_104*(J_10-J_4)

//radiation on surface 11
F_111*A_1=F_11_1*A_11
F_211*A_2=F_11_2*A_11
F_311*A_3=F_11_3*A_11
F_411*A_4=F_11_4*A_11
F_811*A_8=F_11_8*A_11
(E_11-J_11)/((1-ebsilon_2)/(ebsilon_2*A_11))=A_11*F_11_1*(J_11-J_1)+A_11*F_11_2*(J_11-J_2)+A_11*F_11_3*(J_11-J_3)+A_11*F_11_4*(J_11-J_4)+A_11*F_11_8*(J_11-J_8)+A_11*F_1112*(J_11-J_12)

//radiation on surface 12
F_12_1*A_12=A_1*F_112
F_12_2*A_12=A_2*F_212
F_12_3*A_12=A_3*F_312
F_12_4*A_12=A_4*F_412

F_12_11*A_12=A_11*F_1112
(E_12-J_12)/((1-ebsilon_2)/(ebsilon_2*A_12))=A_12*F_12_1*(J_12-J_1)+A_12*F_12_2*(J_12-J_2)+A_12*F_12_3*(J_12-J_3)+A_12*F_12_4*(J_12-J_4)+A_12*F_12_11*(J_12-J_11)

Q_rad_1=(E_1-J_1)/((1-ebsilon_1)/(ebsilon_1*A_1))
Q_rad_2=(E_2-J_2)/((1-ebsilon_3)/(ebsilon_3*A_2))
Q_rad_3=(E_3-J_3)/((1-ebsilon_3)/(ebsilon_3*A_3))
Q_rad_4=(E_4-J_4)/((1-ebsilon_3)/(ebsilon_3*A_4))
Q_rad_5=(E_5-J_5)/((1-ebsilon_2)/(ebsilon_2*A_5))
Q_rad_6=(E_6-J_6)/((1-ebsilon_2)/(ebsilon_2*A_6))
Q_rad_7=(E_7-J_7)/((1-ebsilon_2)/(ebsilon_2*A_7))
Q_rad_8=(E_8-J_8)/((1-ebsilon_2)/(ebsilon_2*A_8))
Q_rad_9=(E_9-J_9)/((1-ebsilon_2)/(ebsilon_2*A_9))
Q_rad_10=(E_10-J_10)/((1-ebsilon_2)/(ebsilon_2*A_10))
Q_rad_11=(E_11-J_11)/((1-ebsilon_2)/(ebsilon_2*A_11))
Q_rad_12=(E_12-J_12)/((1-ebsilon_2)/(ebsilon_2*A_12))

//radiation and convection from surfaces
Q_rad_1+Q_conv_1=q_cond_1
Q_rad_2+Q_conv_2=0
Q_rad_3+Q_conv_3=0
Q_rad_4+Q_conv_4=0
Q_rad_5+Q_conv_5=q_cond_5
Q_rad_6+Q_conv_6=q_cond_6
Q_rad_7+Q_conv_7=q_cond_7
Q_rad_8+Q_conv_8=q_cond_8
Q_rad_9+Q_conv_9=q_cond_9
Q_rad_10+Q_conv_10=q_cond_10
Q_rad_11+Q_conv_11=q_cond_11
Q_rad_12+Q_conv_12=q_cond_12

//convection heat transfer from surfaces

Q_conv_1=h_1*A_1*(T_1-T_13)
Q_conv_2=h_2*A_2*(T_2-T_13)
Q_conv_3=h_3*A_3*(T_3-T_13)
Q_conv_4=h_4*A_4*(T_4-T_13)
Q_conv_5=h_5*A_5*(T_5-T_13)
Q_conv_6=h_6*A_6*(T_6-T_13)
Q_conv_7=h_7*A_7*(T_7-T_13)
Q_conv_8=h_8*A_8*(T_8-T_13)
Q_conv_9=h_9*A_9*(T_9-T_13)
Q_conv_10=h_10*A_10*(T_10-T_13)
Q_conv_11=h_11*A_11*(T_11-T_13)
Q_conv_12=h_12*A_12*(T_12-T_13)

//Conduction
k=15 [W/m-K]
l=0.03 [m] {heated wall thickness}
l_2=0.005 [m] {riser tube thickness}

q=q_cond_1
q_cond_1=k*A_1/l*(T_outer-T_1)
q_cond_5=k*A_5/l_2*(T_5-T_5_i)
q_cond_6=k*A_6/l_2*(T_6-T_6_i)
q_cond_7=k*A_7/l_2*(T_7-T_7_i)
q_cond_8=k*A_8/l_2*(T_8-T_8_i)
q_cond_9=k*A_9/l_2*(T_9-T_9_i)
q_cond_10=k*A_10/l_2*(T_10-T_10_i)
q_cond_11=k*A_11/l_2*(T_11-T_11_i)
q_cond_12=k*A_12/l_2*(T_12-T_12_i)

//mass transfer

q_riser=m*(h_e-h_i)+m*g*(z_e-z_i)
T_14=0.5*(T_i+T_e)

t_i=(50+273.15) [K]
t_e=(52.94+273.15) [K]
p_e=101.303 [kPa]
p_i=101.3 [kPa]
h_e=enthalpy(air_ha,t=t_e,p=p_e)
h_i=enthalpy(air_ha,t=t_i,p=p_i)
z_e=0.2 [m]
z_i=0 [m]

//convection heat transfer coefficients on tube inner surfaces from Flownex
h_i_5=10.0881
h_i_6=11.4918
h_i_7=11.5515
h_i_8=11.6377
h_i_9=10.089
h_i_10=11.5843
h_i_11=11.6923
h_i_12=11.6881

//inner tube areas
A_i5=0.016 [m^2]
A_i6=0.096
A_i7=0.016
A_i8=0.096

A_i9=0.032

A_i10=0.032
A_i11=0.192
A_i12=0.192

{T_14 defined as riser air temperature at the node}
//energy balance on inner surface of tubes.
q_conv_i5=h_i_5*A_i5*(T_5_i-T_14)
q_conv_i6=h_i_6*A_i6*(T_6_i-T_14)
q_conv_i7=h_i_7*A_i7*(T_7_i-T_14)
q_conv_i8=h_i_8*A_i8*(T_8_i-T_14)
q_conv_i9=h_i_9*A_i9*(T_9_i-T_14)
q_conv_i10=h_i_10*A_i10*(T_10_i-T_14)
q_conv_i11=h_i_11*A_i11*(T_11_i-T_14)
q_conv_i12=h_i_12*A_i12*(T_12_i-T_14)

q_conv_i5+q_conv_i6+q_conv_i7+q_conv_i8+q_conv_i9+q_conv_i10+q_conv_i11+q_conv_i12=q_riser

//inner tube radiation view factors
//outer tube
F_5i_6i=0.45049
F_i5_i7=0.090098
F_i5_i8=0.45049
F_6i_5i*A_i6=F_5i_6i*A_i5
F_i6_i7=0.090098
F_i6_i8=0.819804
F_7i_5i*A_i7=F_i5_i7*A_i5
F_i7_i6*A_i7=F_i6_i7*A_i6
F_i7_i8=0.09902
F_8i_5i*A_i8=F_i5_i8*A_i5
F_i8_i6*A_i8=F_i6_i8*A_i6
F_i8_i7*A_i8=F_i7_i8*A_i7

//inner tube
F_9i_10i=0.090098
F_i9_i11=0.45049
F_i9_i12=0.45049
F_10i_9i*A_i10=F_9i_10i*A_i9
F_i10_i11=0.45049
F_i10_i12=0.45049
F_11i_9i=0.090098
F_i11_i10=0.090098
F_i11_i12=0.819804
F_12i_9i=0.090098
F_i12_i10=0.090098
F_i12_i11=0.819804

//inner tube radiation
//outer tubes
(E_5i-J_5i)/((1-ebsilon_2)/(ebsilon_2*A_i5))=A_i5*F_5i_6i*(J_5i-J_6i)+A_i5*F_i5_i7*(J_5i-J_7i)+A_i5*F_i5_i8*(J_5i-J_8i)
(E_6i-J_6i)/((1-ebsilon_2)/(ebsilon_2*A_i6))=A_i6*F_6i_5i*(J_6i-J_5i)+A_i6*F_i6_i7*(J_6i-J_7i)+A_i6*F_i6_i8*(J_6i-J_8i)
(E_7i-J_7i)/((1-ebsilon_2)/(ebsilon_2*A_i7))=A_i7*F_7i_5i*(J_7i-J_5i)+A_i7*F_i7_i6*(J_7i-J_6i)+A_i7*F_i7_i8*(J_7i-J_8i)
(E_8i-J_8i)/((1-ebsilon_2)/(ebsilon_2*A_i8))=A_i8*F_8i_5i*(J_8i-J_5i)+A_i8*F_i8_i6*(J_8i-J_6i)+A_i8*F_i8_i7*(J_8i-J_7i)

//inner tubes

(E_9i-J_9i)/((1-ebsilon_2)/(ebsilon_2*A_i9))=A_i9*F_9i_10i*(J_9i-J_10i)+A_i9*F_i9_i11*(J_9i-J_11i)+A_i9*F_i9_i12*(J_9i-J_12i)
(E_10i-J_10i)/((1-ebsilon_2)/(ebsilon_2*A_i10))=A_i10*F_10i_9i*(J_10i-J_9i)+A_i10*F_i10_i11*(J_10i-J_11i)+A_i10*F_i10_i12*(J_10i-J_12i)
(E_11i-J_11i)/((1-ebsilon_2)/(ebsilon_2*A_i11))=A_i11*F_11i_9i*(J_11i-J_9i)+A_i11*F_i11_i10*(J_11i-J_10i)+A_i11*F_i11_i12*(J_11i-J_12i)
(E_12i-J_12i)/((1-ebsilon_2)/(ebsilon_2*A_i12))=A_i12*F_12i_9i*(J_12i-J_9i)+A_i12*F_i12_i10*(J_12i-J_10i)+A_i12*F_i12_i11*(J_12i-J_11i)

//radiation outer tubes
Q_rad_i5=(E_5i-J_5i)/((1-ebsilon_2)/(ebsilon_2*A_i5))
Q_rad_i6=(E_6i-J_6i)/((1-ebsilon_2)/(ebsilon_2*A_i6))
Q_rad_i7=(E_7i-J_7i)/((1-ebsilon_2)/(ebsilon_2*A_i7))
Q_rad_i8=(E_8i-J_8i)/((1-ebsilon_2)/(ebsilon_2*A_i8))

//radiation inner tubes
Q_rad_i9=(E_9i-J_9i)/((1-ebsilon_2)/(ebsilon_2*A_i9))
Q_rad_i10=(E_10i-J_10i)/((1-ebsilon_2)/(ebsilon_2*A_i10))
Q_rad_i11=(E_11i-J_11i)/((1-ebsilon_2)/(ebsilon_2*A_i11))
Q_rad_i12=(E_12i-J_12i)/((1-ebsilon_2)/(ebsilon_2*A_i12))

E_5i=sigma*T_5_i^4
E_6i=sigma*T_6_i^4
E_7i=sigma*T_7_i^4
E_8i=sigma*T_8_i^4
E_9i=sigma*T_9_i^4
E_10i=sigma*T_10_i^4
E_11i=sigma*T_11_i^4
E_12i=sigma*T_12_i^4

//energy balance outer tubes
Q_rad_i5+q_conv_i5+q_cond_5=0
Q_rad_i6+q_conv_i6+q_cond_6=0
Q_rad_i7+q_conv_i7+q_cond_7=0
Q_rad_i8+q_conv_i8+q_cond_8=0
Q_rad_i9+q_conv_i9+q_cond_9=0
Q_rad_i10+q_conv_i10+q_cond_10=0
Q_rad_i11+q_conv_i11+q_cond_11=0
Q_rad_i12+q_conv_i12+q_cond_12=0

//Convert temperatures to Celcius
T_abs=273.15
T_1C=T_1-T_abs
T_2C=T_2-T_abs
T_3C=T_3-T_abs
T_4C=T_4-T_abs
T_5C=T_5-T_abs
T_6C=T_6-T_abs
T_7C=T_7-T_abs
T_8C=T_8-T_abs
T_9C=T_9-T_abs
T_10C=T_10-T_abs
T_11C=T_11-T_abs
T_12C=T_12-T_abs
T_13C=T_13-T_abs
T_14C=T_14-T_abs